

ADA036872

RADC-TR-76-389
Technical Report
January 1977

LASER ATMOSPHERIC ABSORPTION STUDIES

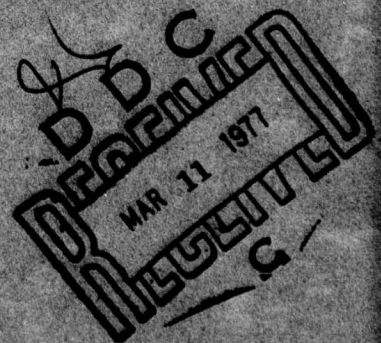
The Ohio State University

Approved for public release; distribution unlimited.

Sponsored by
Defense Advanced Research Projects Agency (DoD)
ARPA Order No. 1279

The views and conclusions contained in this document are those of the authors and should not be interpreted as necessarily representing the official policies, either expressed or implied, of the Defense Advanced Research Projects Agency or the U. S. Government.

ROME AIR DEVELOPMENT CENTER
AIR FORCE SYSTEMS COMMAND
GRIFFISS AIR FORCE BASE, NEW YORK 13441

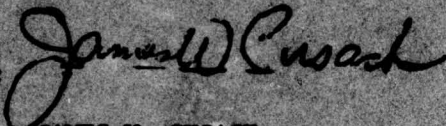


LASER ATMOSPHERIC ABSORPTION STUDIES

This report has been reviewed by the RADC Information Office (OI) and is releasable to the National Technical Information Service (NTIS). At NTIS it will be releasable to the general public, including foreign nations.

This report has been reviewed and approved for publication.

APPROVED:



JAMES W. CUSACK
Project Engineer

Do not return this copy. Retain or destroy.

LASER ATMOSPHERIC ABSORPTION STUDIES

R. K. Long
E. K. Damon
R. J. Nordstrom
J. C. Peterson
M. E. Thomas
J. P. Serafin

Contractor: The Ohio State University
Contract Number: F30602-76-C-0058
Effective Date of Contract: 1 July 1975
Contract Expiration Date: 30 September 1977
Short Title of Work: Laser Atmospheric
Absorption Studies
Program Code Number: 6E20
Period of Work Covered: Feb 76 - Jul 76

Principal Investigator: Dr. Ronald Long
Phone: 614 422-6077
Project Engineer: James W. Cusack
Phone: 315 330-3145

Approved for public release;
distribution unlimited.

This research was supported by the Defense Advanced
Research Projects Agency of the Department of
Defense and was monitored by James W. Cusack (OCSE),
Griffiss AFB NY 13441 under Contract F30602-76-C-0058.



ACCESSION for	
NTS	White Section <input checked="" type="checkbox"/>
BCC	Buff Section <input type="checkbox"/>
UNANNOUNCED	<input type="checkbox"/>
JUSTIFICATION	<input type="checkbox"/>
BY.....	
DISTRIBUTION/AVAILABILITY CODES	
Dist.	AVAIL. OR SPECIAL
A	

See 1473

UNCLASSIFIED

SECURITY CLASSIFICATION OF THIS PAGE (When Data Entered)

19 REPORT DOCUMENTATION PAGE		READ INSTRUCTIONS BEFORE COMPLETING FORM	
1. REPORT NUMBER RADCL-TR-76-389	2. GOVT ACCESSION NO.	3. RECIPIENT'S CATALOG NUMBER	
4. TITLE (and Subtitle) LASER ATMOSPHERIC ABSORPTION STUDIES.		5. TYPE OF REPORT & PERIOD COVERED Interim Report. 1 Feb - 31 Jul 76	
6. PERFORMING ORG. REPORT NUMBER ESL-4232-2		7. CONTRACT OR GRANT NUMBER(s) F30602-76-C-0058, ARPA Order-1279	
7. AUTHOR(s) R. K./Long, J. C./Peterson E. K./Damon, M. E./Thomas R. J./Nordstrom, J. P. Serfin		8. PROGRAM ELEMENT, PROJECT, TASK AREA & WORK UNIT NUMBERS 62301B 12790508	
9. PERFORMING ORGANIZATION NAME AND ADDRESS The Ohio State University/ElectroScience Laboratory Department of Electrical Engineering Columbus OH 43212		10. REPORT DATE January 1977	
11. CONTROLLING OFFICE NAME AND ADDRESS Defense Advanced Research Projects Agency 1400 Wilson Blvd Arlington VA 22209		12. NUMBER OF PAGES 127 133p.	
14. MONITORING AGENCY NAME & ADDRESS (if different from Controlling Office) Rome Air Development Center (OCSE) Griffiss AFB NY 13441		15. SECURITY CLASS. (of this report) UNCLASSIFIED 15a. DECLASSIFICATION/DOWNGRADING SCHEDULE N/A	
16. DISTRIBUTION STATEMENT (of this Report) Approved for public release; distribution unlimited.			
17. DISTRIBUTION STATEMENT (of the abstract entered in Block 20, if different from Report) Same			
18. SUPPLEMENTARY NOTES RADCL Project Engineer: James W. Cusack (OCSE)			
19. KEY WORDS (Continue on reverse side if necessary and identify by block number) Molecular absorption Spectrophone CO ₂ Laser White cell H ₂ O Laser propagation Long-path cell CO ₂ laser Multi-pass cell CO laser			
20. ABSTRACT (Continue on reverse side if necessary and identify by block number) This report describes progress on the various tasks which comprise the research in laser atmospheric propagation. This work includes 1. a review of work done on the study of the infrared water vapor continuum, 2. the design of two stainless steel, temperature controlled absorption cells with White-type optics, 3. design of a non-resonant, differential spectrophone and data recorded on this instrument, 4. design of a stainless steel, resonant spectrophone, 5. and other topics.			

DD FORM 1 JAN 73 1473

EDITION OF 1 NOV 65 IS OBSOLETE

UNCLASSIFIED

SECURITY CLASSIFICATION OF THIS PAGE (When Data Entered)

402251 R

CONTENTS

Section		Page
I	THE WATER VAPOR CONTINUUM	1
II	SPECTROPHONE MEASUREMENTS AT SEVERAL CO ₂ LASER LINES IN THE 10 μ BAND	26
	A. Water Vapor-N ₂	26
	B. CO ₂ -Air	32
III	OZONE SPECTROSCOPY AT LOW TEMPERATURES	38
	A. Ozone Spectroscopy and the CO Laser	38
	B. Two Meter, Temperature, Controlled, Stainless Steel Absorption Cell	39
IV	A DESIGN OF AN ACOUSTICALLY RESONANT SPECTROPHONE WITH VARIABLE DIMENSION AND CONFIGURATION	46
V	WHITE CELL	50
VI	CONTINUING PROJECTS	54
	A. Construction of a DF Laser	54
	B. Modification of Commercial CO ₂ Laser	54
	C. Fourier Transform Spectroscopy	54
	D. Stainless Steel, Nonresonant, Differential Spectrophone	56
	E. IMSAI 8080 Computer	56
	F. SEL 810B Computer	56
VII	ATTENUATION OF INFRARED RADIATION FROM CO ₂ ISOTOPE LASERS BY WATER VAPOR	59
VIII	CONCLUSION	111
REFERENCES		112
APPENDIX A		116

SECTION I

THE WATER VAPOR CONTINUUM

INTRODUCTION

The transmission of infrared radiation through the atmosphere continues to be a subject of considerable interest. Knowledge of the various attenuation processes due to both molecular absorption and aerosol scattering is important to many different scientific disciplines. In meteorologic studies concerning the energy budget for the surface of the earth, for example, contributions from radiation transmitted through the atmosphere to the surface as well as energy radiated away from the surface must be known. The transmission functions which describe these processes are dependent on molecular constituents, particularly H_2O and CO_2 , and also on the aerosol concentrations in the atmosphere.

Infrared transmission studies are also needed to determine optimal spectral regions for infrared imaging systems and the evaluation of infrared sensor performance under various atmospheric conditions. Imaging and sensor systems must prove reliable in the field under all possible circumstances.

Another area in which precise information on the attenuation mechanisms is needed is the study of the propagation of infrared laser radiation. The transmission of laser radiation through the atmosphere has many applications. When considering long path lengths through the atmosphere for projects such as communications, laser ranging, or energy transfer, even small attenuations per meter can become serious.

Early workers in infrared transmission studies recorded the spectral transmittance of the atmosphere to infrared solar radiation. S. P. Langley^{1,2} published several infrared solar spectra. From his work, he concluded that there was practically complete transmission at 10.7μ . A. Adel^{3,4} repeated much of Langley's work and extended the solar spectrum to 24μ . While at The Ohio State University, M. V. Migeotte^{5,6} investigated the infrared solar spectrum from 2μ to 12μ . This work was continued in the early 1950's by J. H. Shaw and co-workers⁷.

The emphasis of this early work was on the identification of atmospheric gases and the accurate determination of absorption features. Many high-resolution maps of the solar spectrum were published which collectively cover the region from 1μ to 350μ .

In 1938, W. M. Elsasser⁸ suggested the existence of a water vapor continuum absorption in the 8μ to 12μ region which he attributed to extreme wings of very strong absorption lines outside this region.

Yates and Taylor⁹ made measurements over horizontal paths using low resolution (10 cm^{-1}) spectroscopy and found greater attenuation than expected from selective absorption alone. The existence of continuum absorption near $10\mu\text{m}$ has also been confirmed in solar spectra by A. Adello¹⁰, R. Anthony¹¹, and W. T. Roach and R. M. Goody¹². In the early 1960's, K. J. Bignell and co-workers¹³ studied continuum absorption in the $10\mu\text{m}$ region at 1 to 2 cm^{-1} resolution using the sun as a source, and in the $20\mu\text{m}$ region using horizontal atmospheric paths and a Nernst source. They guessed that the temperature dependence of the continuum absorption would be negligibly small. Therefore their data are reported without indication of the temperature. In a later paper, however, Bignell¹⁴ reported a strong negative dependence of the continuum absorption coefficient on the temperature, and also reported contributions to this absorption coefficient from a self-broadening term and a foreign broadening term.

D. E. Burch¹⁵ has made laboratory studies of the water vapor continuum in the $8\mu\text{m}$ to $12\mu\text{m}$ region and also in the $4\mu\text{m}$ region¹⁶. In the $8\mu\text{m}$ to $12\mu\text{m}$ region he too found that the continuum absorption coefficient decreased rapidly with temperature. Furthermore, he found that the calculated values for the continuum absorption coefficient based on the Lorentz line shape for the strong water vapor lines were lower than the experimentally measured absorption coefficients at all wavelengths in the $8\mu\text{m}$ to $12\mu\text{m}$ region.

P. Varanasi, S. Chou, and S. S. Penner¹⁷ have suggested that the continuum absorption in this region is due to absorption by water dimer molecules. The absorption coefficient from this mechanism should increase with pressure in the same way as absorption due to the extreme wings of strong lines. The basis for the dimer hypothesis is the strong temperature dependence which is exhibited by the continuum absorption.

CO_2 laser measurements of the $8\mu\text{m}$ to $12\mu\text{m}$ water vapor continuum have been made at this laboratory by J. H. McCoy, D. B. Rensch, and R. K. Long¹⁸. Recent measurements have been made by F. S. Mills, R. K. Long and E. K. Damon¹⁹. These measurements involved the use of a multiple-traversal absorption cell to achieve path lengths of 1 km . Samples of pure water vapor as well as water vapor-air mixtures were studied at several output frequencies of the CO_2 laser. At $\lambda=10.59\mu\text{m}$, McCoy found that the self-broadening contribution to the continuum absorption coefficient was about 200 times stronger than the contribution due to foreign gas broadening¹⁸.

Studies of the absorption of CO_2 laser radiation in the atmosphere are also being performed in the Soviet Union. Absorption coefficients for the continuum absorption at the centers of the P(12) to P(26) laser lines in the $10.4\mu\text{m}$ band of CO_2 have been studied

by I. I. Ippolitov²⁰ and by V. N. Aref'ev et al²¹. A complete review of the influence of molecular absorption on the propagation of CO₂ laser radiation in the atmosphere is given by T. G. Adiks, V. N. Aref'ev, and V. I. Dianov-Klolov²².

Laboratory measurements of the infrared continuum can be divided into two groups depending on whether a laser or blackbody radiation source is used. The advantage of the laser measurement is that more accurate transmittance values are obtainable due to the high power, and excellent frequency and amplitude stability. The major disadvantage is that the radiation is available at only a few fixed frequencies. Information on the continuum absorption at a particular frequency could be obscured by a dominating local absorption line. Local and continuum absorption have different partial pressure dependences, so that this may be used as a test for local effects.

1. The Water Vapor Continuum Between 8 μ m and 12 μ m

Pressure Dependence

The 8 μ m to 12 μ m atmospheric transmission window plays an important role in the energy budget of the surface of the earth, and in the heat balance of the atmosphere since the spectral radiance of a blackbody near 296K is a maximum in this region. Infrared imaging and sensor systems also make extensive use of this spectral region. Attenuation of radiation by continuum absorption in this region, therefore, is important.

A comprehensive study of the water vapor continuum will provide the necessary data for systems design and should also provide an impetus for further theoretical understanding of the mechanism of continuum absorption.

The most recent report on the water vapor continuum in the 8 μ m to 12 μ m region is by R. E. Roberts, L. M. Biberman, and J. E. A. Selby²³. They have accumulated much of the previously published data, including laser measurements from this laboratory, and also unpublished spectroscopic data by D. E. Burch, in an attempt to evaluate the accuracy of the LOWTRAN continuum model of J. E. A. Selby and R. A. McClatchey²⁴.

The amount of radiant energy at frequency ν transmitted through an absorber of length L (in cm) can be expressed as

$$T(\nu) = \exp(-k(\nu)L) \quad (1)$$

where $k(\nu)$ is the absorption coefficient (in cm⁻¹) at frequency ν .

This absorption coefficient is a combination of the attenuation due to molecular absorption and radiation loss due to aerosol scattering. In this discussion, however, it is assumed that the contribution from aerosols is small. From Equation (1), the absorption coefficient can be written

$$K(\nu) = \frac{-1}{L} \ln T(\nu) \quad (2)$$

Before this topic is developed in great detail, it is important to compare this starting point with methods used by other workers. Burch¹⁵ used a different starting point by writing

$$T(\nu) = \exp(-k'(\nu)u) \quad (3)$$

as his first equation. Here $k'(\nu)$ is the absorption coefficient in $(\text{molecule} \cdot \text{cm}^{-2})^{-1}$. We have included the prime to distinguish this coefficient from Equation (2). The quantity u is the absorber thickness expressed in $\text{molecules} \cdot \text{cm}^{-2}$. Burch then writes

$$k'(\nu) = \frac{-1}{u} \ln T(\nu) = C_S^0(\nu) P_{\text{H}_2\text{O}} + C_N^0(\nu) P_N \quad (4)$$

for the continuum absorption coefficient. This expression is based on the assumption that the absorption is due to the extreme wings of collision-broadened lines. In Equation (4), $C_S^0(\nu)$ and $C_N^0(\nu)$ are coefficients denoting the contributions to the absorption coefficient $k'(\nu)$ from self-broadening and foreign gas broadening (usually nitrogen) mechanisms. Burch demonstrated the linear dependence of the continuum absorption coefficient $k'(\nu)$ on the water vapor pressure for a pure sample of H_2O ($P_N = 0$) by plotting $\frac{-1}{u} \ln T(\nu)$ vs $P_{\text{H}_2\text{O}}$ for data taken at $\nu = 844.2 \text{ cm}^{-1}$ at a temperature of 387 K. This plot is shown in Figure 1.

Although this linear dependence as expressed by Burch was based upon the assumption that the continuum absorption is caused by extreme wings of strong lines, Figure 1 does not necessarily substantiate this mechanism. Varanassi et al¹⁷ have proposed that continuum absorption could be due to absorption by the water dimer $(\text{H}_2\text{O})_2$. The absorption coefficient as expressed in Equation (4) caused by absorption by dimer molecules would also be linear in the water vapor pressure²⁵. This statement is analyzed in more detail later in the section on water dimers. Thus, a study of the pressure dependence of the continuum absorption coefficient in the $8\mu\text{m}$ to $12\mu\text{m}$ region does not constitute positive verification of one absorption mechanism over the other.

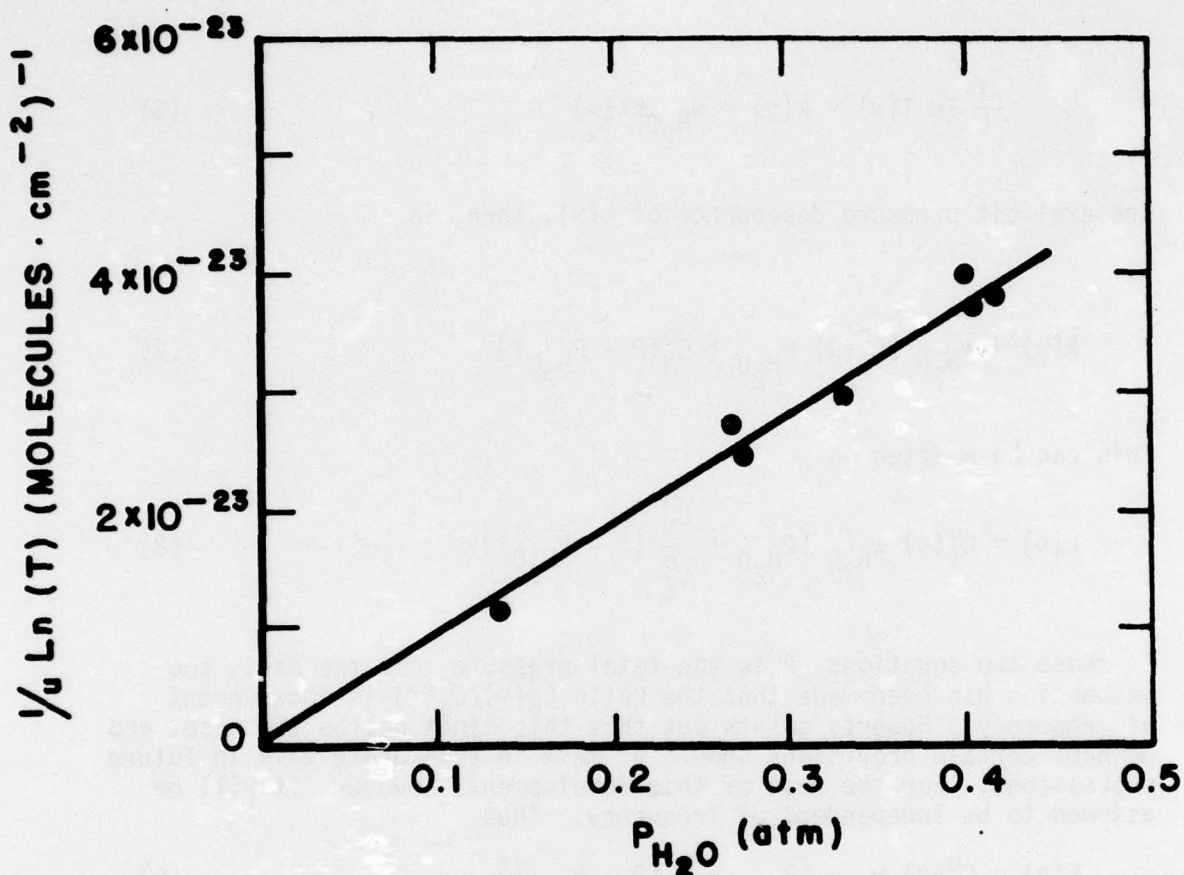


Figure 1. Plot of absorption coefficient $k'(\nu)$ at $\nu = 844.2 \text{ cm}^{-1}$ as defined in Equation (4) as a function of water vapor pressure for a sample of pure water vapor at $T = 387 \text{ K}$. Reproduced from Reference 15.

In order to discuss the results of previous research on the water vapor continuum, we will develop the details expressed in Equations (1) and (2). The absorption coefficient given in Equation (2) can be compared to the absorption coefficient in Equation (4) by noting that

$$u = w_{H_2O} \cdot L \quad (5)$$

where w_{H_2O} is the number density of water vapor molecules in units of molecules $\cdot \text{cm}^{-3}$. From Equations (2) and (4)

$$\frac{-1}{L} \ln T(\nu) = k(\nu) = w_{H_2O} k'(\nu) \quad (6)$$

The explicit pressure dependence of $k(\nu)$, then, is

$$k(\nu) = w_{H_2O} [C_S^0(\nu) P_{H_2O} + C_N^0(P - P_{H_2O})] \quad (7)$$

This can be written

$$k(\nu) = C_S^0(\nu) w_{H_2O} [P_{H_2O} + \frac{C_N^0}{C_S^0} (P - P_{H_2O})] \quad (8)$$

In these two equations, P is the total pressure. In the past, the assumption has been made that the ratio $C_N^0(\nu)/C_S^0(\nu)$ is independent of frequency. Roberts points out that this might not be the case, and perhaps certain provisions should be made to accommodate this in future expressions. For the rest of this development, however, it will be assumed to be independent of frequency. Thus

$$k(\nu) = C_S^0(\nu) w_{H_2O} [P_{H_2O} + \gamma (P - P_{H_2O})] \quad (9)$$

This is the expression in the current LOWTRAN routine.

Several workers have measured $C_S^0(\nu)$ and γ at or near room temperature. Bignell¹⁴ reported a contribution to the continuum absorption coefficient which was linear in water vapor pressure that became equal to the foreign broadened term at a water pressure of about 15 mbar (11.25 torr). From this information, the value of γ which he measured was near 0.015. Values of $C_S^0(\nu)$ measured by Bignell are shown in Figure 5.

Laser absorption studies performed by our laboratory using the P(20) laser line of CO_2 near $10.4\mu m$ suggests that γ is much smaller. McCoy et al reported his data for air broadened water samples in the form of an equation

$$k(\nu = 944.2 \text{ cm}^{-1}) = 4.32 \times 10^{-6} (\text{km}^{-1} \text{ Torr}^{-2}) P_{H_2O} [P + 193 P_{H_2O}] \quad (10)$$

Comparison between this equation and Equation (9) can be made when

$$1/\gamma - 1 = 193 \quad (11-a)$$

$$C_s^0(944.2 \text{ cm}^{-1}) w_{\text{H}_2\text{O}} = 4.32 \times 10^{-6} (\text{km}^{-1} \text{Torr}^{-2}) P_{\text{H}_2\text{O}} \quad (11-b)$$

From Equation (11-a) $\gamma = 0.005$. This is a factor of three lower than the value which was inferred from Bignell's work. The value of $C_s^0(944.2 \text{ cm}^{-1})$ derived from McCoy's equation is

$$\begin{aligned} C_s^0(944.2 \text{ cm}^{-1}) &= \frac{4.32 \times 10^{-6} (760)(700) \times 10^{-5}}{(.005) 2.687 \times 10^{19}} \frac{296}{273} \\ &= 1.85 \times 10^{-22} \text{cm}^2 \text{molecule}^{-1} \text{atm}^{-1} \end{aligned}$$

Burch has not been able to measure γ with any degree of reliability. Roberts performed a linear regression to Burch's data in the $16\mu\text{m}$ to $30\mu\text{m}$ region and extrapolated his results to the $8\mu\text{m}$ to $12\mu\text{m}$ region. Results of this extrapolation show a value of γ from Burch's work to be 0.0008.

Values represented here for γ differ by a factor 20. It is clear that there is a large experimental uncertainty about γ . Roberts suggests that until better measurements are made, the LOWTRAN model should eliminate γ . Further unknowns about γ include its frequency dependence as discussed earlier, and also its temperature dependence.

Several studies of pure water vapor samples have been made in this laboratory. McCoy measured the transmittance at 944.2 cm^{-1} and 1047.1 cm^{-1} through 980 m of water vapor at various partial pressures. The absorption coefficients which he measured at these frequencies were fitted to the equations

$$k(944.2 \text{ cm}^{-1}) = 8.39 \times 10^{-4} P_{\text{H}_2\text{O}}^2 \quad (12-a)$$

$$k(1047.1 \text{ cm}^{-1}) = 6.54 \times 10^{-4} P_{\text{H}_2\text{O}}^2 \quad (12-b)$$

More recently, F. S. Mills and R. K. Long¹⁹ made measurements of the continuum absorption coefficient in pure water vapor at the P(20) laser line of CO_2 at 944.2 cm^{-1} . The data were fitted to the equation

$$k_{\text{Mills}}(944.2 \text{ cm}^{-1}) = 9.67 \times 10^{-4} P_{\text{H}_2\text{O}}^2 \quad (13)$$

The value of $C_s^0(944.2 \text{ cm}^{-1})$ obtained from this fit is $2.24 \times 10^{-22} \text{cm}^2 \text{molecule}^{-1} \text{atm}^{-1}$.

The difference between the fit obtained by McCoy and the fit obtained by Mills is approximately 13%. Figure 2 shows the two results.

V. N. Aref'ev et al²¹ have also studied the transmittance of pure water vapor samples. For these studies, a multiple-transversal cell with a base path of 50 m was used to achieve path lengths of 3 km. The CO₂ laser which was used as a source was not stabilized, and it oscillated alternately on the P(16), P(20), P(22), and P(24) transitions in the 10.4 μ m band.

Results of their work done at 294 K are reproduced in Figure 3. The dashed curve represents the results of McCoy et al¹⁸, as expressed in Equation (12-a). Aref'ev chose to fit his data to an expression of the form

$$T = \exp(-(0.031w + 0.029w^2)) \quad (14)$$

where w is the centimeters of precipitable water in the 3 km path. This can be written for arbitrary path length in terms of the water vapor density a (in gm/m³).

$$T = \exp(-(3.1a + 0.87a^2) \times 10^{-3}L) \quad (15)$$

The absorption coefficient in the form

$$k = (3.1a + 0.87a^2) \times 10^{-3} \quad (16)$$

with a term which is linear in the absorber amount for pure water samples is not in agreement with the results of McCoy and of Mills and Long in Figure 2. In the units chosen by Burch, this linear term in Equation (16) would become a nonzero intercept to Figure 1.

In light of this discrepancy, we have examined the data of Figure 3 very carefully. Using a computer graphics technique, we digitized the data of Figure 3 two separate times to create independent data sets. We then ran several curve fit routines on these data sets to determine the necessity of the linear term in Equation (16).

The two independent data sets were fit to a $P_{H_2O}^2$ dependence by converting gm/m³ to Torr. The conversion used was 1 gm/m³ = 1.033 Torr at 294 K. Figures 4 (a) and 4 (b) show plots of $-(1/L)\ln(t)$ in km⁻¹ as a function of $P_{H_2O}^2$ for each of the data sets. Allowance was made in the curve fit for the fact that the best straight line might not pass through the origin due to systematic or instrumentation errors in the experiment. Results of these fits are shown in Table I. Also shown are the least square fits to McCoy's data and the data of Mills and Long. The RMS errors of the two data sets from Aref'ev indicate a good fit to the data and we feel that the linear term in Equation (16) is unnecessary.

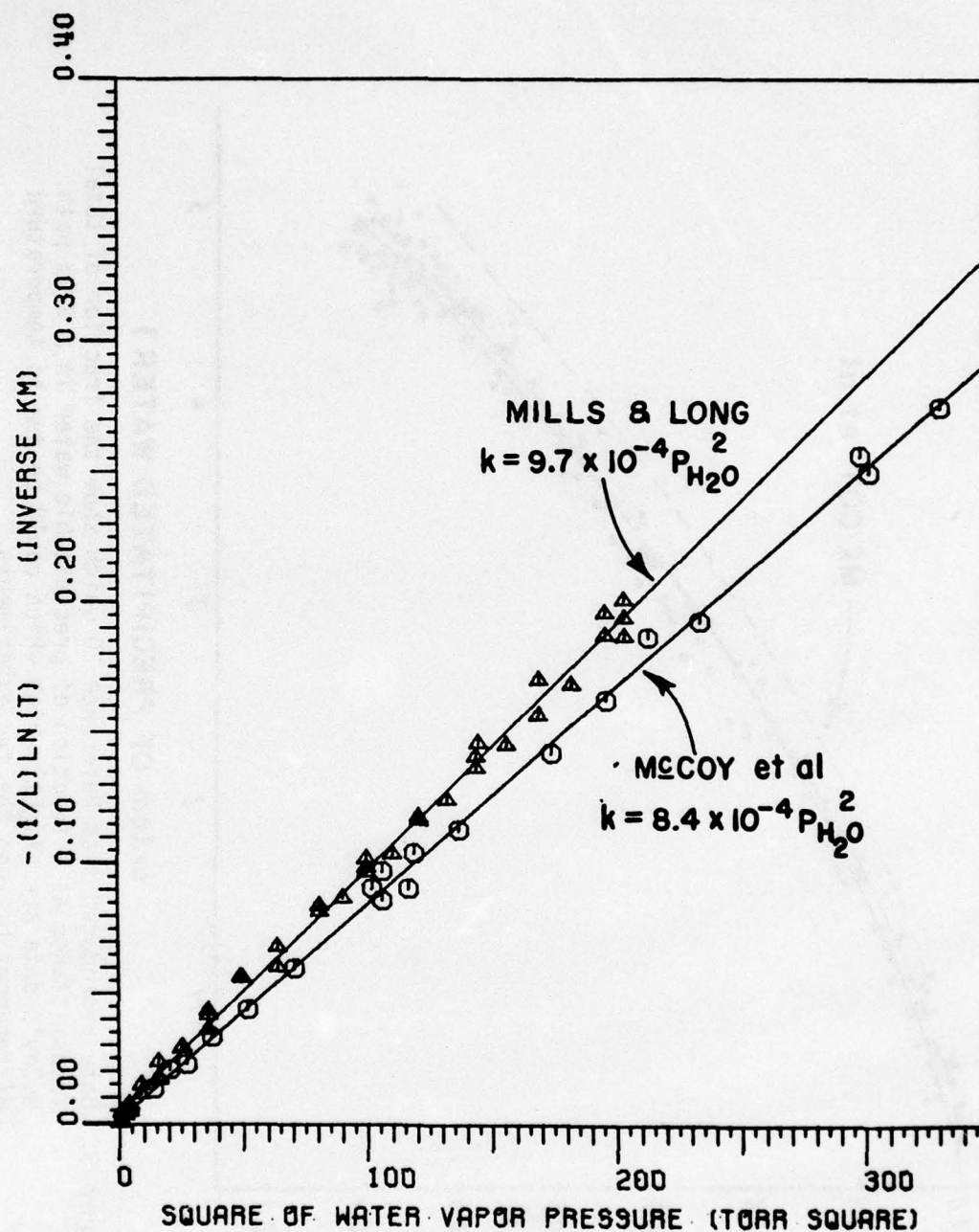


Figure 2. Comparison of the results of McCoy et al. and the results of Mills and Long for absorption of the P(20) laser line of CO_2 by pure water vapor samples.

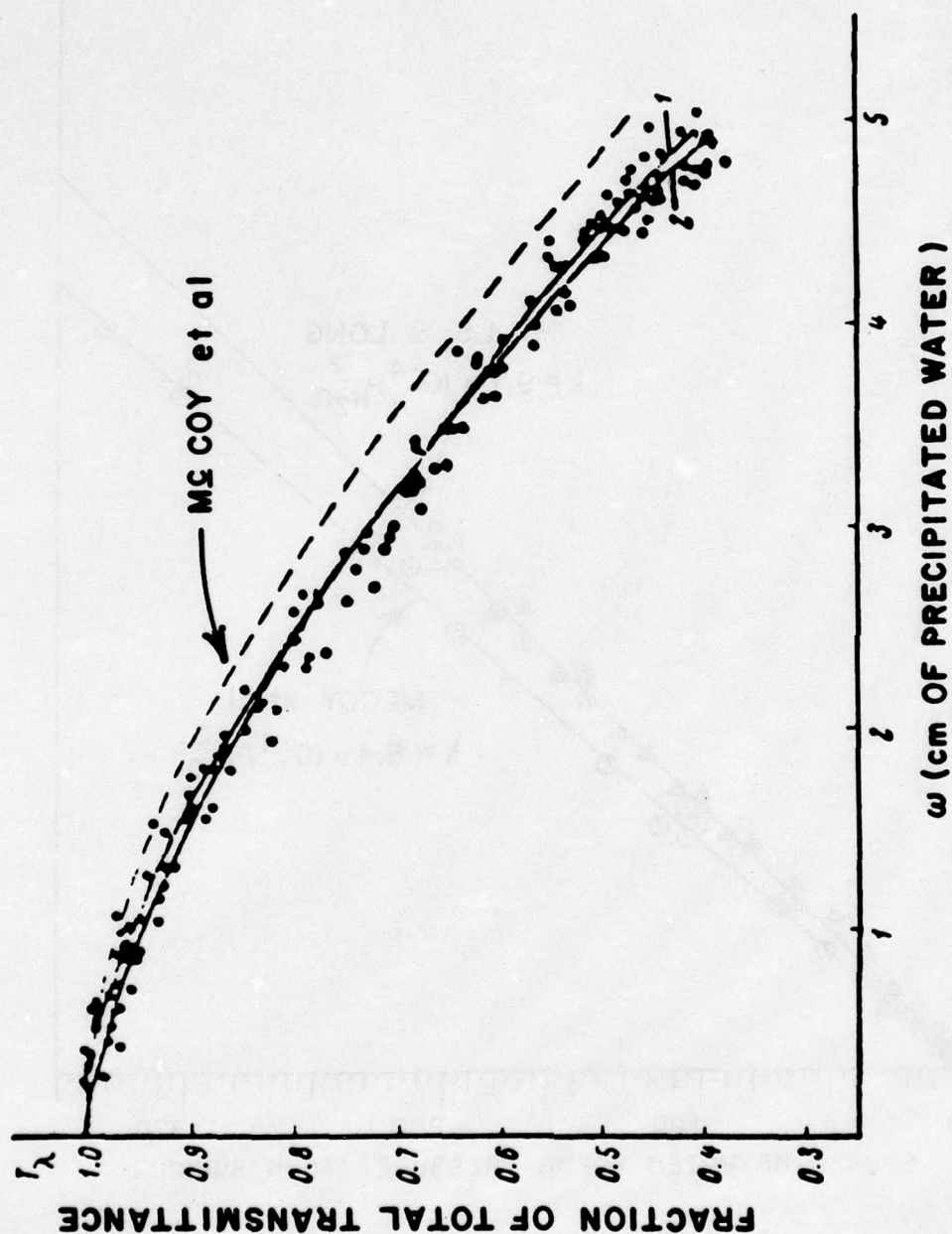


Figure 3. Data reproduced from Reference 20 which show the fraction of total transmittance as a function of precipitable water in a 3 km path. McCoy's data are slightly high which could be due to temperature differences between the two experiments.

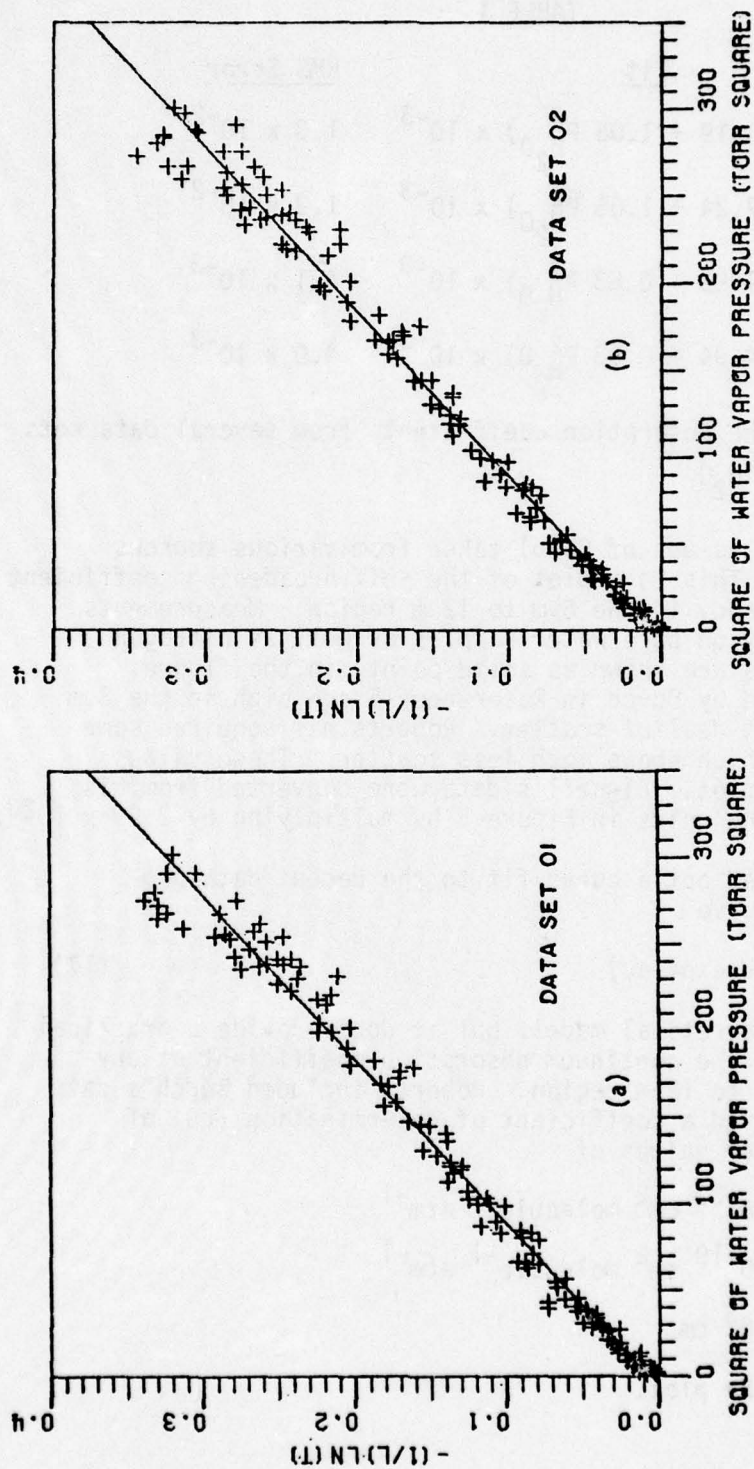


Figure 4 (a-b). Plots of absorption coefficient $k(v)$ as defined by Equation (2) as a function of $P_{H_2O}^2$ for two independent digitizations of the data in Figure 3. Results of the linear least square fits are shown in Table I.

TABLE I

<u>Data Set</u>	<u>Fit</u>	<u>RMS Error</u>
01	$k = (6.19 + 1.06 P_{H_2O}^2) \times 10^{-3}$	1.3×10^{-2}
02	$k = (7.24 + 1.05 P_{H_2O}^2) \times 10^{-3}$	1.3×10^{-2}
McCoy	$k = (1.95 + 0.83 P_{H_2O}^2) \times 10^{-3}$	4.1×10^{-3}
Mills and Long	$k = (4.94 + 0.93 P_{H_2O}^2) \times 10^{-3}$	4.0×10^{-3}

Least square fits of the absorption coefficients from several data sets to the form $k = a + b P_{H_2O}^2$.

Comparison of the values of $C_S^0(\nu)$ taken from various sources is shown in Figure 5. This is a plot of the self-broadening coefficient as a function of frequency in the $8\mu\text{m}$ to $12\mu\text{m}$ region. Measurements made at this laboratory on pure water samples as well as nitrogen broadened water samples are shown as solid points in the figure. Original data published by Burch in Reference 15 are high in the $8\mu\text{m}$ region and show a great deal of scatter. Roberts has acquired some recent data by Burch which shows much less scatter. These values are also shown in the plot. Bignell's data were converted from his units of $\text{cm}^2 \text{cm}^{-1}$ to the units in Figure 5 by multiplying by 2.99×10^{23} .

Roberts has carried out a curve fit to the recent data provided by Burch. His curve

$$C_S^0(\nu) = a + b \cdot \exp(-\sigma \nu) \quad (17)$$

is not based on any theoretical model, but it does provide a practical method for calculating the continuum absorption coefficient at any frequency ν in the $8\mu\text{m}$ to $12\mu\text{m}$ region. Roberts included Burch's data out to 30 m, and achieved a coefficient of determination (r^2) of 0.992 with the parameter values of

$$a = 1.25 \times 10^{-22} \text{ cm}^2 \text{ molecule}^{-1} \text{ atm}^{-1}$$

$$b = 1.67 \times 10^{-19} \text{ cm}^2 \text{ molecule}^{-1} \text{ atm}^{-1}$$

$$\sigma = 7.87 \times 10^3 \text{ cm}$$

This fit is shown in the plot.

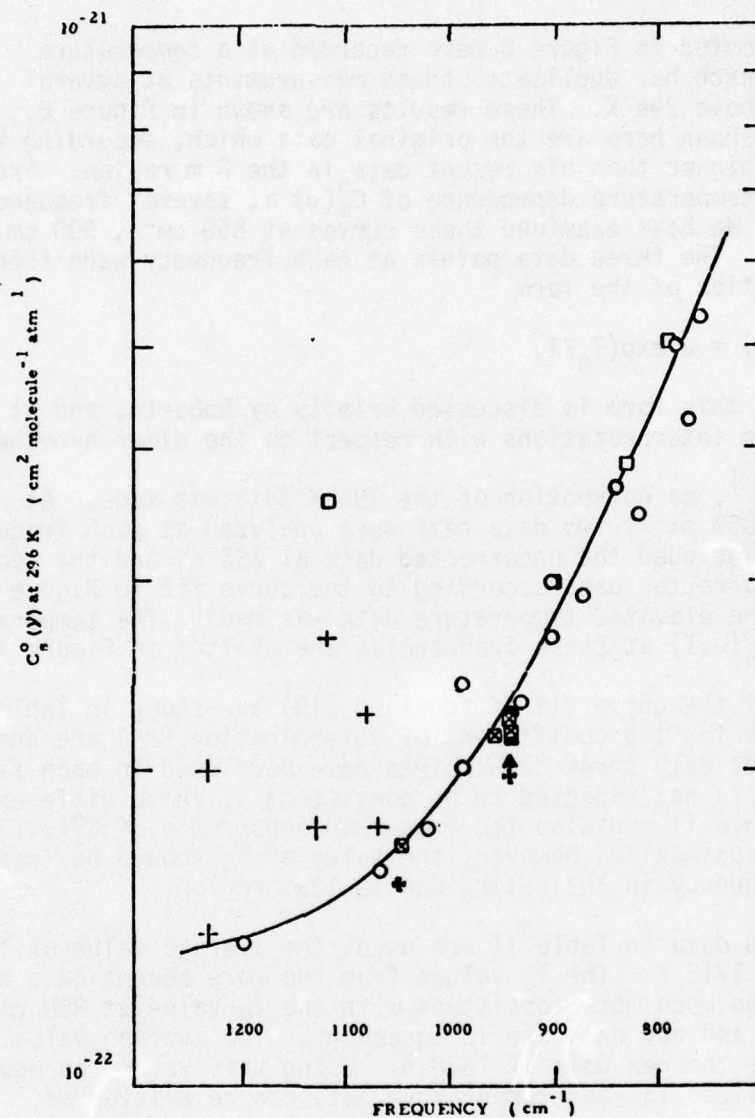


Figure 5. Accumulation of data from several sources on the frequency dependence of the self-broadening coefficient near 296 K in the 8 μ m to 12 μ m atmospheric transmission window. Legend:

- | | | |
|---|--------------------------------------|--------------|
| + | Original Burch data near 8 μ m | Reference 15 |
| ○ | Unpublished Burch data | |
| □ | Bignell | Reference 14 |
| + | McCoy, pure H ₂ O samples | Reference 18 |
| ▲ | McCoy, air broadened | Reference 18 |
| ■ | Mills, Long, pure H ₂ O | Reference 25 |
| ● | Mills, Long, nitrogen broadened | Reference 25 |
| ■ | Mills, Long, Damon | Reference 19 |

Temperature Dependence

Data presented in Figure 5 were recorded at a temperature near 296 K. Burch has duplicated these measurements at several temperatures above 296 K. These results are shown in Figure 6. The data at 296 K shown here are the original data which, according to Figure 5, are higher than his recent data in the 8 μ m region. From Figure 6, the temperature dependence of $C_S^0(\nu)$ at several frequencies can be found. We have examined these curves at 850 cm^{-1} , 900 cm^{-1} , and 1000 cm^{-1} . The three data points at each frequency were then fit to an equation of the form

$$C_S^0(\nu) = a \exp(T_0/T) \quad (18)$$

An equation of this form is discussed briefly by Roberts, and it has interesting interpretations with respect to the dimer hypothesis.

At 850 cm^{-1} , no correction of the 296 K data was made. At 900 cm^{-1} and 1000 cm^{-1} , two data sets were analyzed at each frequency. The first set included the uncorrected data at 296 K, and the second set included corrected data according to the curve fit in Figure 5. No change of the elevated temperature data was made. The temperature profiles for $C_S^0(\nu, T)$ at these frequencies are plotted in Figure 7.

Results of the curve fit of Equation (18) are shown in Table II. The high values for the coefficient of determination (r^2) are due to the fact that only three data points have been used in each fit. The value of a is not expected to be consistent at these different frequencies since it contains the frequency dependence of $C_S^0(\nu, T)$. To a first approximation, however, the value of T_0 should be independent of frequency in the entire 8 μ m to 12 μ m region.

If the old data in Table II are used, the average value of T_0 is found to be 1718 K. The T_0 values from the more recent data by Burch seem to be much more consistent with the T_0 value at 850 cm^{-1} , where both old and new data are in agreement. The average value of T_0 derived from the new data is 1638 K. Using this value, an equation which is normalized to room temperature data can be written as

$$C_S^0(\nu, T) = C_S^0(\nu) \exp \left[1638 \text{ K} \left(\frac{1}{T} - \frac{1}{296 \text{ K}} \right) \right] \quad (19)$$

$C_S^0(\nu)$ is the self-broadening coefficient at 296 K.

No measurements of any kind have been made to study the temperature dependence of continuum absorption from air broadened water vapor samples. This study would prove particularly interesting, and would determine what effect, if any, the temperature has on the parameter γ .

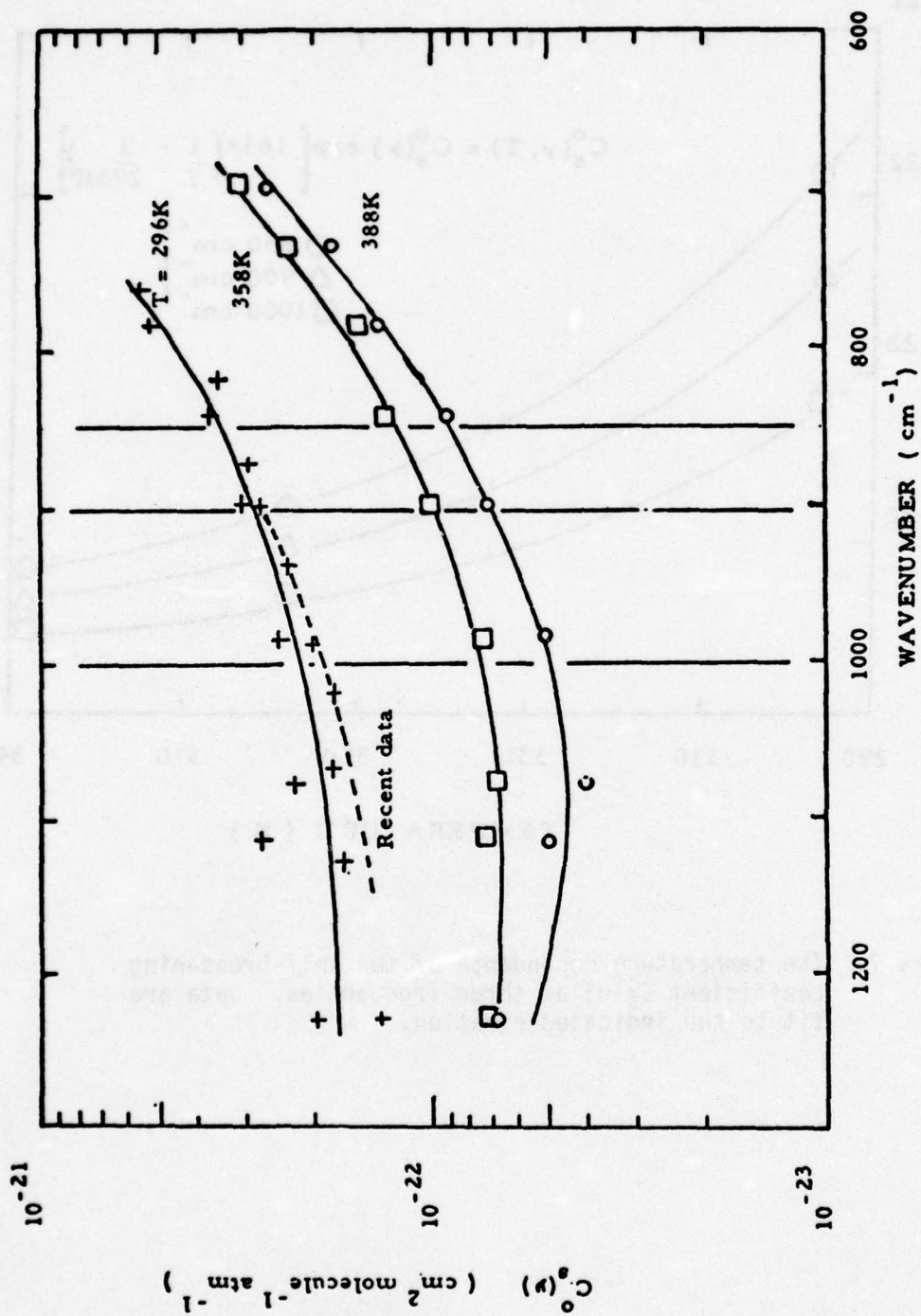


Figure 6. The self-broadening coefficient $C_s^O(v)$ at several temperatures. The dashed line at 296 K represents the curve fit to recent data in Figure 5.

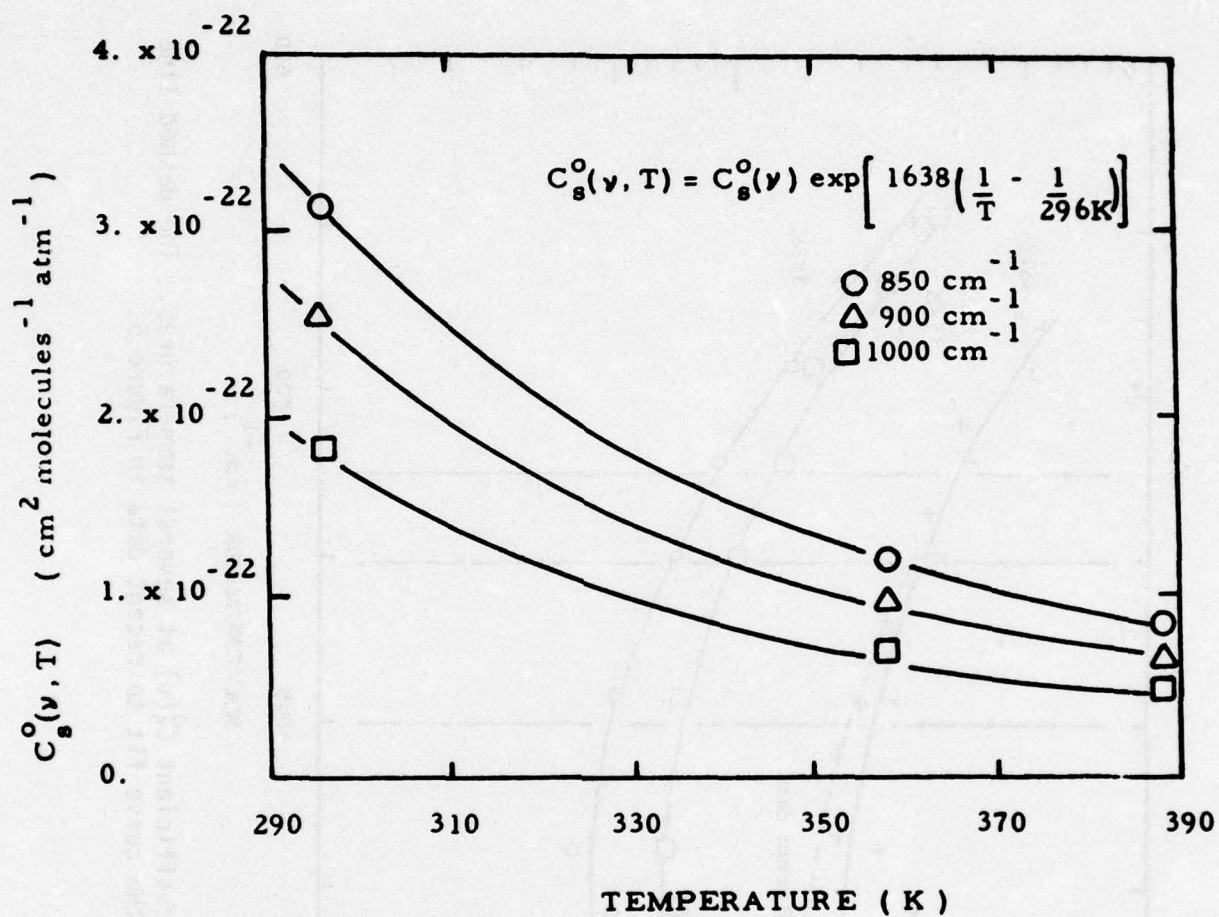


Figure 7. The temperature dependence of the self-broadening coefficient $C_s^0(\nu)$ at three frequencies. Data are fit to the indicated equation.

TABLE II

	old 850 cm^{-1}	new 900 cm^{-1}	old 1000 cm^{-1}	new 1000 cm^{-1}
a	1.265×10^{-24}	8.047×10^{-25}	4.755×10^{-25}	6.959×10^{-25}
T_0	1.635×10^3	1.628×10^3	1.792×10^3	1.650×10^3
r^2	.999	1.000	1.000	.999

Coefficients for Equation (18) determined from a least square fit of Burch's data at several frequencies.

V. N. Aref'ev carried out measurements of the continuum absorption coefficients at the centers of the P(16), P(20), P(22), and P(24) CO₂ laser lines in the 10.4 μm band. As mentioned before, their laser oscillated alternately on each of the lines, and no special steps were taken to separate the results obtained. Measurements were carried out at temperatures of 293 K, 323 K, and 353 K as reported by Adiks et al.²² on pure water samples. Results of this work were reported in the form of an equation

$$k = 1.76 \times 10^{-3} a + 0.42 \times 10^{-6} a^2 \exp \left[\frac{-\Delta H}{RT} \right] \quad (20)$$

In this equation, a is the amount of water vapor in units of gm·m⁻³ and k is in km⁻¹. Since frequency components were not separated, this expression is an average over the four laser lines. In comparing this work with other laser measurements it is assumed that Equation (20) is valid at the P(20) laser line position. The value of $-\Delta H/R$ reported was 2273 K.

The presence of a term which is linear in the absorber amount has been questioned earlier in this report. The fact that it is now assumed to be independent of temperature makes this term even more suspect. An equation of the form shown in Equation (20) is not in agreement with Equations (8), (10), and (19). Furthermore, it does not even agree well with Equation (16), as can be seen by using $T = 294$ K in Equation (20) to write

$$k = (1.76a + 0.96a^2) \times 10^{-3} \quad (21)$$

Other workers have estimated the size of the exponential factor T_0 in Equation (18). Roberts has summarized these results in his report on the water vapor continuum²³. Rather than reporting the value which Aref'ev and Dianov-Kloloov found as 2273 K, Roberts fit their data to an equation of the form given in Equation (16). Results of this fit give $T_0 = 1810$ K. Table III summarized values of the exponential constant found by several workers. In all of this work, errors of ±200 K are not uncommon.

TABLE III

Reference	T_0 (K)
Burch ¹⁵ (old data)	1718
Burch (new data)	1638
Aref'ev ²²	2273
Aref'ev*	1810
Bignell ¹⁴	1800
Varanasi et al. ¹⁷	2000

*Using Aref'ev data and fitting to Equation (19).

A Case for Water Dimer Absorption

Burch found that the water vapor continuum absorption coefficients in the 8 μ m to 12 μ m region are significantly larger than the calculated values based on extreme wings of strong Lorentz water lines. Figure 8 shows that the discrepancy is a full order of magnitude. The simple Lorentz line shape has the form

$$k(\nu) = \frac{1}{\pi} \frac{S\alpha}{(\nu-\nu_0)^2 + \alpha^2} \quad (22)$$

and the full Lorentz line shape has the form

$$k(\nu) = \frac{1}{\pi} \frac{\nu}{\nu_0} \left[\frac{S\alpha}{(\nu-\nu_0)^2 + \alpha^2} - \frac{S\alpha}{(\nu+\nu_0)^2 + \alpha^2} \right] \quad (23)$$

where S is the intensity, α is the halfwidth, and ν_0 is the center frequency of the absorption line. For infrared frequencies, $\nu+\nu_0 \gg \alpha$, and the second term in Equation (23) is negligible.

The fact that the experimentally observed absorption is greater than the calculated absorption is just the opposite from the continuum absorption caused by CO_2 in the 14 μ m region. For the CO_2 continuum, the absorption coefficient is smaller than the calculated absorption based on wings of Lorentz lines. The suggestion has been made that the increased absorption for the case of water vapor is due to absorption by $(\text{H}_2\text{O})_2$ dimer molecules.¹⁷

The water dimer molecule is in equilibrium with water vapor through the dissociation-association reactions $(\text{H}_2\text{O})_2 \rightleftharpoons 2 \text{H}_2\text{O}$. The equilibrium constant for these reactions is

$$k_{\text{Eq}} = \frac{p_{\text{H}_2\text{O}}^2}{p_{\text{D}}} \quad (24)$$

where the subscript D refers to the dimer.

Energy transmitted by a gas of dimer molecules is expected to follow the usual

$$T_D(\nu) = \exp(-k_D(\nu)u_D) \quad (25)$$

where $k_D(\nu)$ is the absorption coefficient of the dimer gas and u_D is the optical thickness which can be written by Equation (5) as $u_D = w_D \cdot L$. From Equation (25), $k_D(\nu)$ can be written as

$$k_D(\nu) = \frac{-1}{u_D} \ln T_D(\nu) \quad (26)$$

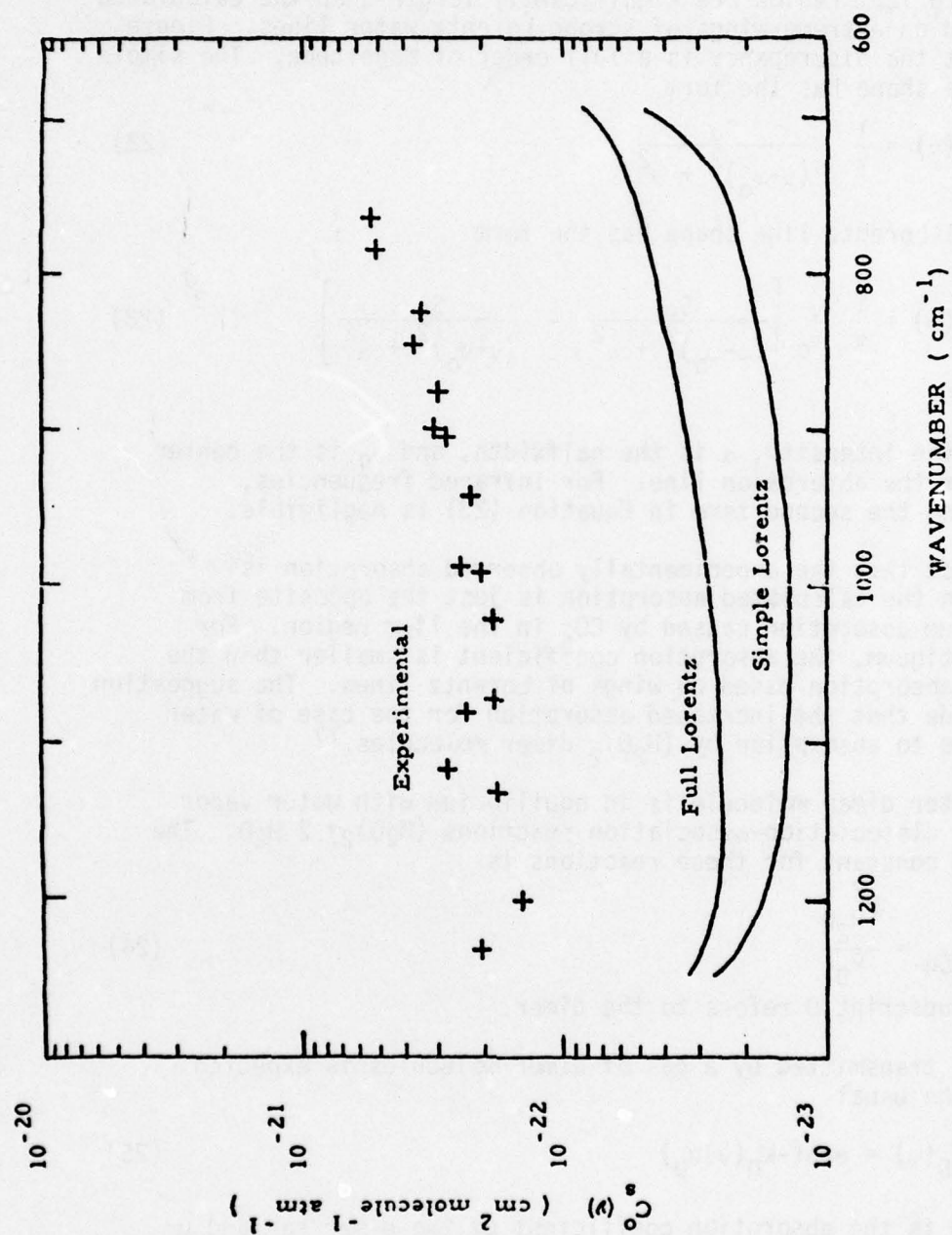


Figure 8. Comparison of experimental values of $C_s^0(\nu)$ at 296 K with calculated values assuming the continuum absorption is due to the extreme wings of simple Lorentz lines, or of full Lorentz lines. Reproduced from Reference 15.

If the water dimer is indeed causing the absorption in the 8 μ m to 12 μ m region, then $k_D(\nu)$ is the experimentally measured absorption coefficient. However, this coefficient is measured experimentally with respect to the concentration of water vapor (u_{H_2O}) not with respect to dimer concentration. From Equation (24), u_D can be converted to u_{H_2O} .

$$u_D = \frac{1}{k_{Eq}} u_{H_2O} P_{H_2O} \quad (27)$$

Substitution of this expression into Equation (26) gives

$$k_D(\nu) = \frac{k_{Eq}}{P_{H_2O}} \frac{-1}{u_{H_2O}} \ln T_D(\nu) \quad (28)$$

Rearranging terms gives

$$\frac{-1}{u_{H_2O}} \ln T_D(\nu) = \frac{k_D(\nu)}{k_{Eq}} P_{H_2O} \quad (29)$$

The left hand side of this equation is the expression which would be measured as in Figure 1, assuming the continuum absorption is caused by water vapor. Ignoring dimer-dimer contributions to $k_D(\nu)$, this expression is linear in the water vapor pressure. This is the same pressure dependence as Burch used, assuming that the continuum was caused by extreme wings of very strong lines. Therefore, a study of the pressure dependence of continuum absorption in the 8 μ m to 12 μ m region is not expected to support one absorption mechanism over the other.

The temperature dependence of the continuum absorption has been cited by many as strong evidence for the mechanism of dimer absorption.^{17,22} If dimers are responsible for the absorption, the absorption coefficient should have a temperature dependence of the form $\exp(E/RT)$, where E is the bonding energy of the dimer. Results of temperature studies by several workers show that the temperature dependence of the continuum absorption coefficient can be fitted to an exponential form. Figure 7 demonstrates this fit. Table III shows that a reasonable estimate for the constant E/R is approximately 1800 K. On the basis of a hydrogen-hydrogen bond, the bonding energy for the water dimer has been estimated at 3 to 5 kcal/mole.^{17,22} Using $R = 2$ cal/mole $^\circ$ K, these bond energies give a value of T_0 between 1500 K and 2500 K.

The agreement between the temperature dependence of the water vapor continuum and the temperature dependence of dimer formation plus the fact that continuum absorption is much stronger than predicted from Lorentz lines can be taken as strong evidence in favor of the

dimer absorption mechanism. However, as Burch points out,²⁶ so little is known about the true shapes of the extreme wings of water vapor lines that their contribution cannot be ruled out.

Results such as Equations (9), (17), and (19) are largely empirical and do not depend on a particular absorption mechanism. They generate curves which are fitted to the data and thus represent algorithms for evaluating the absorption coefficient under specific environmental conditions. As such, these results do not possess any power to predict results of experiments outside the limitations of the variables. Absolute determination of the mechanism of continuum absorption in the $8\mu\text{m}$ to $12\mu\text{m}$ region would enable predictions of the behavior of this absorption under new circumstances to be made.

One idea which may help to determine the absorption mechanism is to study samples of D_2O instead of H_2O . The isotopic shift in the ν_2 band from $6.3\mu\text{m}$ to $8.5\mu\text{m}$ would efficiently bring the CO_2 laser emission frequencies closer to the band center for a different look at absorption due to the wings of strong lines. A close look at the pressure and temperature dependence of the continuum absorption of D_2O might well shed considerable insight on the continuum absorption of H_2O .

The Water Vapor Continuum in the Region of $4\mu\text{m}$

D. Burch¹⁵ has studied continuum absorption in the $4\mu\text{m}$ region using a long path absorption cell and a grating spectrometer. Continuum absorption in this region arises from two effects. One is water vapor absorption which has been attributed to the extreme wings of strong water lines in the bands at $6.3\mu\text{m}$ and $2.7\mu\text{m}$. The other is pressure induced nitrogen absorption.

Burch found the experiment difficult to perform and his accuracy was less than he had anticipated. The major difficulty was due to the fact that the absorption in this region due to the water vapor continuum is close to two orders of magnitude smaller than continuum absorption near $10\mu\text{m}$. As a result, he had to use very high temperatures (up to 428 K), with water vapor pressures of 100 Torr could be achieved. This led to problems of water vapor absorption onto the cooler mirrors which reduced reflectivity. Figure 9 is a plot of the self-broadening coefficient $C_S^0(\nu)$ for water vapor absorption in this region from 2400 cm^{-1} to 2800 cm^{-1} at several different temperatures. The magnitude of the values of $C_S^0(\nu)$ in this plot should be compared to the magnitude of $C_S^0(\nu)$ in Figures 5 and 6.

If the temperature dependence of the water vapor continuum absorption in the 4 m region is accurately represented by Equation (18), then plots of $\ln(C_S^0(\nu))$ as a function of $1/T$ for various frequency

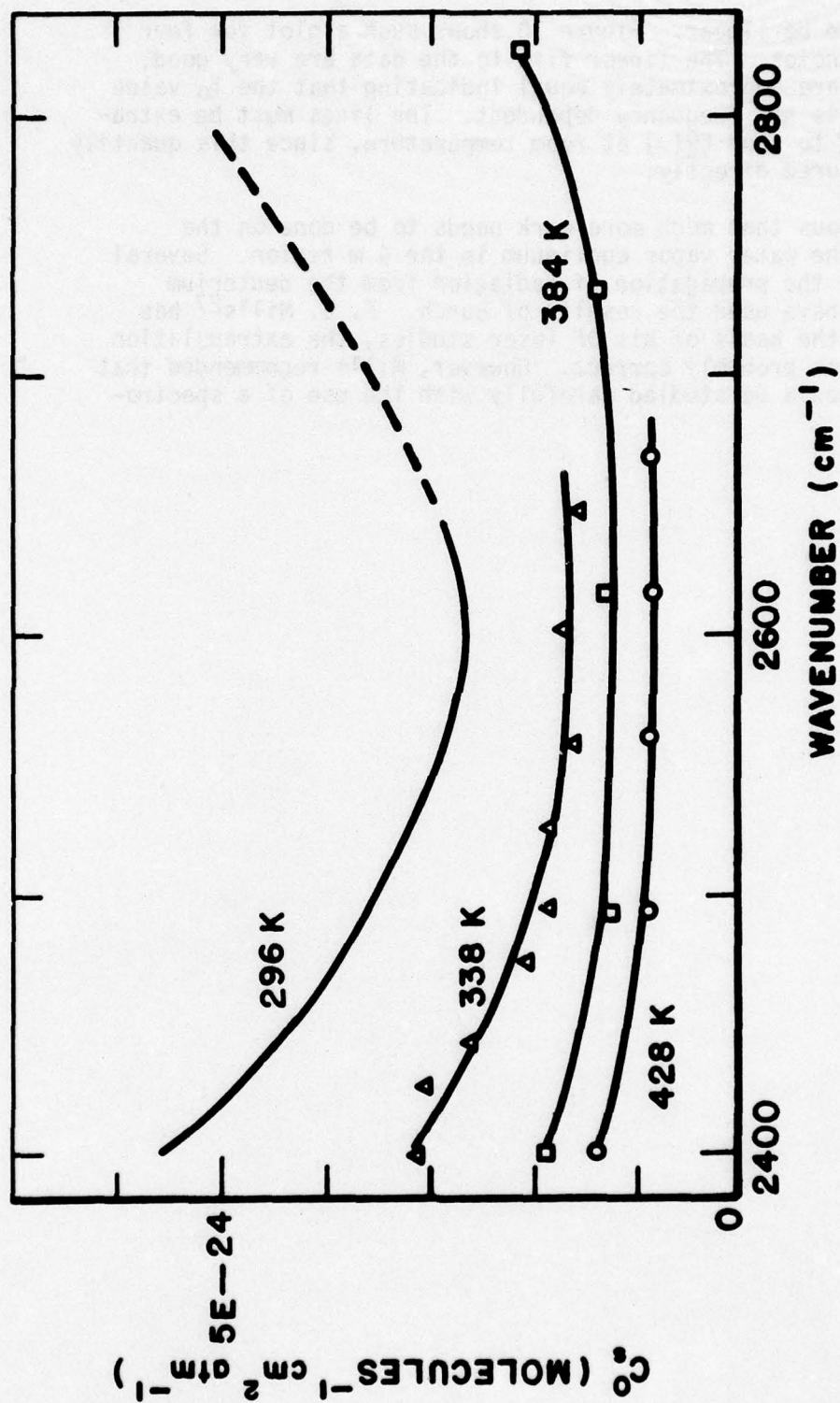


Figure 9. Spectral plots of $C_S^O(\nu)$ between 2400 cm^{-1} and 2820 cm^{-1} for pure H_2O at four temperatures. The curve at 296 K is constructed with the help of Figure 10. Reproduced from Reference 15.

positions should be linear. Figure 10 shows such a plot for four selected frequencies. The linear fits to the data are very good, and the slopes are approximately equal indicating that the T_0 value in this region is not frequency dependent. The lines must be extrapolated outward to find $CQ(v)$ at room temperature, since this quantity can not be measured directly.

It is obvious that much more work needs to be done on the absorption of the water vapor continuum in the 4 μ region. Several studies^{27,28} of the propagation of radiation from the deuterium fluoride laser have used the results of Burch. F. S. Mills²⁷ has stated that on the basis of his DF laser studies, the extrapolation done by Burch was probably correct. However, Mills recommended that this problem should be studied carefully with the use of a spectrophone.

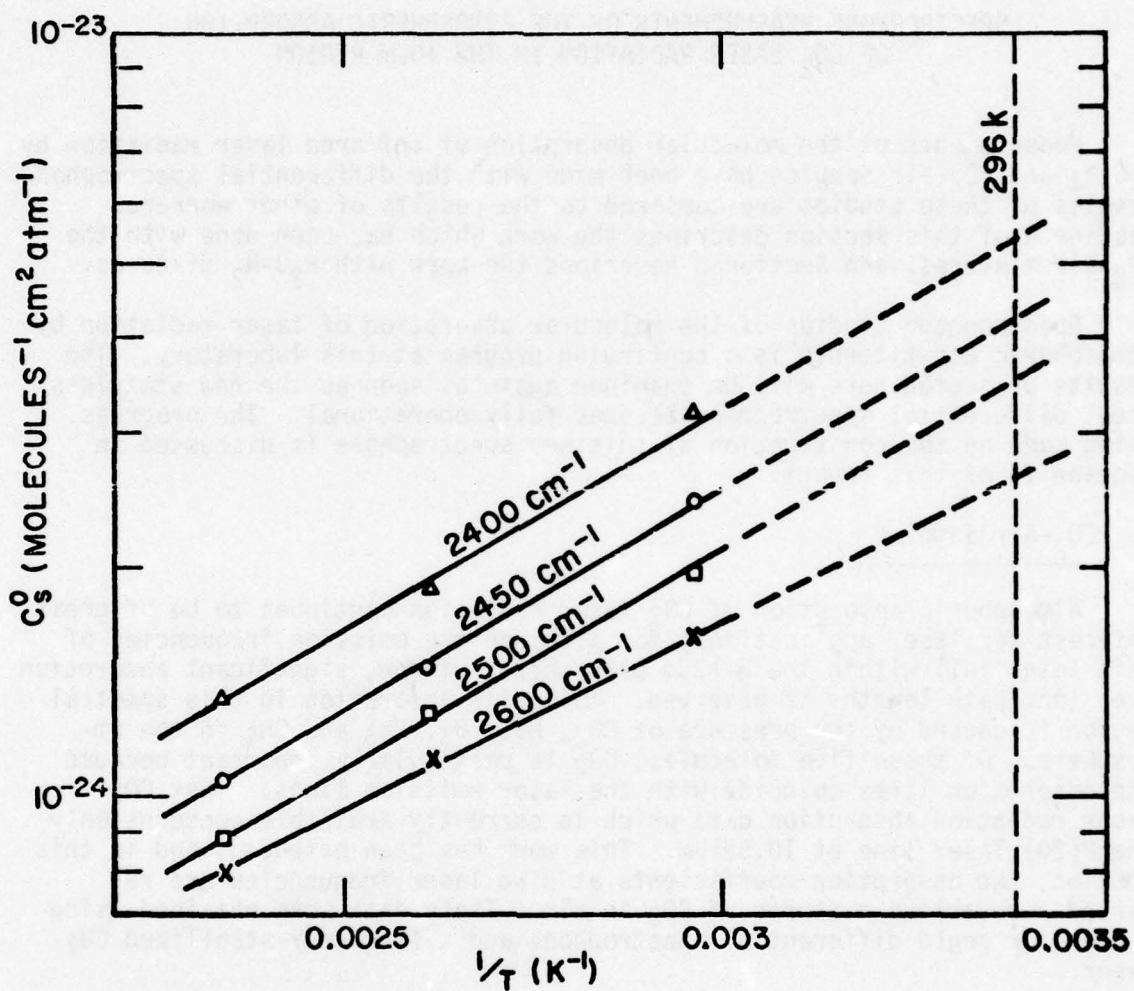


Figure 10. Semi-Logarithmic plots of $C_S^0(\nu)$ vs $1/T$ for four different frequencies. The plots are extrapolated to $T=296$ K to find $C_S^0(\nu)$ at room temperature.

SECTION II

SPECTROPHONE MEASUREMENTS OF THE ATMOSPHERIC ABSORPTION OF CO₂ LASER RADIATION IN THE 10 μ m REGION

Measurements of the molecular absorption of infrared laser radiation by H₂O-N₂ and CO₂-air samples have been made with the differential spectrophone. Results of these studies are compared to the results of other workers. Section A of this section describes the work which has been done with the CO₂-air mixtures, and Section B describes the work with H₂O-N₂ mixtures.

Spectrophone studies of the molecular absorption of laser radiation by atmospheric constituents is a continuing program at this laboratory. The results presented here will be examined again as soon as the new stainless steel differential spectrophone becomes fully operational. The progress being made on the construction of this new spectrophone is discussed in Section VI of this report.

A. CO₂-Air Samples

Atmospheric absorption of CO₂ laser radiation continues to be of great interest for laser applications, for although the emission frequencies of this laser fall within the 8-12 μ m atmospheric window, significant absorption over long path lengths is observed. Molecular absorption in this spectral region is caused by the presence of CO₂, H₂O, O₃, NH₃ and CH₄ in the atmosphere. Of these five molecules, CO₂ is particularly important because the absorption lines coincide with the laser emission lines. Most CO₂ laser radiation absorption data which is currently available concerns only the P(20) laser line at 10.591 μ m. This work has been extended, and in this section, the absorption coefficients at nine laser frequencies are reported for various mixtures of CO₂ in air. These data were obtained using a Brewster angle differential spectrophone and a frequency-stabilized CO₂ laser.

The instrument used to perform these measurements was designed by Professor E. K. Damon²⁹ in an effort to achieve improved sensitivity over the conventional spectrophone by considerably reducing the effects of absorption in the end windows. In order to accomplish this objective, two chambers of different lengths but equal volumes are optically coupled and a differential capacitive manometer is connected across the two cells as shown in Figure 11. When the spectrophone contains an inert gas sample, the window absorption in each chamber will produce equal signals (in magnitude and phase) on opposite sides of the differential pressure sensor. The net result is that there will be a null signal from the transducer.

When an absorbing gas sample is being measured, the pressure signals from cells A and B consist of two parts -- one caused by the windows and another caused by molecular absorption in the gas. Assuming matched windows and equal volumes, the window pressure signal will be equal in

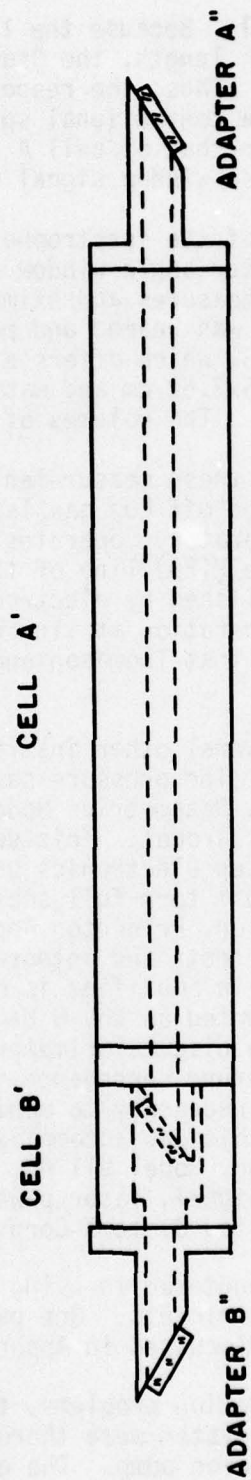


Figure 11. Brewster angle of differential spectrophone.

both chambers and therefore cancel. Because the laser energy absorbed by the gas is proportional to path length, the "sample signal" will be greater in cell A than in cell B. Thus, the response of this instrument is roughly equivalent to that of a conventional spectrophone whose length is equal to the difference between that of cell A and cell B with the important difference that the false window signal will be minimized.

The long and short cavities of the spectrophone were machined from aluminum, as were the three Brewster angle window adapters on which NaCl windows are mounted. The cell A measures approximately 5x5x30 cm and includes a 30 cm long hole, which was reamed and polished to a final diameter of 1.031 cm. The cell B, which offers a relatively short path to the incident beam, measured 5x5x7.62 cm and was machined to have a volume equal to that of cavity A. The volumes of both cells are 38 cc.

The radiation source used in these measurements was a frequency stabilized, grating tunable, sealed off CO₂ gas laser. This laser, which was constructed at this laboratory, operates at a nominal power of two watts in the TEM₀₀ mode on the P(20) line of the 10 μ m band. The frequency stabilization is accomplished by electronically tuning the cavity length to maintain laser operation at line center. The stabilizer design was adapted from one that Thomason and Elbers³⁰ used with a commercial laser.

In addition to the laser, several other instruments were involved in the experiment, see Figure 12. The pressure sensor used with the differential spectrophone is a C.G.S. Datametrics Model 523-15 differential electronic manometer, trade named Barocel. This sensor has a full scale range of 1 torr while the associated electronics unit offers a selection of higher sensitivities down to 10⁻⁴ torr full scale. The pressure signal was processed by a lock-in amplifier, Princeton Applied Research Corporation Model 128A, which synchronously detects and integrates the pressure signal. The reference signal for the lock-in amplifier is obtained from an infrared diode-phototransistor pair mounted on the 8 Hz mechanical chopper. The laser power was monitored by a disc calorimeter, Scientech Model 3600. Because of the significant temperature dependence in the absorption coefficient for CO₂ gas samples, it was necessary to monitor continuously the temperature of the spectrophone; this was accomplished with an electronic thermometer, Stow Laboratories, Inc. Model 911 PL. The raw data which includes the integrated pressure signal, laser power, temperature, and the time of day were recorded by a United Systems Corp. Model 1267 data logger.

The most serious problem encountered in using the spectrophone for measuring small absorption is contaminants. One particular contamination problem which was encountered is discussed in Appendix A.

In order to minimize contamination problems, the instrument and its associated stainless steel vacuum system were thoroughly cleaned and out-gassed using heating tape and a Vacion pump. The gas samples were introduced using the manifold and pressure gauges shown schematically in Figure 13. This gas handling system was constructed from stainless steel fittings and bellows-sealed vacuum valves which were also systematically cleaned.

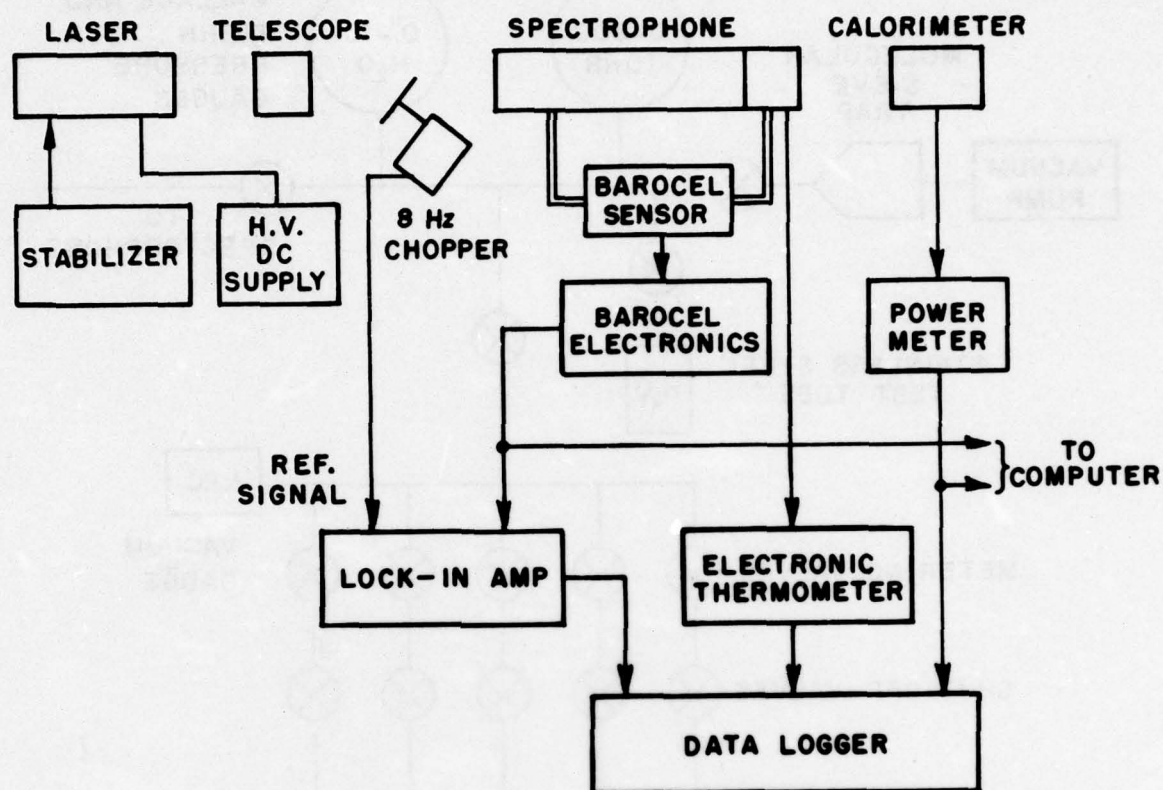


Fig. 12. Experimental design for measurement of absorption of laser radiation by gases.

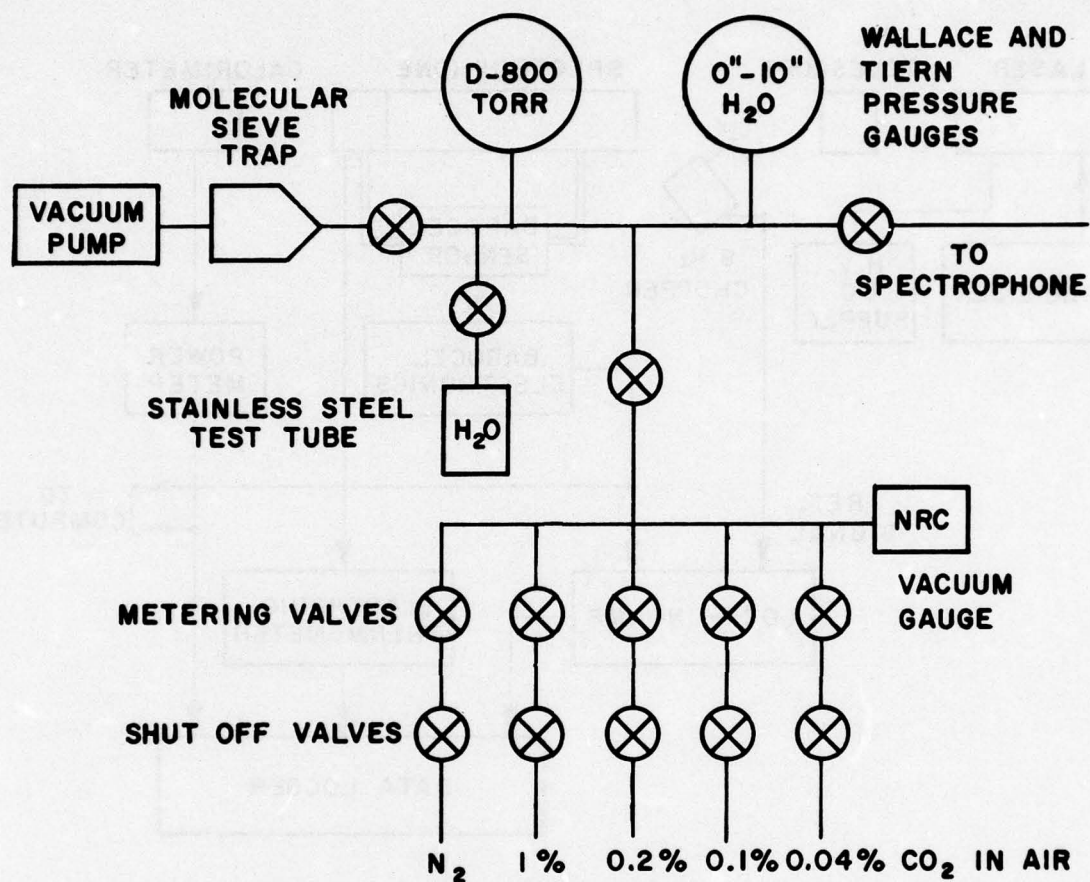


Figure 13. The gas handling system.

The CO₂ mixtures were obtained from Primary Standard gas cylinders containing 1.0%, 0.2%, 0.1% and 0.04% CO₂ in air; concentrations near 0.5%, which were also measured were obtained by mixing the 1% sample gas in equal parts with gas from .04% CO₂ cylinder.

Measurements at CO₂ concentration of .04%, 0.1%, 0.2%, 0.52% and 1% were performed on each of the nine laser lines. The results of several independent observations were consistent to within 1% for all lines at all concentrations. In particular, measurements on the 10.59 μ m P(20) line were conducted on four occasions; the first and last of which were separated by more than a week. All measurements were performed at the ambient temperature of the laboratory (\sim 24°C) which was not strictly constant. No attempt was made to account for the observed temperature fluctuations, although they were recorded by the data-logger.

A more important phenomenon associated with spectrophone measurements of CO₂ absorption is kinetic cooling³¹. The use of a spectrophone for measuring absorption depends upon the condition that the absorbed radiant energy is proportional to the temperature rise in the gas sample. A further consideration is the rate at which this energy transfer takes place. The case of CO₂ in air deserves special attention, since the absorbed energy can be initially stored in the form of internal vibration-rotation energy. This process has the initial effect of cooling the gas sample and thereby inducing a time lag in the anticipated temperature rise. This phenomena, called kinetic cooling, is especially important here where the transient response of the spectrophone is being used to obtain absorption measurements. Kinetic cooling causes the phase of the pressure signal (as determined by the lock-in amplifier relative to the 8 Hz reference signal) to be a function of the relative concentrations of CO₂ and N₂.³² A determination of the absorption coefficient requires measuring the magnitude of the total pressure signal, thus it was necessary to resolve the pressure signal into orthogonal (in-phase and quadrature) components (using the phase control of the lock-in amplifier) from which the magnitude (and phase) of the total pressure signal was determined.

Calibration of the spectrophone was based on White cell measurements of CO₂ in air on the 10.59 μ m P(20) by Mills³³. The calibration obtained from this line was assumed to be valid for all the other frequencies which were considered in this work. As a check on the internal consistency of this calibration, water vapor measurements were conducted on the R(20) line of the 10 μ m band and compared (based on the CO₂ in air calibration at 10.59 μ m) with previous White cell measurements³³. The two measurements were observed to be in very close agreement (less than 1% difference).

Results of the CO₂ measurements are given in Table I. Also tabulated here are the results of Henry³⁴, who has performed White cell measurements of CO₂ in air absorption for the P(16) line(s); where possible, a comparison between the two studies indicates agreement.

Further comparisons with the numerous $10.59\mu\text{m}$ CO_2 absorption studies³⁵ have not been attempted here because of the wide variation in the results reported (order of magnitude variations are observed) in the literature.

TABLE IV

Line	cm^{-1}	This Study km^{-1}	Henry [34] km^{-1}	% Difference
P(28)	936.800	.054		
P(26)	938.684	.060		
P(24)	940.544	.070		
P(22)	942.380	.073		
P(20)	944.190	.078		
P(18)	945.976	.078		
P(16)	947.738	.077	.076	1.3
P(14)	949.476	.074		
P(12)	951.189	.069		

Absorption Coefficients for 330 ppm CO_2 in Air at
Nine CO_2 Laser Lines.

B. Water Vapor- N_2 Samples

Data have also been obtained on several different laser lines of the 00^0_1 - 10^0_0 band of CO_2 for water vapor samples in nitrogen. The absorption of the laser radiation has been measured for water vapor pressures from 1 torr to 10 torr. Total pressure within the spectrophone was maintained at 760 torr with N_2 .

Calibration of the spectrophone was based upon long path, multiple traversal absorption cell measurements of attenuation of the P(20) CO_2 laser line at $10.591\mu\text{m}$ by CO_2 in N_2 . This calibration was discussed in the previous section.

The results obtained on the spectrophone for the absorption of CO_2 laser radiation by 5 torr and 10 torr of water vapor are presented in Table V. Also included are results from work done at JPL³⁶. The discrepancies between the two data sets are significant, and they indicate that further studies are needed. Figure 14 shows a comparison of the two data sets recorded at 10 torr partial pressure of water vapor. Agreement at the P(20) calibration point is good, but other frequencies show wide variations in the measured absorption coefficients.

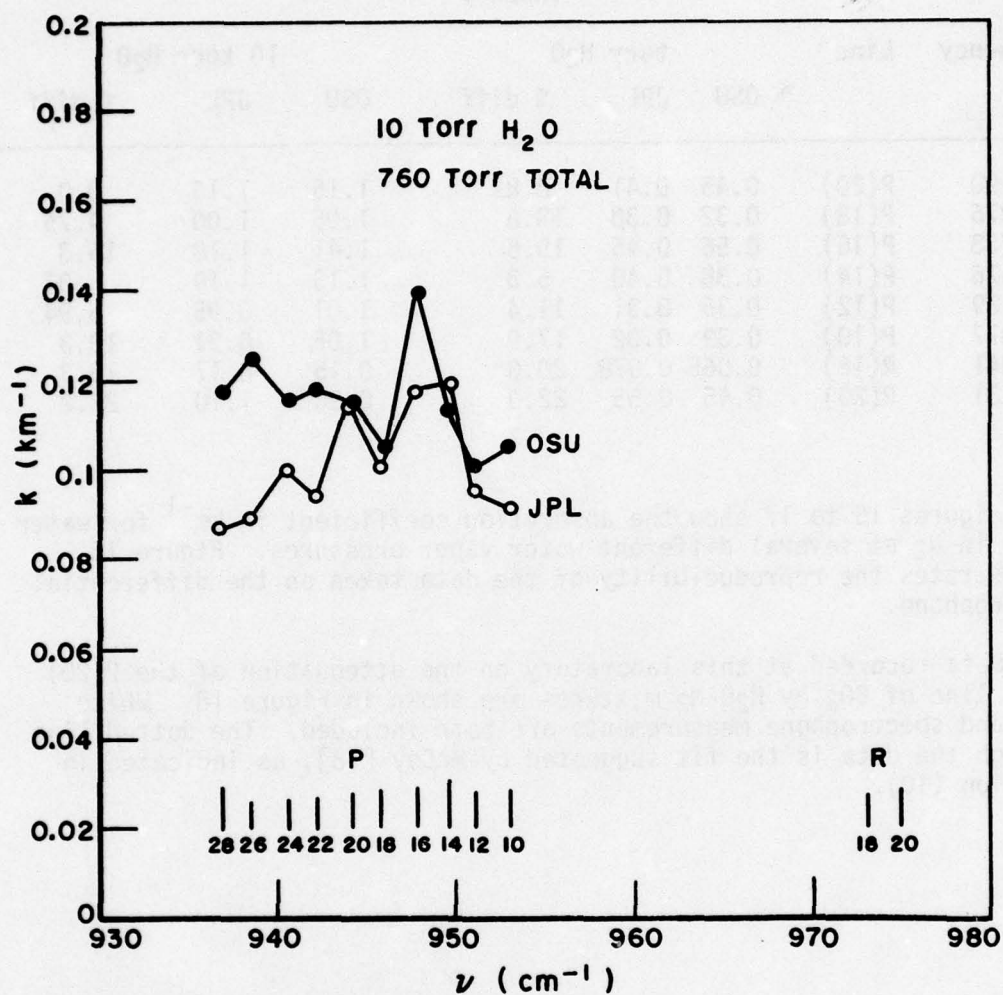


Figure 14. Comparison of data recorded at this Laboratory to the data at JPL.

TABLE V

Frequency	Line	torr H ₂ O			10 torr H ₂ O		
		OSU	JPL	% diff	OSU	JPL	% diff
944.190	P(20)	0.45	0.41	8.89	1.15	1.15	0.0
945.976	P(18)	0.32	0.38	18.8	1.05	1.00	4.76
947.738	P(16)	0.56	0.45	19.6	1.41	1.18	16.3
949.476	P(14)	0.38	0.40	5.3	1.13	1.19	.97
951.189	P(12)	0.35	0.31	11.4	1.01	0.95	5.94
956.877	P(10)	0.39	0.32	17.9	1.05	0.91	13.3
954.341	R(16)	0.065	0.078	20.0	0.15	0.17	13.3
957.131	R(20)	0.45	0.55	22.0	0.90	1.10	22.2

Figures 15 to 17 show the absorption coefficient in km^{-1} for water vapor in N_2 at several different water vapor pressures. Figure 15 demonstrates the reproducibility of the data taken on the differential spectrophone.

Data recorded at this laboratory on the attenuation of the P(20) laser line of CO_2 by $\text{H}_2\text{O}-\text{N}_2$ mixtures are shown in Figure 18. White cell and spectrophone measurements are both included. The dotted line through the data is the fit suggested by McCoy [18], as indicated in Equation (10).

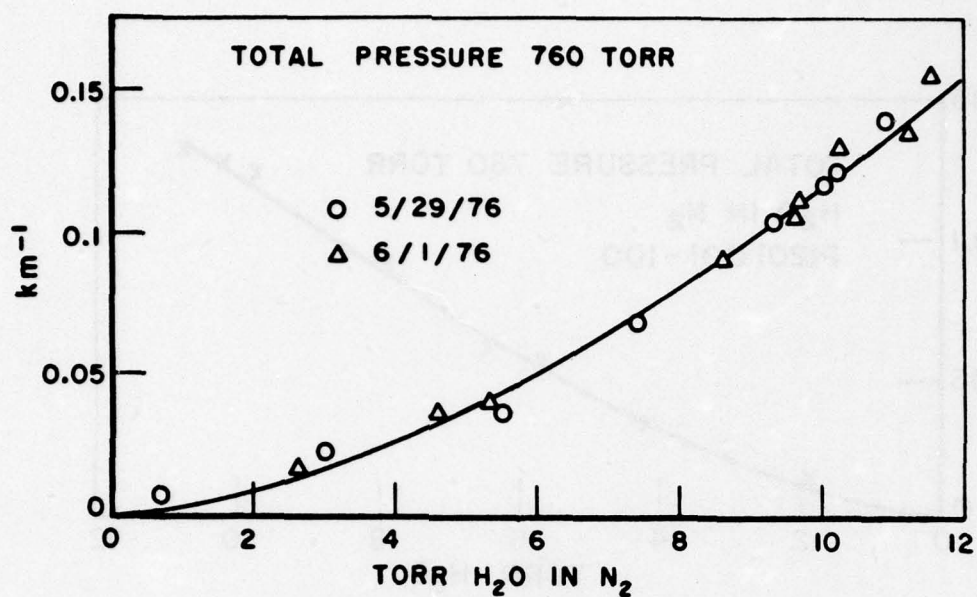


Figure 15. Water vapor absorption coefficient for CO₂ laser P(22) line at 942.380 cm^{-1} .

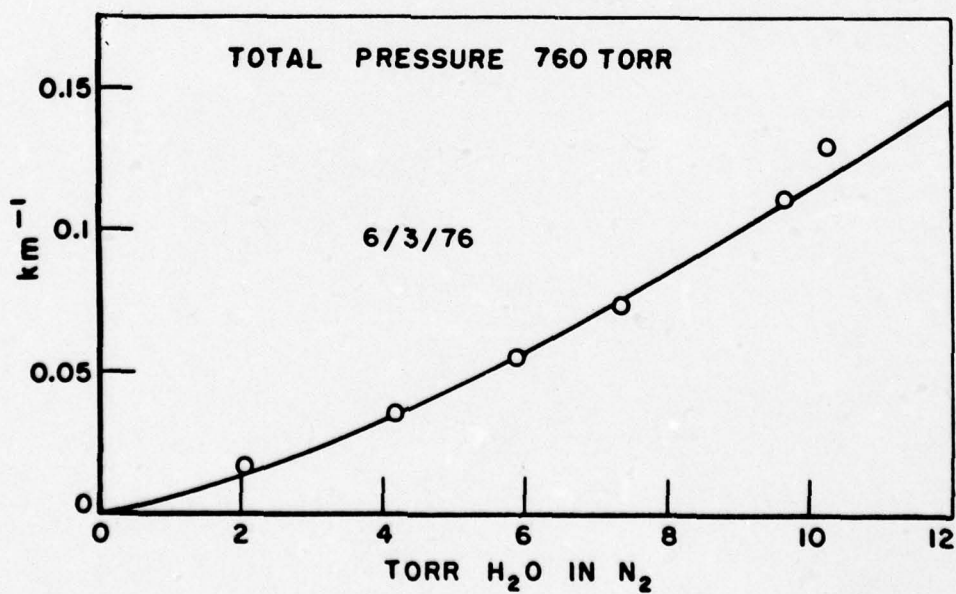


Figure 16. Water vapor absorption coefficient for CO₂ laser P(24) line at 940.544 cm^{-1} .

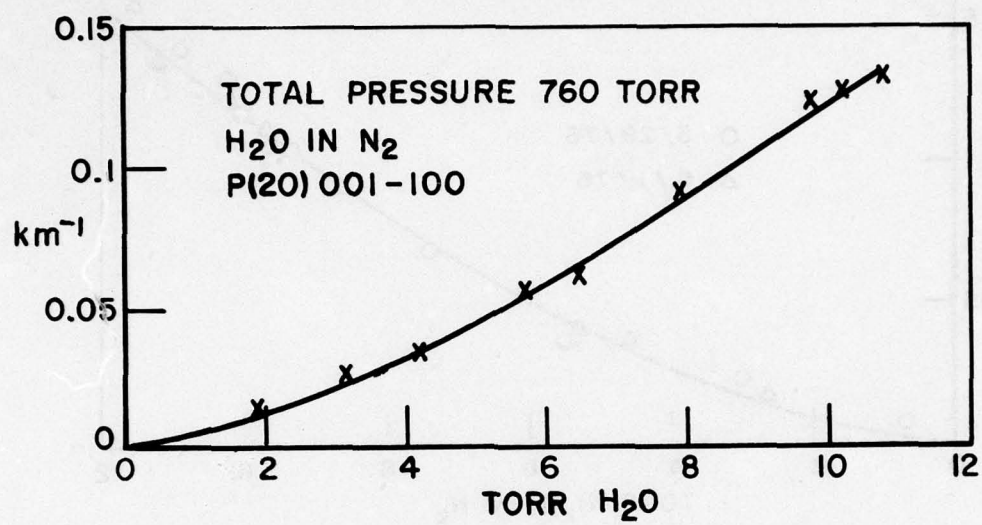


Figure 17.

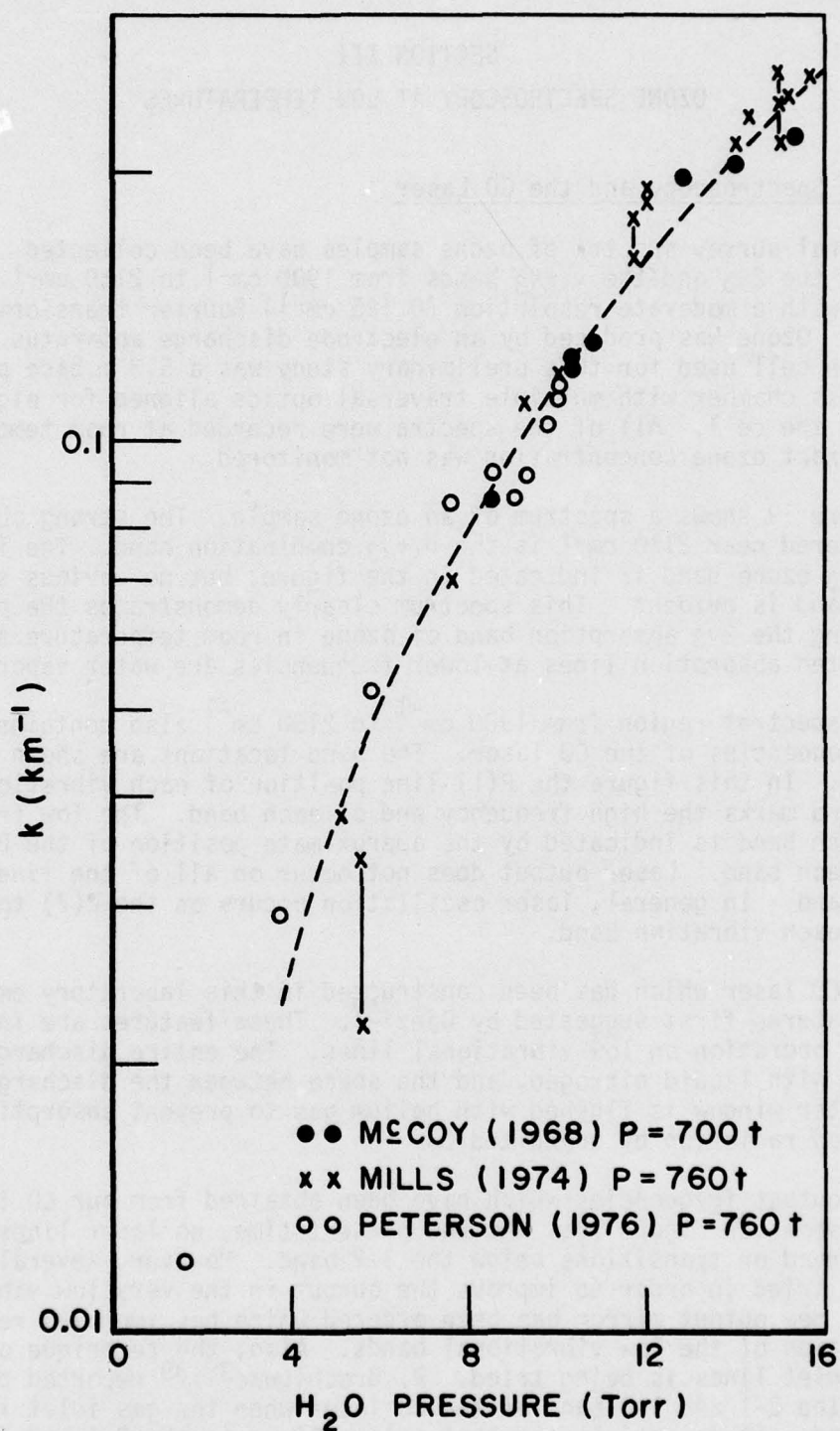


Figure 18. Comparison of White cell and spectrophone measurements made at this Laboratory.

SECTION III

OZONE SPECTROSCOPY AT LOW TEMPERATURES

A. Ozone Spectroscopy and the CO Laser

Several survey spectra of ozone samples have been collected. The region of the $2\nu_3$ and the $\nu_1+\nu_3$ bands from 1900 cm^{-1} to 2150 cm^{-1} was recorded with a moderate resolution (0.125 cm^{-1}) Fourier transform instrument. Ozone was produced by an electrode discharge apparatus. The absorption cell used for this preliminary study was a 5.3 m base path pyrex glass chamber with multiple traversal optics aligned for eight passes of the cell. All of the spectra were recorded at room temperature, and the exact ozone concentration was not monitored.

Figure 19 shows a spectrum of an ozone sample. The strong absorption band centered near 2110 cm^{-1} is the $\nu_1+\nu_3$ combination band. The location of the $2\nu_3$ ozone band is indicated in the figure, but no obvious structure of this band is evident. This spectrum clearly demonstrates the problems of studying the $2\nu_3$ absorption band of ozone in room temperature spectra. The isolated absorption lines at lower frequencies are water vapor lines.

The spectral region from 1900 cm^{-1} to 2150 cm^{-1} also contains many output frequencies of the CO laser. The band locations are shown in Figure 19. In this figure the P(1) line position of each vibration transition band marks the high frequency end of each band. The low frequency end of each band is indicated by the approximate position of the P(20) line in each band. Laser output does not occur on all of the lines within a given band. In general, laser oscillation occurs on the P(7) to P(16) lines in each vibration band.

The CO laser which has been constructed in this laboratory employs design features first suggested by Djezi³⁷. These features are intended to permit operation on low vibrational lines. The entire discharge length is cooled with liquid nitrogen, and the space between the discharge and the Brewster window is flushed with helium gas to prevent absorption of the emitted radiation by unexcited CO.

The output frequencies which have been obtained from our CO laser are also shown in Figure 19a. At the present time, no laser lines have been observed on transitions below the 3-2 band. However, several ideas are being tried in order to improve the output in the very low vibrational lines. A new output mirror has been ordered which has improved reflectance in the region of the low vibrational bands. Also, the technique of cooling the gas inlet lines is being tried. P. Brechignac^{38,39} reported observing lines in the 2-1 and 1-0 band of the CO laser when the gas inlet lines were cooled. It is anticipated that output lines in the 2-1 and 1-0 bands will be found before the temperature controlled, two meter absorption cell is ready to be used with the CO laser.

The relative power of the output frequencies currently achievable is shown in Figure 19b. The power of each line is measured relative to approximately 100 mw on the P(12) line of the 7-6 vibration band. This chart, which appeared in a previous monthly letter, is plotted with the high frequencies to the left. The rapid decrease in output in the 4-3 and 3-2 bands demonstrate that the improvements discussed above will have to be implemented before output in the low vibrational bands can be achieved.

B. Two Meter, Temperature Controlled, Stainless Steel Absorption Cell

A stainless steel absorption cell has been designed and the final assembly is nearing completion. This absorption cell will contain a multiple-traversal mirror system of the standard White design⁴⁰. The base path length of this optical system was chosen to be 2m. This length should insure good temperature uniformity along the cell, and permits the use of an immersion bath method for temperature control. The size of the cell is not too long that it cannot be portable. A set of gold coated, 2m radius-of-curvature mirrors are available for use in this chamber. With those mirrors, total path lengths in excess of 100 m can be achieved.

Stainless steel was chosen as the construction material for the absorption cell because of its excellent resistance to corrosion by ozone. Many experimenters who have worked with ozone have reported the formation of CO and CO₂ inside their cells as the ozone decays.^{41,42} In order to reduce the possible sources of carbon inside our cell, and for improved weld quality, an extra-low-carbon composition, type 316 stainless steel was chosen for the chamber and mirror mounts.

The chamber is constructed from 3/16 inch thick stainless plate rolled into a tube. An elliptical shaped end cap is welded to one end of the tube, and another elliptical cap is bolted onto the other end with stainless steel flanges. This end allows access to the inside of the chamber for positioning the mirrors. Overall length of the absorption cell is 252 cm. Figure 20a shows a drawing of the chamber.

The entire chamber will be immersed in a bath of liquid coolant. Although this cooling method requires a large amount of coolant in comparison to a wrapped coil method, the temperature bath is better suited to phase change cooling. In this process, the thermal energy removed from the chamber produces a phase change in the coolant without a corresponding temperature change (latent heat). Several coolants are being considered, and styrofoam insulation is being applied to the outside of the tank to insulate the bath-cell system down to liquid nitrogen temperature. Other possible coolants include dry ice-alcohol and dry ice-acetone slurries.

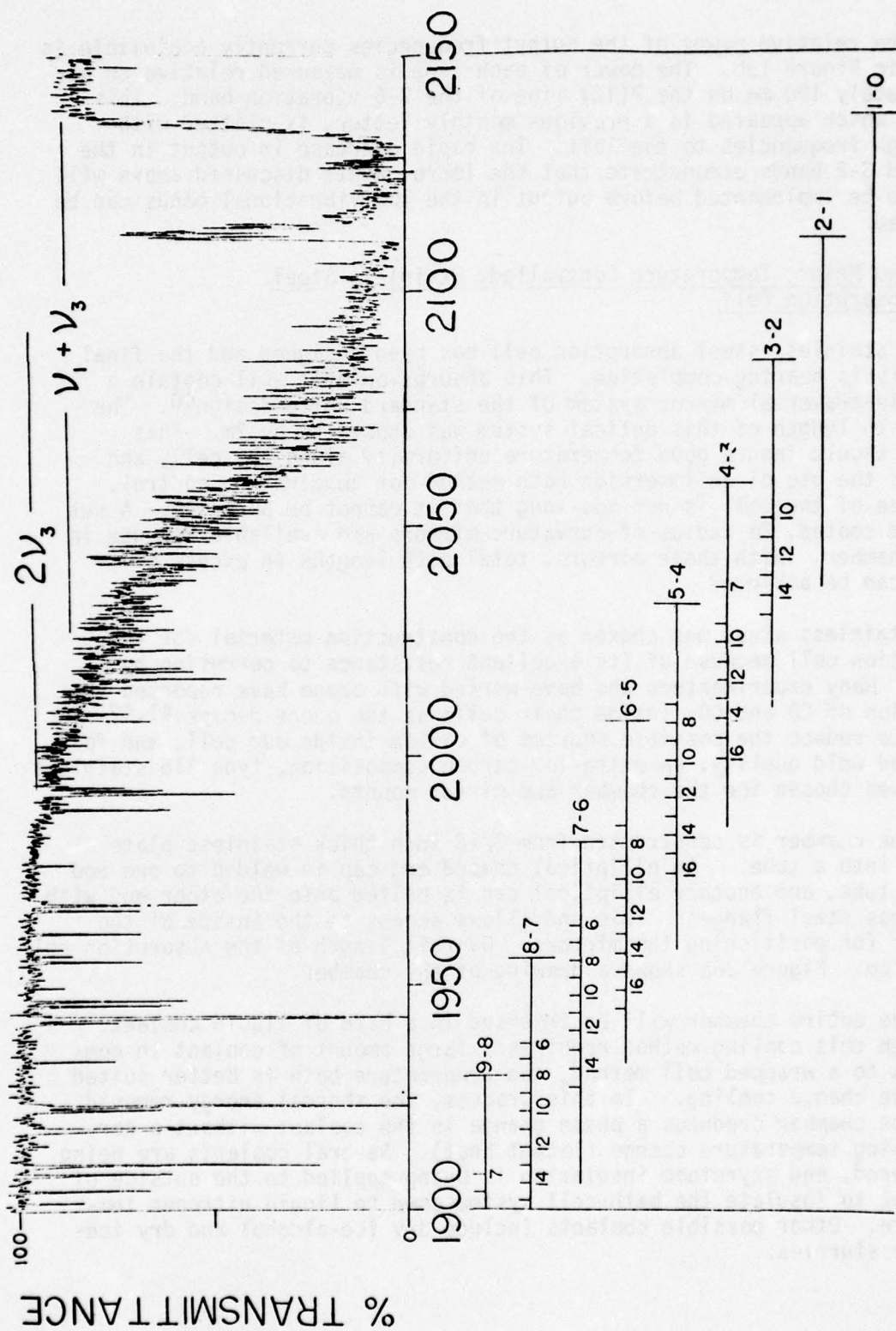


Figure 19a. Ozone spectrum in the region from 1900 cm^{-1} to 2150 cm^{-1} . CO laser lines are also shown.

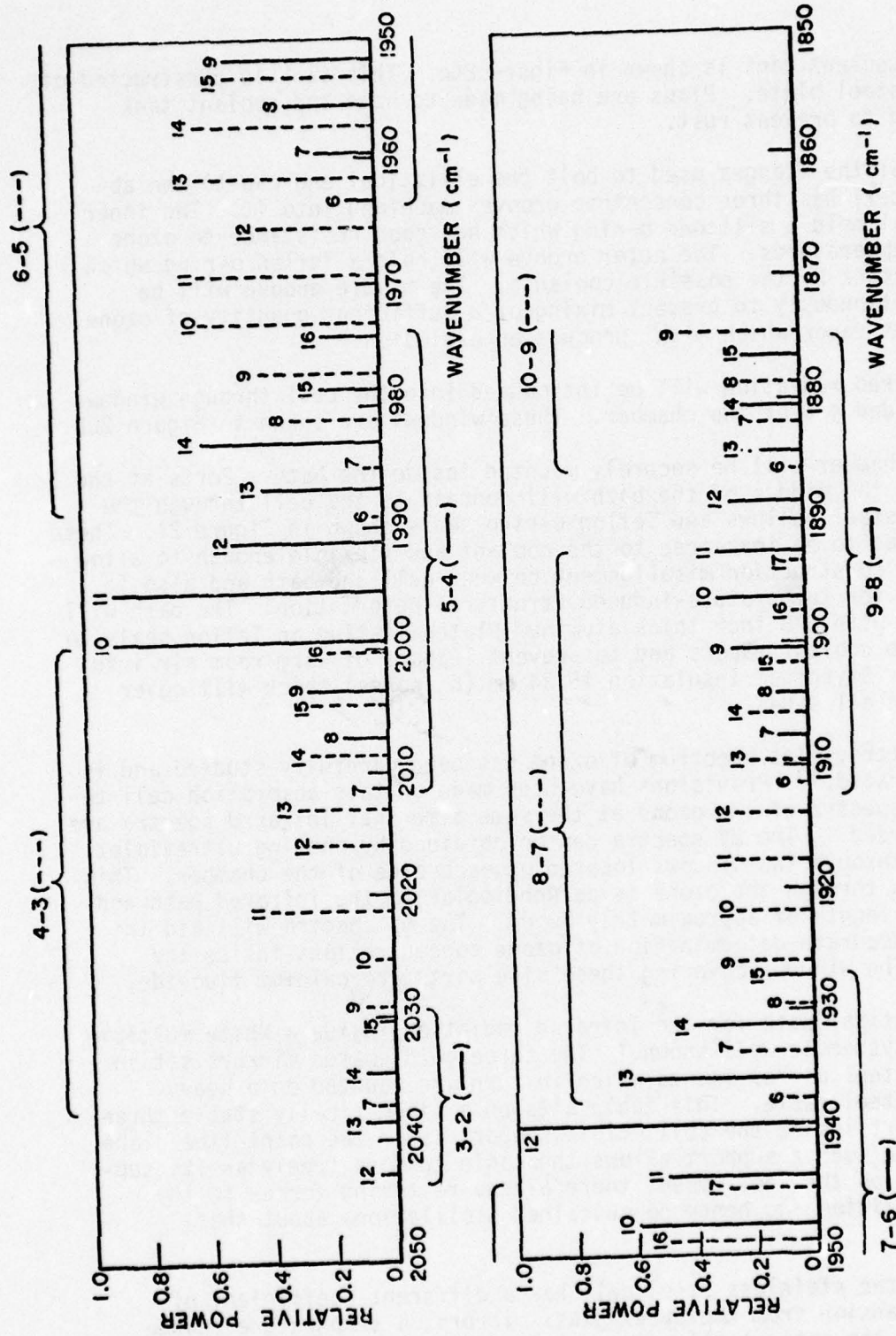


Figure 19b. Output power of CO laser relative to the 100 mw output of the P(12) line in the 7-6 band.

The coolant tank is shown in Figure 20c. This tank is constructed of 1/4 inch steel plate. Plans are being made to have the coolant tank galvanized to prevent rust.

One of the flanges used to bolt the elliptical end cap to the absorption cell has three concentric grooves machined into it. The inner groove will hold a silicone o-ring which has good resistance to ozone and low temperatures. The outer groove will hold a Teflon o-ring which resists attack by the possible coolants. The middle groove will be pumped continuously to prevent mixing of a sufficient quantity of ozone and coolant vapor which might produce an explosion.

Infrared radiation will be introduced into the cell through windows at the welded end of the chamber. These windows are shown in Figure 20b.

The chamber will be securely mounted inside the bath. Ports at the end and in the middle of the bath will connect to the cell through the stainless steel bellows and Teflon o-ring seals shown in Figure 21. These are designed to be leak-free to the coolant and flexible enough to allow for slight construction misalignment between cell and bath and also to compensate for temperature-induced structural deformation. The bath will be covered with 3/8 inch thick aluminum plates resting on Teflon seals to contain the coolant vapors and to prevent leakage of warm room air into the bath. Styrofoam insulation 15.24 cm (6 inches) thick will cover the bath on all sides.

The ultraviolet spectrum of ozone has been carefully studied and is well calibrated.⁴³ Provisions have been made on this absorption cell to record UV spectra of the ozone at the same time that infrared spectra are being recorded. The UV spectra can be obtained by passing ultraviolet radiation through two windows located on each side of the chamber. This single pass through the ozone is perpendicular to the infrared path and has a path length of approximately 70 cm. The UV spectra will aid in making an accurate determination of ozone concentrations inside the chamber. The windows covering these side ports are calcium fluoride.

The optical path for the infrared radiation inside a White multiple traversal system is well known.¹ The three gold-coated mirrors sit in stainless steel mirror mounts which in turn are mounted on a heavy stainless steel table. This table sits on a kinematically stable three point support inside the cell. This support is of the point-line-plane type. Since such a support allows the table to move freely as its support points on the cell move, there are no restoring forces to the original position and hence no sustained oscillations about that position.

Since the stainless steel cell has a different coefficient of thermal expansion from the pyrex glass mirrors, a temperature change will change the optical alignment. A temperature change of 85 K should

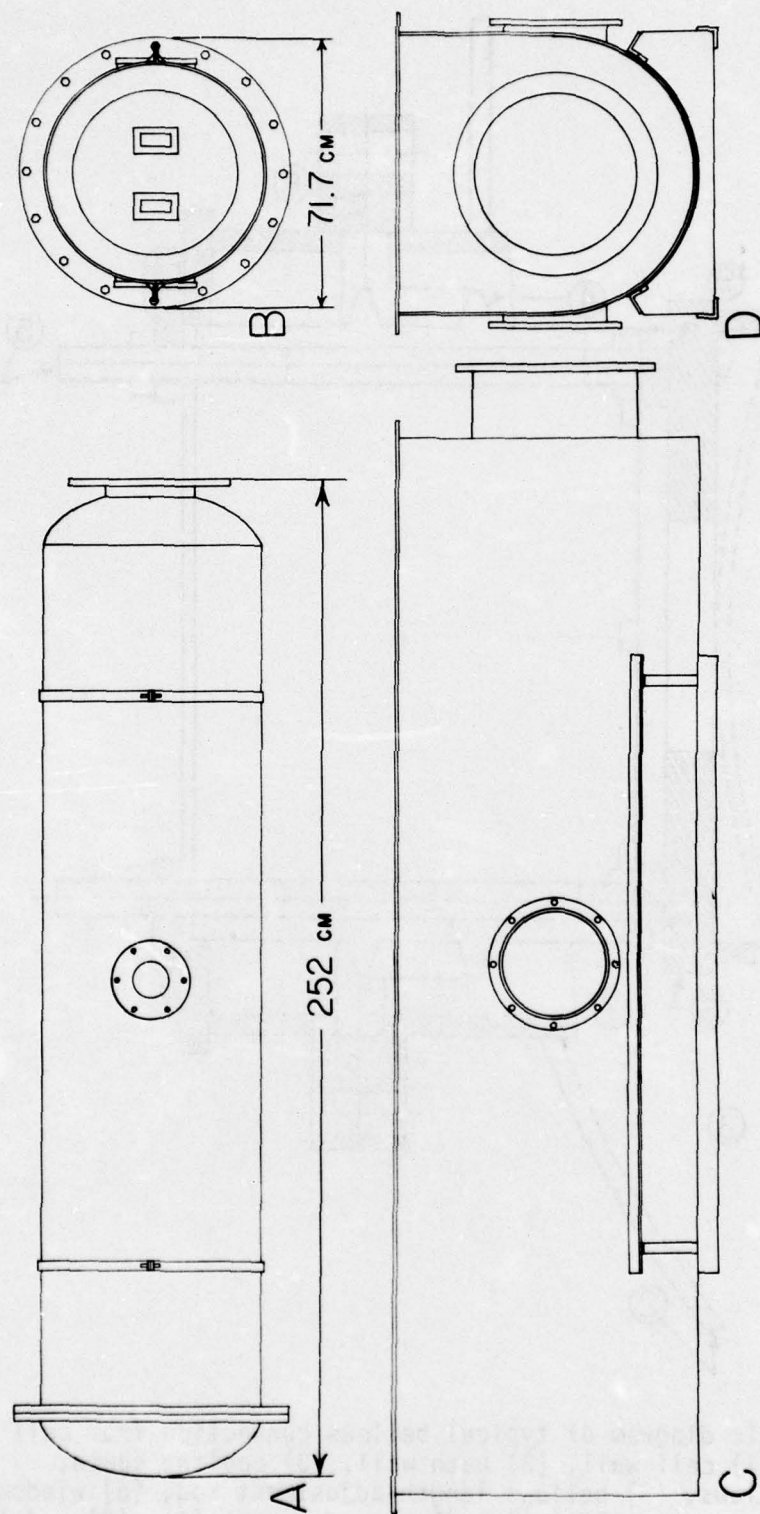


Figure 20. Schematic diagrams of the cell and bath. (A) sideview of cell showing window for ultraviolet radiation, (B) end view of cell showing windows for infrared radiation, (C) side view of bath, (D) end view of bath. Bath is shown without insulation.

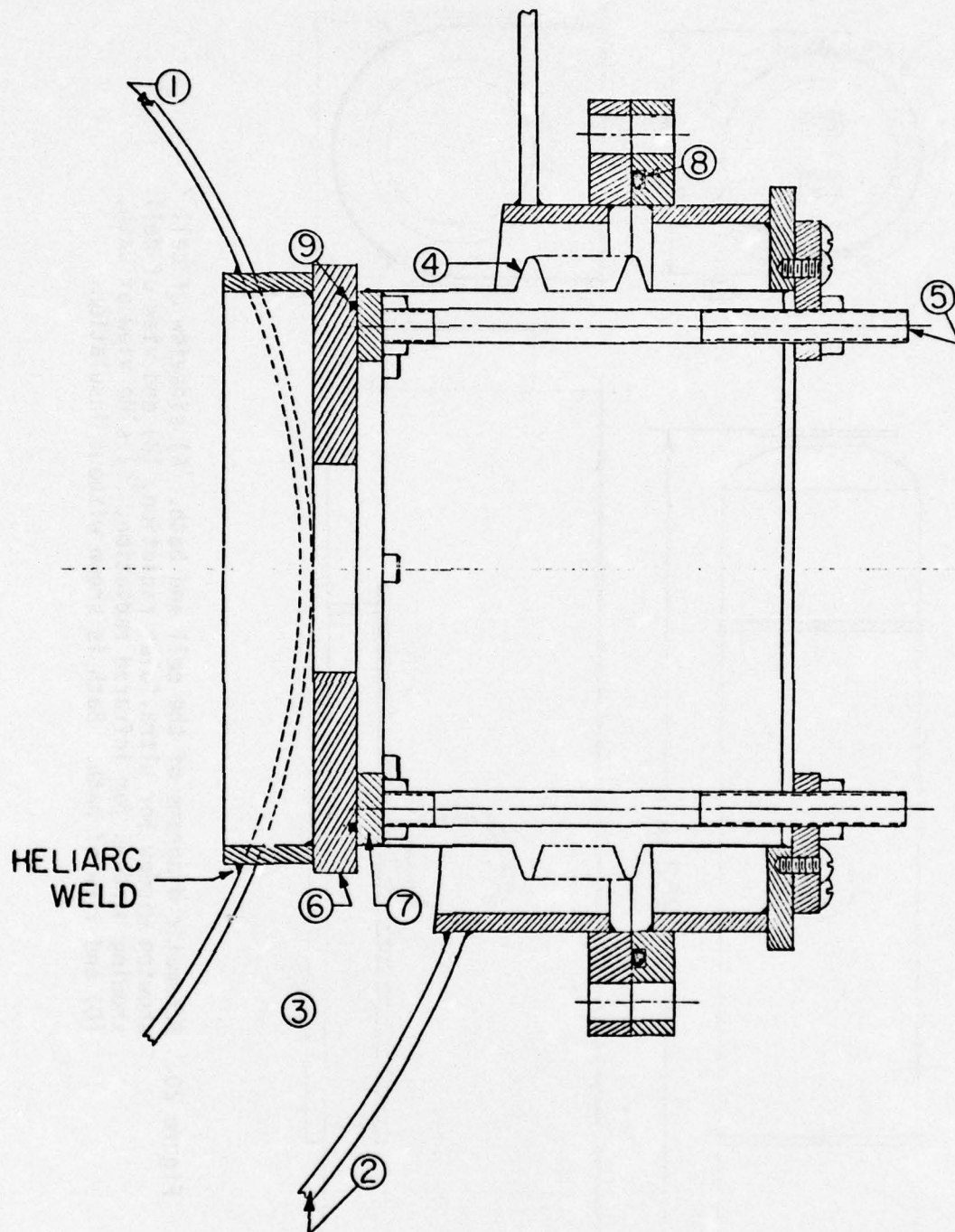


Figure 21. Schematic diagram of typical bellows connection from cell to bath. (1) cell wall, (2) bath wall, (3) coolant space, (4) bellows, (5) bellows length-adjustment rod, (6) window mounting plate, (7) mating flanges for port (6), (8) and (9), teflon o-rings.

produce a contraction of 3 mm of the cell with respect to the radius of curvature of the mirrors. In addition warping and bending of the cell can change the alignment. Provisions have been made to realign the mirrors after the cell has cooled down. This will be accomplished by feedthroughs similar to the design of Blickensderfer et al⁴⁴.

Once the absorption cell has been cooled, condensation of water vapor on the outsides of the windows will be a problem. In anticipation of this, all of the infrared input optics will be housed in a compartment which is constantly flushed with dry nitrogen.

At the present time, all of the major construction is finished. Figure 22 shows the stainless steel chamber suspended above the temperature bath. The styrofoam insulation is partially assembled for the photograph. The cloth material around the outside of the temperature bath is a woven glass impregnated with Teflon. This material was wrapped around the tank in the unlikely event that a leak developed and coolant escaped from the tank.

The cell has been positioned within the temperature bath and the bellows assemblies have been connected between the cell and the bath to make sure that all pieces fit. After the bath has been rust-proofed, the completed assembly will be moved into position next to the Ebert spectrometer.

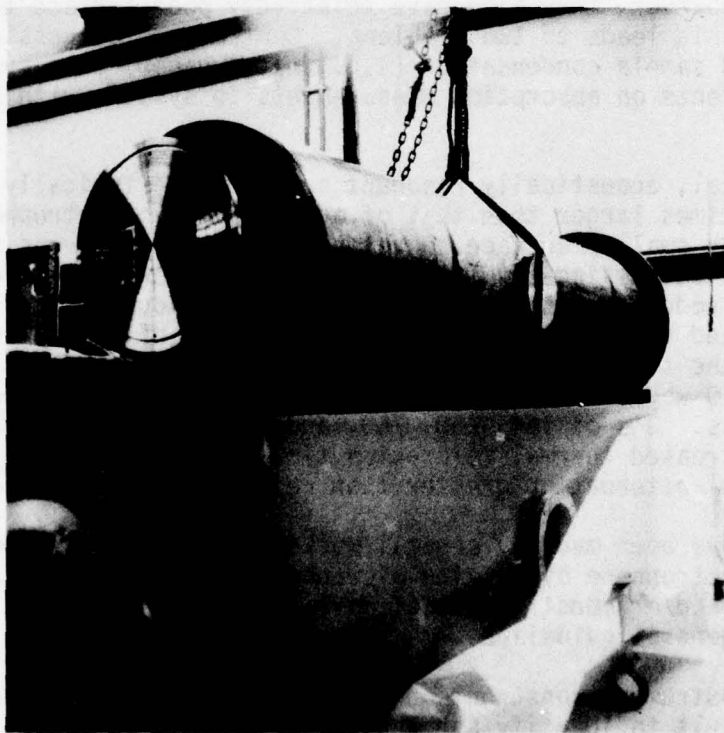


Figure 22. The 2-meter absorption cell and cooling bath.

SECTION VI

A DESIGN OF AN ACOUSTICALLY RESONANT SPECTROPHONE WITH VARIABLE DIMENSION AND CONFIGURATION

The importance of measuring atmospheric molecular absorption coefficients has been recognized for some time. Conventionally these measurements are made using multi-traversal (White) absorption cells. Trusty⁴⁵ has shown that when the transmittance is greater than 91%, an error of 1% in transmittance measurement will result in an error greater than 10% in the calculated absorption coefficient. For a transmittance greater than 99%, the corresponding error in the absorption coefficient would be greater than 100% for a 1% error in measured transmittance. Thus, for low concentrations of weak absorbers, long path lengths must be used.

In order to eliminate the above problem, a number of workers⁴⁵⁻⁵⁰ have used spectrophones with which measurements are independent of path length. Usually, spectrophones are more portable and require much smaller sample gas volumes than White cells.

Most spectrophones have been of the acoustically nonresonant type^{45,46,50}. These usually have the highest illuminated volume to non-illuminated volume ratio. However, they also have relatively poor surface to volume (S/N) ratios. This leads to two problems. Contaminant outgassing from system walls and sample condensation (e.g., water vapor) onto system walls have greater effects on absorption measurements in systems with high S/N ratios.

A cylindrical, acoustically resonant spectrophone typically has a radius several times larger than that of a nonresonant spectrophone. This results in a much smaller surface to volume ratio which reduces the problems from contaminant outgassing and sample gas condensation. The pressure responsivity is reduced in the resonant spectrophone due to the increase in non-illuminated volume, but this can be more than offset by resonant enhancement of the signal. For a resonant to nonresonant radius ratio of 10 the acoustic Q would need to be at least 100 to offset the pressure responsivity loss. Q's of 164, 200, 750, and 890 have been reported.⁴⁷⁻⁴⁹ However, the increased thermal relaxation time due to the larger radius results in signal attenuation greater than resonant enhancement.^{36,48}

Attempts have been made by several workers to optimize response of the resonant spectrophone by varying microphone placement (usually depth of penetration) and/or construction of more than one instrument. Rosengren⁴⁹ has given some general guidelines.

Multiple instrument construction is time consuming and expensive, and it is difficult to identify and analyze all of the causes of any difference in performance between the instruments. The intent here is to present a description of a resonant spectrophone designed to have a

maximum of independent parameters. This design is presently being implemented, and a schematic sketch of it is shown in Figure 23.

The resonant chamber is cylindrical and it consists of an 8" I.D. seamless pipe and 8" diameter disks as end plates which slide inside the pipe on spring loaded teflon. The end plates are secured by three threaded rods spaced 120 degrees apart at each end of the pipe. Figure 23 shows only one rod at each end to avoid cluttering the sketch. These rods are fastened by nuts to brackets which are welded to the outside of the pipe. The spectrophone has six ports. Three are in the middle of the cylinder spaced 90 degrees apart along the circumference. Two more are centered in the end plates. These five ports are identical so that the configuration of the spectrophone may be changed, which will be discussed later.

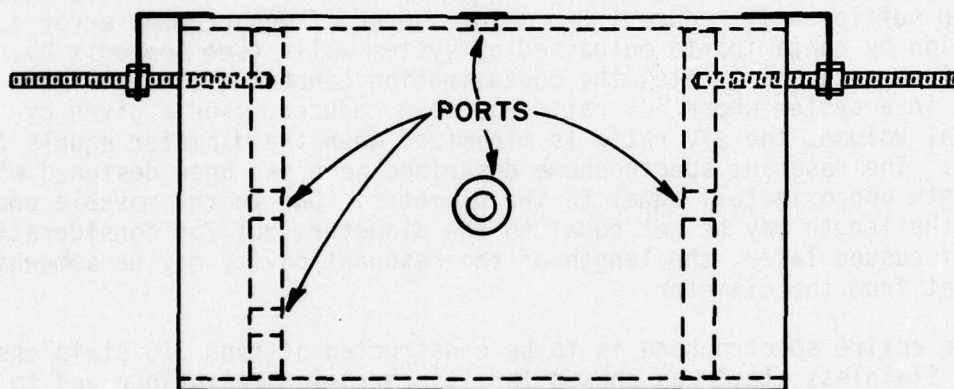


Figure 23. Design of the resonant spectrophone.

The sixth port is to be connected to a vacuum and gas handling system and is located so as to minimize any perturbation to the resonant cavity. This position is on one of the end plates and is located a distance equal to 0.6 times the radius from the center of the end plate. This position is the location of an acoustic mode for the first radial resonant mode. A seventh port similar to the sixth could be added later which would allow measurements to be made with flowing samples. This would facilitate field measurements of absorption coefficients or the determination of the presence and concentration of atmospheric absorbers or pollutants.

The major objectives guiding this design have been:

1. Low surface to volume ratio.
2. Maximum practical use of high vacuum techniques and materials.
3. Sample cell geometry as close to a right circular cylinder as practical.
4. Maximum practical configuration flexibility.

It is well known that a given cylindrical volume will be enclosed by the smallest possible surface when the diameter of the cylinder equals its length. However, for a number of reasons, the lengths of nonresonant spectrophones are much greater than their diameter. This results in a poor surface to volume ratio, but window noise (false signal due to EM absorption at the window surface) is greatly reduced. When window noise has been sufficiently reduced, the major source of measurement error is absorption by contaminants outgassed by system walls (see Appendix A). For a given outgassing rate, the contamination concentration will be lowered in a system whose S/V ratio has been reduced. For a given cylindrical volume, the S/V ratio is minimized when the diameter equals the lengths. The resonant spectrophone described here has been designed with the length approximately equal to the diameter. Due to the movable end walls, the length may be set equal to the diameter; but for considerations to be discussed later, the length of the resonant cavity may be somewhat different from the diameter.

The entire spectrophone is to be constructed of type 316 stainless steel. Stainless steel was chosen for its corrosion resistance and to minimize water vapor adsorption.^{51,52} Spectrophones have been constructed from aluminum, glass, brass, and Pyrex glass. Brass should be avoided in vacuum systems which might be subjected to temperatures greater than room temperature. This is due to the high vapor pressure of zinc.⁵¹ Pyrex and other high alkali content glasses have been found to adsorb more water than glasses with low alkali content such as quartz or fused silica.⁵³ It has also been found that Pyrex glass used in the construction of CO₂ lasers which has been cleaned and baked out still outgasses contaminants which significantly reduce CO₂ laser output.⁵⁴

Small deviations from cylindrical geometry within the spectrophone will cause perturbations to the resonant frequency and will also create coupling between acoustic modes. Therefore, efforts are being made to minimize any structural deviations from the cylindrical shape. All ports not in use will be capped with plugs that mount flush with the inner surface.

The excitation of the spectrophone can be changed by mounting windows in to two side ports which are on a common diameter, and by placing a microphone in one of the end ports. In this configuration, axial modes can be excited. The second harmonic would be efficiently coupled, and this frequency is 15% lower than the fundamental radial resonance in a spectrophone with equal length and diameter.^{47,48}

The movable end walls and several ports allow the configuration to be quite flexible. With windows in the ports on the end plates and a microphone in one of the ports on the cylindrical wall, the spectrophone will become a conventional axially excited spectrophone with radial resonance.

By moving both end plates in the same direction by the same amount, the effects of microphone placement along the length of the cavity may be studied. Varying the separation between the end plates will allow the study of the effects of changes in volume, absorption path length, and window separation. Background signals due to contaminants and the possibility of cancelling window noise by making the end plate separation equal to an odd integral number of half wavelengths of fundamental radial resonant frequency will be particularly interesting to study.

Once an optimum configuration is determined, the prototype should be suitable for making absorption measurements without compromise with respect to material of construction or configuration. Future development should also be relatively easy to incorporate.

SECTION V

WHITE CELL

The design philosophy of the new multi-pass absorption cell was documented in a previous report.⁵⁵ Briefly, the vacuum chamber is 40 feet long and 24 inches in diameter. Mirror spacing is 10.785 meters (35.4 feet) with multi-pass capability to at least one km. The system is stainless steel, and can be temperature controlled between -60°C and $+60^{\circ}\text{C}$.

The main vacuum chamber has been constructed and is in place on its air-supported mount. The optical tables are similarly mounted. Figure 24 shows the vacuum chamber mounted to the frame. External cooling connections and the temperature control system are being fabricated and installed. Components for the insulating jacket are on hand and will be installed as soon as plumbing connections are made and the system is vacuum checked. Figure 25 shows the stacking configuration for the urethane insulation.

The main optics mounts have been fabricated and are being fitted and assembled. The three main cervit mirrors have been received and will be coated in the near future. Electronics for the stepper motor optical drives have been constructed and tested, and will be integrated with the physical mounts shortly.

The support for the two-mirror and of the White optical system is shown in Figures 26a and 26b. The upper figure shows the front of the mount where the cervit mirrors will be held. The lower figure shows the back of the mount. The stepper motor assemblies are housed in leak-tight containers. One container has been removed for observation of the stepper motor and the large anti-backlash gear.

The general system plan is now well enough established that entrance optics, the sample handling system, gauging, and auxiliary systems are being designed.

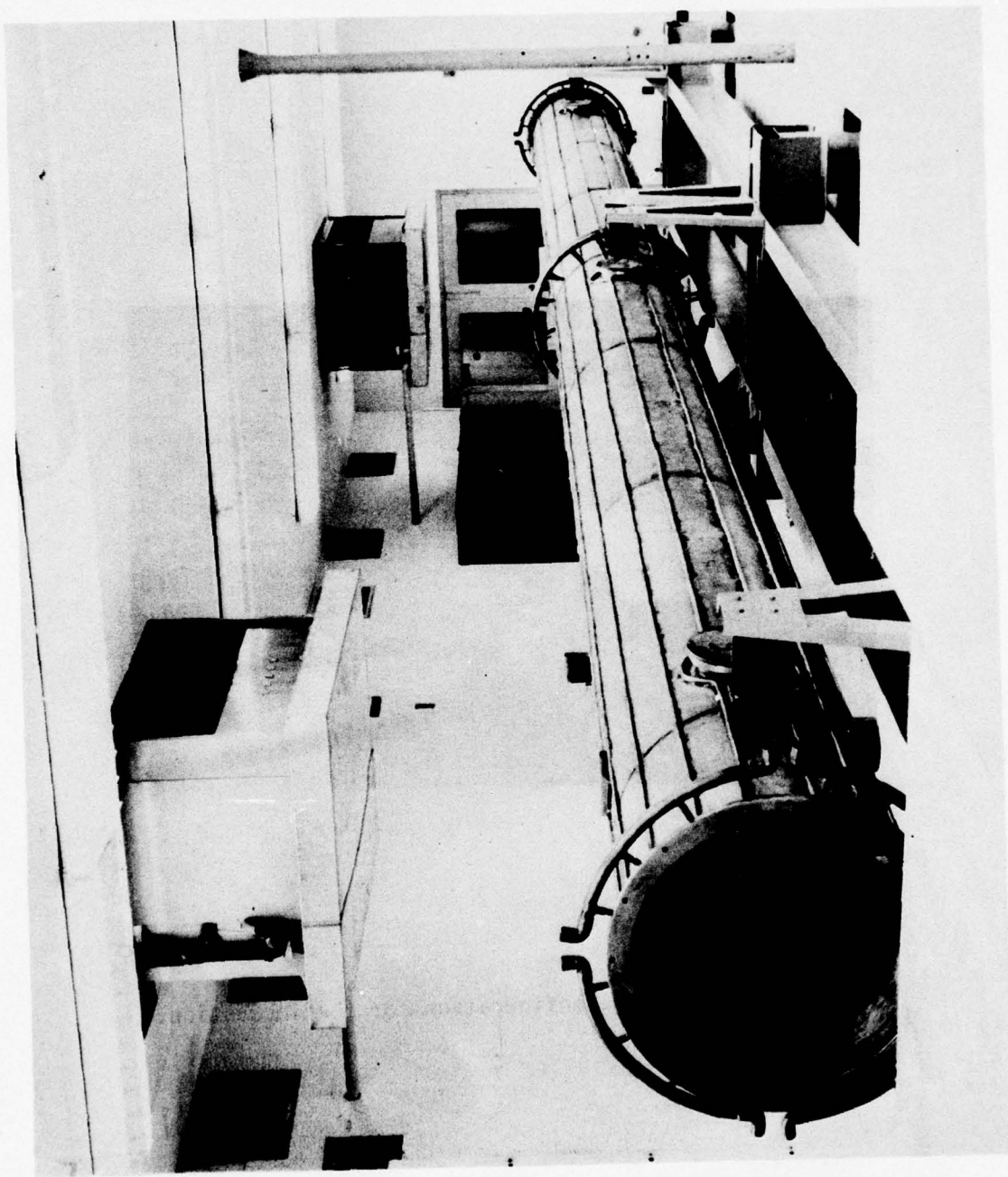


Figure 24. The 10.8 meter White cell.

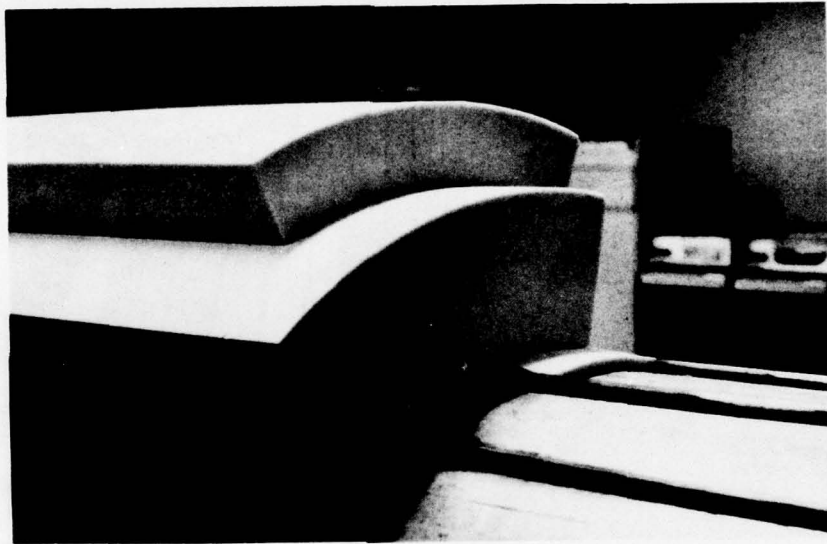


Figure 25. Stacking configuration for the insulation.

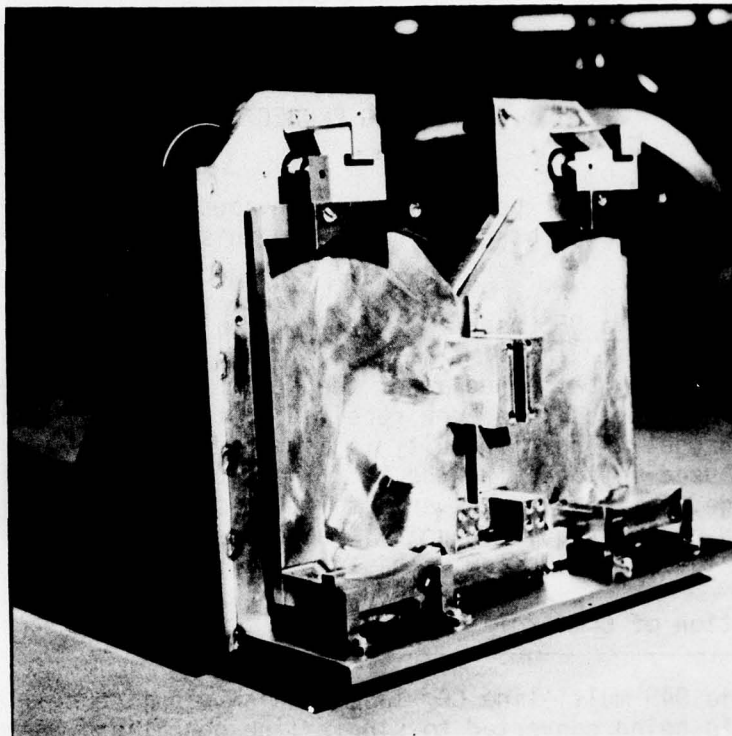


Figure 26a. Front view of the mirror mounts for the 10.8 m White cell.

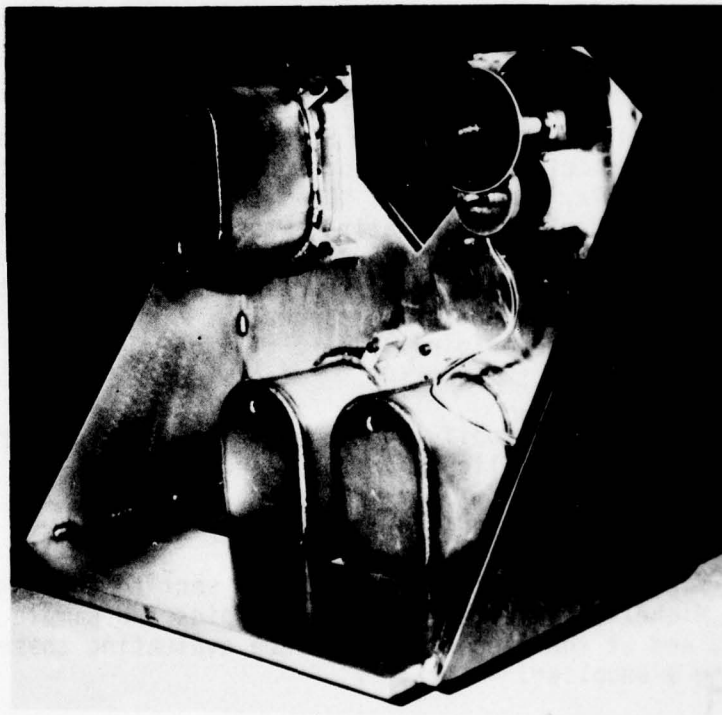


Figure 26b. Back view of the mirror mounts showing the stepper motors.

SECTION VI

CONTINUING PROJECTS

Besides the efforts reported in the previous sections, progress is being made in a number of other efforts. In this section, these are discussed.

A. Construction of a DF Laser

The cw DF laser, patterned after the design of Hinchey, is not yet operational. New optics have been received, but would not allow operation on a single channel. The difficulty is ascribed, at least partially, to the hole size used in injecting the D₂. The current holes are believed to be too large, so that the gas enters with too low a velocity to cause uniform mixing and consequent chemical reactions of a single plane transverse to the main gas flow. This problem is being corrected.

B. Modification of Commercial CO₂ Laser

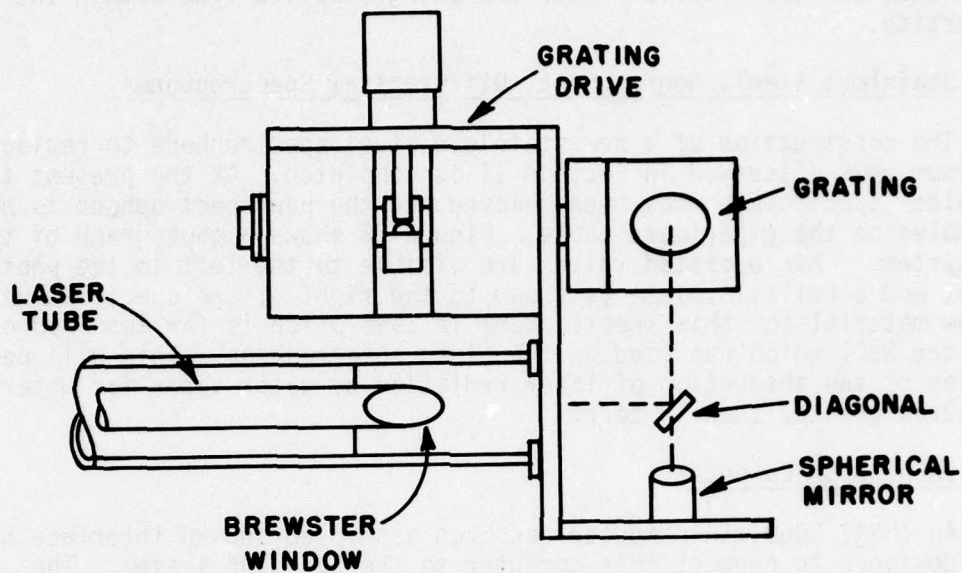
A Sylvania 948 multi-line CO₂ laser, which was made available to the program, is being converted to single-line operation. Because the output reflector on the Model 948 is flat and internal to the plasma tube, a conventional grating resonator can not be used. The existing laser used an external, totally reflecting spherical mirror on a PZT mount for cavity length control. For alignment stability, the grating optics must have a corresponding curvature.

The retrofit selected is shown in Figure 27. The diagonal mirror is used because of space restrictions on the laser mounting plate. As indicated in Figure 27a, the diagonal turns the beam in a horizontal plane. The beam is thus incident on the grating, whose axis of rotation is parallel to the tube axis. The grating is set slightly (approx. 4°) from the Littrow angle so that the diffracted beam passes just over the diagonal mirror and is incident on the spherical mirror. This mirror and PZT mount are from the original laser. The beam then retraces itself, thus double-passing the grating. A top view is shown in Figure 27b.

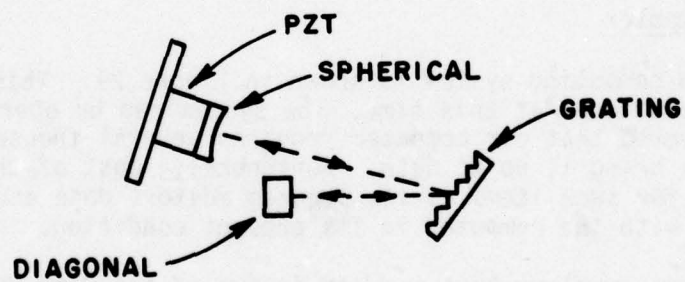
The grating mount for modifying the laser has been constructed, and is now being installed and aligned in the laser.

C. Fourier Transform Spectroscopy

Requests for quotation of price have been sent to three manufacturers of rapid-scan Michelson interferometers. The bids and sample spectra have been received, and at the present time we are evaluating these data before choosing a supplier.



(a)



(b)

Figure 27. Retrofit for line selection of the Sylvania 948 CO₂ laser.

Funds for the interferometer are being supplied from within the university.

D. Stainless Steel, Nonresonant, Differential Spectrophone

The construction of a new stainless steel spectrophone to replace the aluminum unit discussed in Section II is completed. At the present time, the older spectrophone has been removed and the new spectrophone is being assembled on the experiment table. Figure 28 shows a photograph of the new system. Air operated valves are visible to the left in the photograph, and a ballast volume is shown to the right of the spectrophone window material for this spectrophone in ZnSe which is far less hydroscopic than the NaCl which was used on the older spectrophone. This will permit studies of the absorption of laser radiation by water vapor for water vapor pressures greater than 10 torr.

E. IMSAI 8080 Computer

An IMSAI 8080 minicomputer has been assembled and an interface has been designed to connect this computer to the SEL 810B system. The primary function of the minicomputer will be as a teletype scanner for multiple user operation of the 810B facility. However, the minicomputer has the versatility to perform other data acquisition tasks. With the addition of an A/D converter, the computer can read temperature sensors associated with the 10-m absorption cell, and it can control the stepper motor mirror alignment within the cell.

F. SEL 810B Computer

The SEL 810B computing system is shown in Figure 29. This computer is being made operational at this time. The system can be operated, but it was discovered that our computer requires several thousand wiring changes to bring it up to date. Fortunately, most of the software development for such items as the program editor, data acquisition, etc. can be done with the computer in its present condition.

Minor hardware problems have occurred in two of the disc drive units, but these should not be difficult to repair. Also, a CRT display unit which is connected to the system needs software before it can be operated.

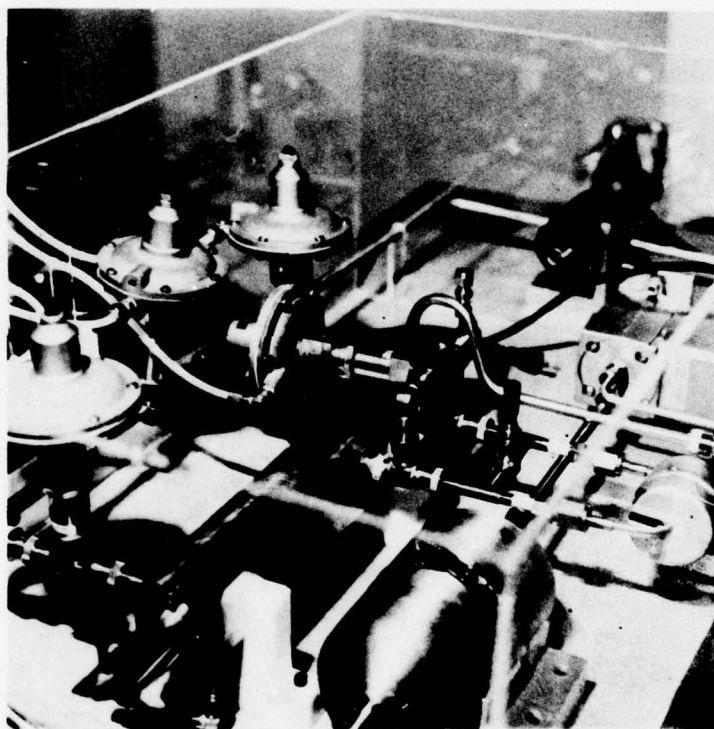


Figure 28. The new stainless steel spectrophone.

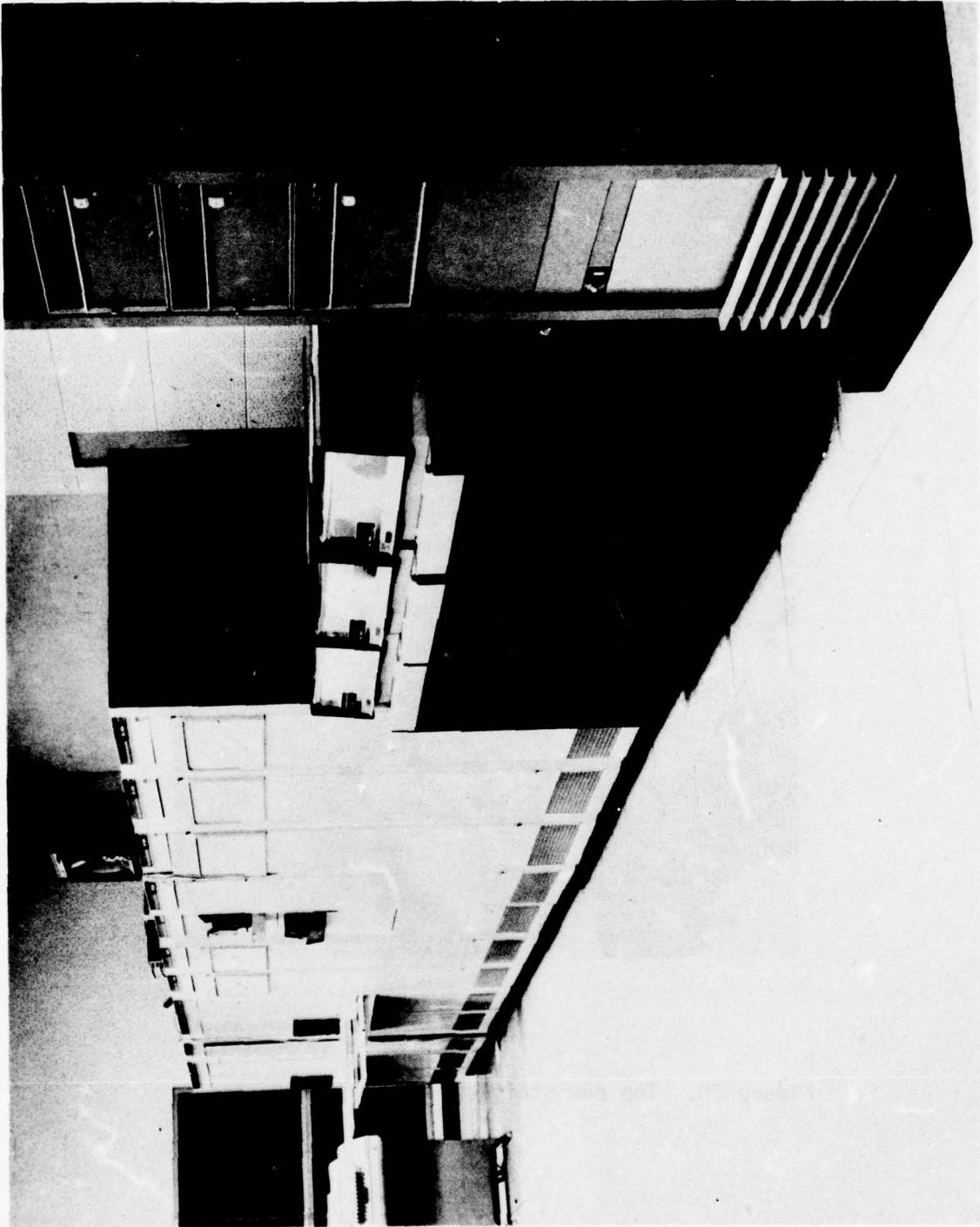


Figure 29. The SEL 810B computing system.

SECTION VII
ATTENUATION OF INFRARED RADIATION FROM CO₂
ISOTOPE LASERS BY WATER VAPOR

Lasers operating on the transitions of the isotopic variations of the carbon dioxide molecule have provided new frequencies in the infrared with which to probe the atmosphere. Isotope laser action in the 10 μ m region was first reported by Wieder and McCurdy⁵⁶ in the ¹²C ¹⁸O₂ isotope and by Jacobs and Bowers⁵⁷ in the ¹³C ¹⁶O₂ isotope. The laser transition frequencies for these isotopes as well as the ¹³C ¹⁸O₂ isotope have been measured to better than 3 MHz (0.0001 cm⁻¹) by Freed et al.⁵⁸

Recently, Buchwald et al.⁵⁹ reported the generation of laser radiation in the 16 μ m to 18 μ m region by optically pumping various isotopes of CO₂ with a pulsed HF laser. Numerous lines near 4.3 μ m were also generated.

In this report, the attenuation by water vapor of laser radiation from the isotopes of CO₂ is examined. Atmospheric conditions of 70°F (294 K) and a total pressure of 760 torr with water vapor pressures of 1, 3, 5, 10, and 15 torr were used in the calculation of absorption coefficients. The atmospheric abundance of HDO at each water vapor pressure was accounted for and included with the H₂O as an absorber.

Plots of the log of the absorption coefficient for atmospheric temperature of 70°F, a total pressure of 760 torr, and a water vapor pressure of 15 torr have been prepared. These atmospheric conditions were chosen because they correspond to the sea level conditions of the midlatitude summer model of McClatchey et al.⁶⁰

The absorption coefficients are calculated from the AFCRL Atmospheric Absorption Line Parameters Compilation.⁶¹ This listing provides the parameters necessary to compute infrared and far-infrared spectra of the permanent atmospheric gases. The accuracy of the parameters for absorption lines in the 8 μ m to 12 μ m spectral region has been studied, and it was found that CO₂ line parameters near 9.4 μ m are in error in the most recent listing.⁶² The absorption parameters of water vapor, however, produce accurate spectra in this region.

The program used to calculate the spectra from the parameters has been described previously.⁶³ In the calculations, the Lorentz line shape was used for the water vapor lines.

The isotopes of CO₂ are coded in this report according to a scheme used by McClatchey.^{60,61} The CO₂ molecule has the appearance O-C-O, and a three digit number corresponding to the last digits of the nucleon numbers of the three atoms can be used to identify the isotope. Thus the ¹⁸O-¹²C-¹⁸O isotope is coded 828, and the ¹⁸O-¹²C-¹⁶O isotope is coded 826 which is identical to 628.

Tables VI to XI list the transition frequencies for the P(30) to R(30) lines in the 10 m region of the 828, 636, and 838 isotopes. These frequencies were taken from Reference 58. Also listed in each table are the absorption coefficients in km^{-1} which were calculated from the AFCRL Line Listing at the laser frequencies. Water vapor pressures of 1, 3, 5, 10 and 15 torr were used in this calculation. No continuum absorption was included.

Figures 30 to 60 show the log of the calculated absorption coefficients for 15 torr of water vapor at 70°F (294k) with a total pressure of 760 torr. The laser line positions for each of the above isotopic variations are labeled in each figure.

Tables XII to XVI list the laser frequencies from Reference 59 for 17 m and 4.3 m output for optically pumped 828 and 628 isotopes. The spectral regions of these laser lines are plotted in Figures 61 through 71.

TABLE VI

Frequency cm ⁻¹	Line	Absorption Coefficients in km ⁻¹ for Water Vapor Pressures				
		1 torr	3 torr	5 torr	10 torr	15 torr
943.229	P(30)	1.200E-4	3.638E-4	6.126E-4	1.257E-3	1.932E-3
944.997	P(28)	1.740E-2	5.214E-2	8.683E-2	1.733E-1	2.593E-1
946.738	P(26)	6.517E-3	1.952E-2	3.247E-2	6.465E-2	9.650E-2
948.452	P(24)	1.886E-2	5.712E-2	9.613E-2	1.968E-1	3.021E-1
950.140	P(22)	2.343E-4	7.103E-4	1.196E-3	2.454E-3	3.773E-3
951.801	P(20)	1.293E-4	3.920E-4	6.602E-4	1.354E-3	2.082E-3
953.436	P(18)	1.151E-2	3.479E-2	5.840E-2	1.188E-1	1.812E-1
955.044	P(16)	4.093E-3	1.240E-2	2.085E-2	4.267E-2	6.544E-2
956.626	P(14)	1.784E-4	5.409E-4	9.108E-4	1.868E-3	2.872E-3
958.181	P(12)	1.014E-4	3.074E-4	5.176E-4	1.062E-3	1.632E-3
959.709	P(10)	5.714E-3	1.716E-2	2.863E-2	5.738E-2	8.620E-2
961.212	P(8)	8.090E-4	2.446E-3	4.107E-3	8.367E-3	1.277E-2
962.687	P(6)	7.437E-5	2.254E-4	3.796E-4	7.787E-4	1.197E-3
964.136	P(4)	6.417E-5	1.945E-4	3.276E-4	6.719E-4	1.033E-3
965.559	P(2)	5.817E-4	1.763E-3	2.967E-3	6.079E-3	9.335E-3
967.644	R(0)	2.616E-4	7.928E-4	1.335E-3	2.738E-3	4.208E-3
969.000	R(2)	1.164E-4	3.529E-4	5.942E-4	1.219E-3	1.874E-3
970.330	R(4)	7.565E-3	2.252E-2	3.724E-2	7.306E-2	1.076E-1
971.633	R(6)	8.767E-3	2.646E-2	4.436E-2	8.997E-2	1.368E-1
972.910	R(8)	7.214E-4	2.185E-3	3.676E-3	7.525E-3	1.155E-2
974.160	R(10)	4.680E-3	1.417E-2	2.383E-2	4.871E-2	7.463E-2
975.384	R(12)	9.863E-4	2.990E-3	5.034E-3	1.032E-2	1.587E-2
976.580	R(14)	1.424E-3	4.316E-3	7.267E-3	1.490E-2	2.290E-2
977.750	R(16)	2.312E-3	7.004E-3	1.179E-2	2.413E-2	3.703E-2
978.893	R(18)	7.712E-4	2.331E-3	3.913E-3	7.964E-3	1.215E-2
980.010	R(20)	1.067E-4	3.234E-4	5.446E-4	1.117E-3	1.717E-3
981.099	R(22)	4.103E-4	1.243E-3	2.092E-3	4.284E-3	6.575E-3
982.161	R(24)	3.290E-3	9.851E-3	1.638E-2	3.259E-2	4.860E-2
983.196	R(26)	1.282E-4	3.887E-4	6.544E-4	1.342E-3	2.063E-3
984.203	R(28)	8.014E-3	2.408E-2	4.021E-2	8.072E-2	1.215E-1
985.184	R(30)	8.260E-5	2.504E-4	4.216E-4	8.647E-4	1.329E-3

Calculated absorption coefficients for 5 water vapor pressures at laser frequencies of the $00^{\circ}1-[10^{\circ}0,02^{\circ}0]_1$ transitions in the 828 isotope of CO_2 .

TABLE VII

Frequency cm ⁻¹	Line	Absorption Coefficients in km ⁻¹ for Water Vapor Pressures				
		1 torr	3 torr	5 torr	10 torr	15 torr
1060.836	P(30)	6.660E-4	2.019E-3	3.399E-3	6.972E-3	1.072E-2
1062.495	P(28)	1.813E-2	5.469E-2	9.164E-2	1.856E-1	2.818E-1
1064.135	P(26)	7.621E-4	2.303E-3	3.868E-3	7.878E-3	1.203E-2
1065.756	P(24)	9.277E-3	2.812E-2	4.733E-2	9.703E-2	1.491E-1
1067.359	P(22)	1.489E-3	4.512E-3	7.598E-3	1.558E-2	2.396E-2
1068.942	P(20)	5.271E-4	1.590E-3	2.663E-3	5.395E-3	8.194E-3
1070.507	P(18)	2.088E-4	6.329E-4	1.066E-3	2.186E-3	3.360E-3
1072.052	P(16)	8.949E-4	2.708E-3	4.553E-3	9.301E-3	1.424E-2
1073.579	P(14)	1.394E-3	4.223E-3	7.107E-3	1.456E-2	2.235E-2
1075.086	P(12)	1.948E-3	5.904E-3	9.938E-3	2.037E-2	3.129E-2
1076.574	P(10)	7.485E-4	2.268E-3	3.819E-3	7.829E-3	1.203E-2
1078.042	P(8)	1.300E-4	3.940E-4	6.635E-4	1.361E-3	2.092E-3
1079.492	P(6)	1.189E-4	3.599E-4	6.054E-4	1.238E-3	1.898E-3
1080.921	P(4)	2.342E-3	6.979E-3	1.156E-2	2.274E-2	3.360E-2
1082.332	P(2)	1.376E-4	4.172E-4	7.025E-4	1.441E-3	2.215E-3
1084.411	R(0)	2.543E-4	7.707E-4	1.298E-3	2.661E-3	4.090E-3
1085.773	R(2)	1.376E-3	4.170E-3	7.017E-3	1.437E-2	2.206E-2
1087.115	R(4)	2.403E-4	7.282E-4	1.226E-3	2.513E-3	3.861E-3
1088.438	R(6)	3.613E-4	1.095E-3	1.844E-3	3.782E-3	5.815E-3
1089.741	R(8)	5.848E-4	1.773E-3	2.985E-3	6.122E-3	9.412E-3
1091.025	R(10)	2.358E-2	7.136E-2	1.200E-1	2.452E-1	3.756E-1
1092.289	R(12)	1.125E-3	3.410E-3	5.742E-3	1.178E-2	1.810E-2
1093.534	R(14)	2.758E-3	8.213E-3	1.359E-2	2.670E-2	3.938E-2
1094.759	R(16)	4.907E-4	1.476E-3	2.465E-3	4.465E-3	7.483E-3
1095.964	R(18)	2.565E-4	7.774E-4	1.309E-3	2.683E-3	4.124E-3
1097.151	R(20)	3.466E-4	1.051E-3	1.769E-3	3.629E-3	5.579E-3
1098.317	R(22)	8.656E-4	2.624E-3	4.418E-3	9.061E-3	1.393E-2
1099.465	R(24)	3.369E-2	1.018E-1	1.710E-1	3.483E-1	5.318E-1
1100.593	R(26)	3.300E-3	1.000E-2	1.684E-2	3.453E-2	5.308E-2
1101.701	R(28)	2.257E-2	6.833E-2	1.149E-1	2.349E-1	3.598E-1
1102.790	R(30)	5.073E-3	1.523E-2	2.540E-2	5.087E-2	7.643E-2

Calculated absorption coefficients for 5 water vapor pressures at laser frequencies of the $00^01-[10^00,02^00]_{11}$ transitions in the 828 isotope of CO_2 .

TABLE VIII

Frequency cm ⁻¹	Line	Absorption Coefficients in km ⁻¹ for Water Vapor Pressures				
		1 torr	3 torr	5 torr	10 torr	15 torr
887.919	P(30)	2.683E-3	8.133E-3	1.369E-2	2.808E-2	4.317E-2
889.756	P(28)	1.436E-3	4.353E-3	7.329E-3	1.503E-2	2.309E-2
891.574	P(26)	2.000E-3	6.060E-3	1.020E-2	2.091E-2	3.211E-2
893.372	P(24)	1.114E-4	3.376E-4	5.684E-4	1.166E-3	1.793E-3
895.150	P(22)	9.050E-5	2.743E-4	4.619E-4	9.474E-4	1.457E-3
896.909	P(20)	1.449E-4	4.393E-4	7.397E-4	1.517E-3	2.332E-3
898.649	P(18)	9.537E-5	2.891E-4	4.867E-4	9.982E-4	1.534E-3
900.368	P(16)	4.499E-5	1.364E-4	2.296E-4	4.711E-4	7.242E-4
902.069	P(14)	7.041E-5	2.134E-4	3.594E-4	7.371E-4	1.133E-3
903.750	P(12)	9.200E-5	2.789E-4	4.696E-4	9.634E-4	1.481E-3
905.411	P(10)	4.557E-3	1.371E-2	2.289E-2	4.603E-2	6.935E-2
907.053	P(8)	9.925E-4	3.008E-3	5.064E-3	1.038E-2	1.596E-2
908.675	P(6)	1.672E-2	5.067E-2	8.528E-2	1.747E-1	2.684E-1
910.278	P(4)	7.369E-3	2.223E-2	3.724E-2	7.545E-2	1.146E-1
911.861	P(2)	2.526E-4	7.657E-4	1.289E-3	2.645E-3	4.066E-3
914.199	R(0)	8.232E-3	2.490E-2	4.183E-2	8.532E-2	1.304E-1
915.734	R(2)	1.428E-4	4.329E-4	7.289E-4	1.495E-3	2.299E-3
917.249	R(4)	2.027E-4	6.144E-4	1.035E-3	2.122E-3	3.263E-3
918.744	R(6)	2.183E-3	6.616E-3	1.114E-2	2.282E-2	3.505E-2
920.219	R(8)	3.642E-4	1.104E-3	1.859E-3	3.814E-3	5.864E-3
921.675	R(10)	3.138E-2	9.436E-2	1.576E-1	3.169E-1	4.775E-1
923.111	R(12)	1.227E-3	3.719E-3	6.259E-3	1.282E-2	1.969E-2
924.528	R(14)	2.565E-3	7.774E-3	1.309E-2	2.683E-2	4.123E-2
925.924	R(16)	8.662E-4	2.625E-3	4.420E-3	9.063E-3	1.393E-2
927.300	R(18)	1.806E-4	5.474E-4	9.217E-4	1.891E-3	2.907E-3
928.657	R(20)	8.654E-3	2.572E-2	4.248E-2	8.307E-2	1.219E-1
929.993	R(22)	3.368E-4	1.016E-3	1.704E-3	3.455E-3	5.253E-3
931.309	R(24)	6.427E-5	1.948E-4	3.281E-4	6.729E-4	1.035E-3
932.605	R(26)	8.413E-5	2.550E-4	4.294E-4	8.805E-4	1.353E-3
933.881	R(28)	3.155E-5	9.564E-5	1.611E-4	3.304E-4	5.079E-4
935.136	R(30)	6.111E-4	1.834E-3	3.059E-3	6.124E-3	9.190E-3

Calculated absorption coefficients for 5 water vapor pressures at laser frequencies of the $00^{\circ}1-[10^{\circ}0,02^{\circ}0]_1$ transitions in the 636 isotope of CO₂.

TABLE IX

Frequency cm ⁻¹	Line	Absorption Coefficients in km ⁻¹ for Water Vapor Pressures				
		1 torr	3 torr	5 torr	10 torr	15 torr
991.071	P(30)	4.362E-5	1.322E-4	2.226E-4	4.566E-4	7.020E-4
993.042	P(28)	7.988E-5	2.412E-4	4.045E-4	8.217E-4	1.251E-3
994.986	P(26)	1.571E-4	4.760E-4	8.014E-4	1.643E-3	2.524E-3
996.901	P(24)	7.898E-5	2.394E-4	4.032E-4	8.270E-4	1.271E-3
998.788	P(22)	3.755E-2	1.116E-1	1.842E-1	3.601E-1	5.280E-1
1000.647	P(20)	1.532E-3	4.642E-3	7.813E-3	1.600E-2	2.457E-2
1002.478	P(18)	1.567E-4	4.748E-4	7.995E-4	1.640E-3	2.520E-3
1004.280	P(16)	2.948E-3	8.844E-3	1.474E-2	2.949E-2	4.424E-2
1006.053	P(14)	1.116E-4	3.378E-4	5.679E-4	1.160E-3	1.777E-3
1007.798	P(12)	3.160E-4	9.500E-4	1.587E-3	3.190E-3	4.810E-3
1009.514	P(10)	9.260E-4	2.785E-3	4.653E-3	9.367E-3	1.415E-2
1011.201	P(8)	1.390E-3	4.214E-3	7.094E-3	1.454E-2	2.242E-2
1012.859	P(6)	2.780E-4	8.428E-4	1.419E-3	2.911E-3	4.476E-3
1014.488	P(4)	1.433E-1	4.293E-1	7.144E-1	1.423E-0	2.125E-0
1016.088	P(2)	4.091E-4	1.240E-3	2.088E-3	4.280E-3	6.577E-3
1018.434	R(0)	1.502E-3	4.551E-3	7.662E-3	1.571E-2	2.414E-2
1019.961	R(2)	3.415E-4	1.035E-3	1.742E-3	3.571E-3	5.485E-3
1021.459	R(4)	3.919E-4	1.175E-3	1.957E-3	3.912E-3	5.867E-3
1022.928	R(6)	8.631E-5	2.616E-4	4.406E-4	9.036E-4	1.389E-3
1024.368	R(8)	6.957E-5	2.109E-4	3.551E-4	7.284E-4	1.120E-3
1025.778	R(10)	2.064E-4	6.254E-4	1.053E-3	2.156E-3	3.311E-3
1027.160	R(12)	3.641E-4	1.104E-3	1.859E-3	3.813E-3	5.861E-3
1028.512	R(14)	8.018E-3	2.428E-2	4.085E-2	8.360E-2	1.282E-1
1029.835	R(16)	6.730E-3	2.035E-2	3.417E-2	6.963E-2	1.063E-1
1031.129	R(18)	4.972E-4	1.507E-3	2.538E-3	5.204E-3	7.999E-3
1032.394	R(20)	1.280E-3	3.876E-3	6.518E-3	1.332E-2	2.041E-2
1033.631	R(22)	2.078E-4	6.300E-4	1.061E-3	2.176E-3	3.345E-3
1034.838	R(24)	3.273E-4	9.913E-4	1.668E-3	3.413E-3	5.235E-3
1036.017	R(26)	7.380E-5	2.237E-4	3.767E-4	7.727E-4	1.188E-3
1037.167	R(28)	1.226E-4	3.716E-4	6.256E-4	1.283E-3	1.972E-3
1038.289	R(30)	7.788E-4	2.359E-3	3.969E-3	8.126E-3	1.247E-2

Calculated absorption coefficients for 5 water vapor pressures at laser frequencies of the $00^{\circ}1-[10^{\circ}0,02^{\circ}0]_{II}$ transitions in the 636 isotope of CO_2 .

TABLE X

Frequency cm ⁻¹	Line	Absorption Coefficients in km ⁻¹ for Water Vapor Pressures				
		1 torr	3 torr	5 torr	10 torr	15 torr
905.323	P(30)	1.432E-3	4.332E-3	7.280E-3	1.485E-2	2.271E-2
907.033	P(28)	1.068E-3	3.237E-3	5.449E-3	1.117E-2	1.716E-2
908.720	P(26)	2.358E-2	7.144E-2	1.202E-1	2.462E-1	3.780E-1
910.384	P(24)	1.981E-2	5.909E-2	9.792E-2	1.931E-1	2.855E-1
912.026	P(22)	2.750E-4	8.334E-4	1.403E-3	2.876E-3	4.419E-3
913.644	P(20)	1.039E-3	3.145E-3	5.291E-3	1.082E-2	1.660E-2
915.241	P(18)	1.956E-4	5.930E-4	9.985E-4	2.048E-3	3.149E-3
916.815	P(16)	2.593E-4	7.833E-4	1.314E-3	2.672E-3	4.073E-3
918.366	P(14)	1.517E-2	4.586E-2	7.698E-2	1.567E-1	2.390E-1
919.894	P(12)	3.134E-4	9.501E-4	1.600E-3	3.282E-3	5.046E-3
921.401	P(10)	3.314E-3	1.004E-2	1.690E-2	3.464E-2	5.322E-2
922.884	P(8)	1.917E-3	5.807E-3	9.770E-3	2.000E-2	3.069E-2
924.345	P(6)	1.443E-3	4.375E-3	7.366E-3	1.510E-2	2.322E-2
925.784	P(4)	1.291E-3	3.913E-3	6.588E-3	1.350E-2	2.074E-2
927.200	P(2)	1.884E-4	5.710E-4	9.615E-4	1.972E-3	3.033E-3
929.282	R(0)	1.326E-3	4.015E-3	6.755E-3	1.382E-2	2.120E-2
930.642	R(2)	2.356E-4	7.122E-4	1.196E-3	2.434E-3	3.714E-3
931.978	R(4)	2.681E-4	8.094E-4	1.357E-3	2.757E-3	4.196E-3
933.295	R(6)	3.527E-5	1.069E-4	1.801E-4	3.694E-4	5.679E-4
934.587	R(8)	4.244E-5	1.286E-4	2.166E-4	4.442E-4	6.828E-4
935.856	R(10)	3.849E-5	1.167E-4	1.965E-4	4.030E-4	6.196E-4
937.103	R(12)	2.001E-4	6.062E-4	1.021E-3	2.092E-3	3.213E-3
938.327	R(14)	9.330E-5	2.828E-4	4.761E-4	9.763E-4	1.501E-3
939.528	R(16)	1.411E-4	4.267E-4	7.167E-4	1.461E-3	2.232E-3
940.707	R(18)	3.867E-4	1.172E-3	1.973E-3	4.047E-3	6.220E-3
941.862	R(20)	2.336E-4	7.081E-4	1.192E-3	2.445E-3	3.759E-3
942.995	R(22)	1.044E-4	3.163E-4	5.327E-4	1.093E-3	1.680E-3
944.104	R(24)	4.796E-4	1.453E-3	2.446E-3	5.010E-3	7.693E-3
945.190	R(26)	1.460E-3	4.423E-3	7.445E-3	1.526E-2	2.343E-2
946.253	R(28)	4.559E-4	1.382E-3	2.326E-3	4.770E-3	7.329E-3
947.292	R(30)	9.105E-4	2.760E-3	4.648E-3	9.532E-3	1.465E-2

Calculated absorption coefficients for 5 water vapor pressures at laser frequencies of the $00^{\circ}1-[10^{\circ}0,02^{\circ}0]_1$ transitions in the 838 isotope of CO_2 .

TABLE XI

Frequency cm ⁻¹	Line	Absorption Coefficients in km ⁻¹ for Water Vapor Pressures				
		1 torr	3 torr	5 torr	10 torr	15 torr
1003.802	P(30)	5.596E-3	1.690E-2	2.836E-2	5.765E-2	8.782E-2
1005.487	P(28)	1.249E-4	3.786E-4	6.373E-4	1.306E-3	2.006E-3
1007.153	P(26)	2.381E-3	7.170E-3	1.199E-2	2.419E-2	3.657E-2
1008.798	P(24)	1.826E-4	5.534E-4	9.318E-4	1.911E-3	2.938E-3
1010.422	P(22)	2.239E-3	6.786E-3	1.142E-2	2.342E-2	3.598E-2
1012.025	P(20)	2.609E-4	7.910E-4	1.332E-3	2.732E-3	4.356E-3
1013.608	P(18)	7.486E-4	2.269E-3	3.821E-3	7.836E-3	1.205E-2
1015.170	P(16)	1.022E-3	3.098E-3	5.217E-3	1.070E-2	1.645E-2
1016.711	P(14)	7.236E-4	2.189E-3	3.679E-3	7.512E-3	1.150E-2
1018.231	P(12)	3.403E-3	1.031E-2	1.735E-2	3.555E-2	5.458E-2
1019.730	P(10)	1.579E-3	4.769E-3	8.001E-3	1.626E-2	2.476E-2
1021.208	P(8)	1.379E-4	4.180E-4	7.039E-4	1.444E-3	2.219E-3
1022.664	P(6)	1.148E-4	3.481E-4	5.861E-4	1.202E-3	1.848E-3
1024.100	P(4)	6.587E-5	1.997E-4	3.362E-4	6.897E-4	1.060E-3
1025.514	P(2)	1.059E-4	3.211E-4	5.407E-4	1.109E-3	1.705E-3
1027.595	R(0)	1.253E-3	3.777E-3	6.326E-3	1.280E-2	1.943E-2
1028.956	R(2)	2.605E-3	7.895E-3	1.329E-2	2.725E-2	4.187E-2
1030.295	R(4)	1.620E-3	4.908E-3	8.261E-3	1.693E-2	2.601E-2
1031.613	R(6)	4.247E-4	1.287E-3	2.167E-3	4.444E-3	6.830E-3
1032.910	R(8)	2.748E-3	8.361E-3	1.398E-2	2.854E-2	4.368E-2
1034.186	R(10)	1.131E-4	3.429E-4	5.774E-4	1.184E-3	1.821E-3
1035.440	R(12)	1.599E-4	4.846E-4	8.158E-4	1.672E-3	2.569E-3
1036.673	R(14)	9.034E-5	2.738E-4	4.611E-4	9.456E-4	1.454E-3
1037.884	R(16)	1.131E-3	3.422E-3	5.754E-3	1.176E-2	1.801E-2
1039.074	R(18)	1.143E-3	3.464E-3	5.931E-3	1.195E-2	1.835E-2
1040.243	R(20)	3.695E-4	1.120E-3	1.886E-3	3.867E-3	5.944E-3
1041.391	R(22)	1.751E-4	5.302E-4	8.921E-4	1.826E-3	2.801E-3
1042.518	R(24)	5.518E-2	1.653E-1	2.751E-1	5.479E-1	8.180E-1
1043.623	R(26)	1.183E-4	3.585E-4	6.037E-4	1.238E-3	1.904E-3
1044.708	R(28)	8.123E-5	2.462E-4	4.146E-4	8.504E-4	1.307E-3
1045.771	R(30)	1.023E-4	3.088E-4	5.176E-4	1.050E-3	1.597E-3

Calculated absorption coefficients for 5 water vapor pressures at laser frequencies of the $00^{\circ}1-[10^{\circ}0,02^{\circ}0]_{II}$ transitions in the 838 isotope of CO₂.

ABSORBERS: WATER VAPOR
 AMOUNT (TCRA): 15
 TEMP (DEG F): 70.0
 CARBON-12, OXYGEN-18
 09/02/76
 TOTAL PRESSURE (TORR): 760.0

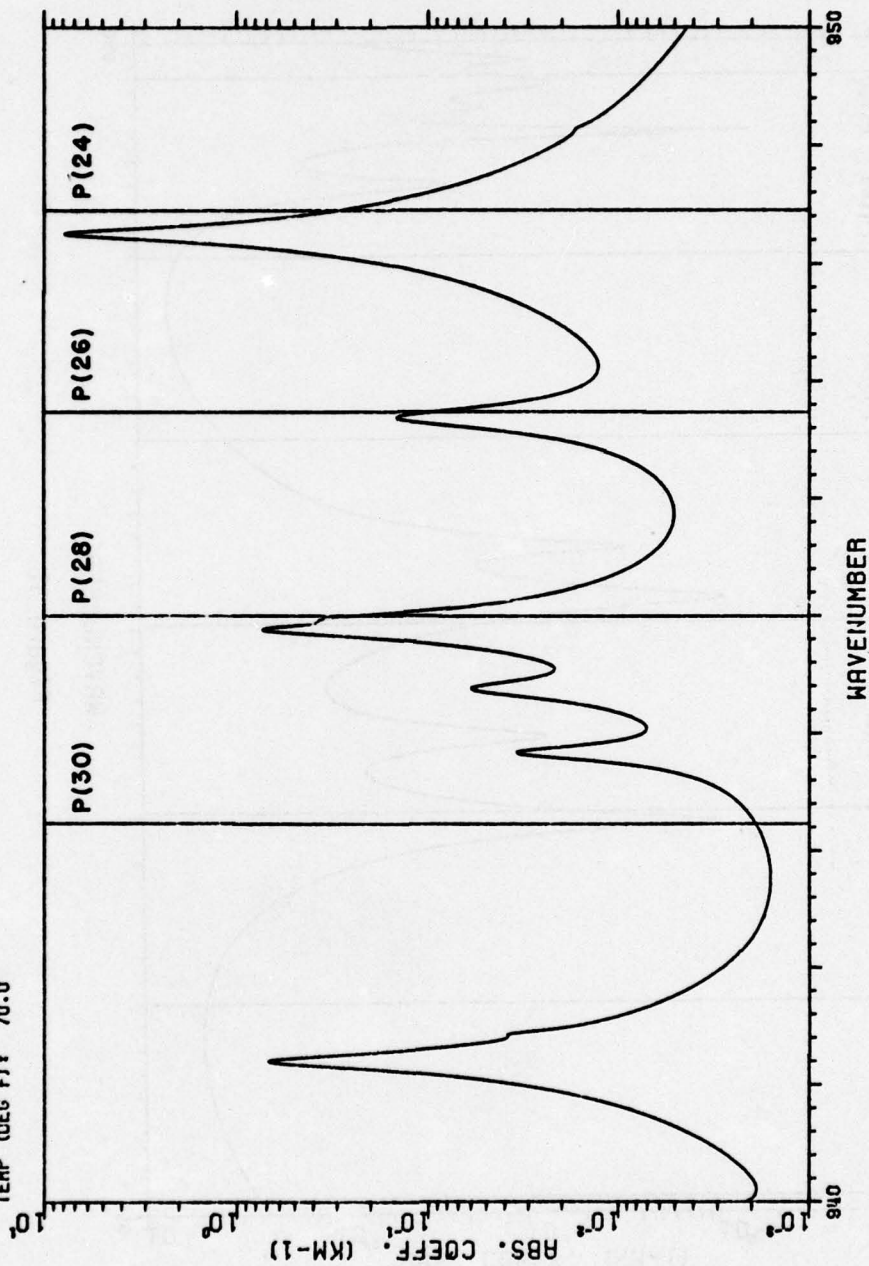
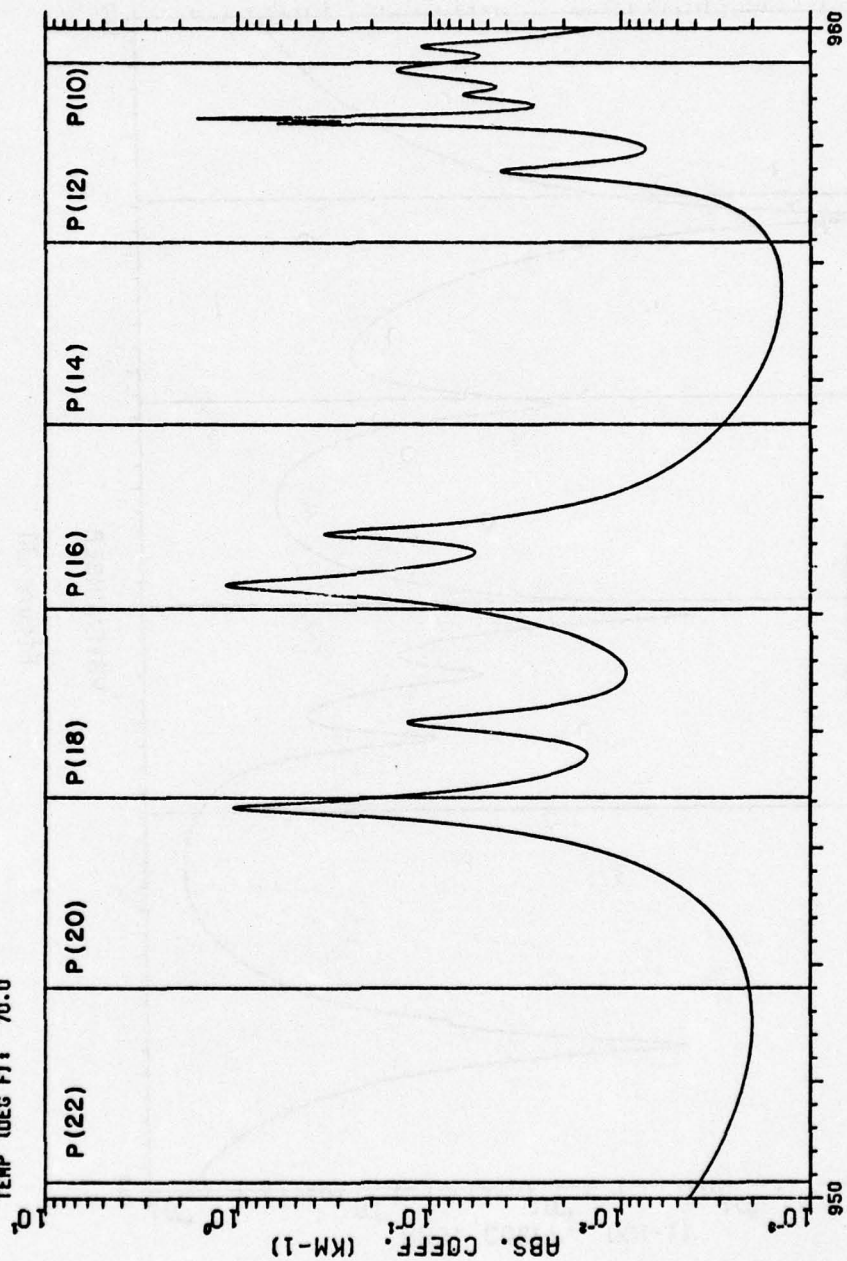


Figure 30

09/02/76
TOTAL PRESSURE (TORR) : 760.0

CARBON-12, OXYGEN-18

ABSORBERS: WATER VAPOR
AMOUNT (TORR) : 15
TEMP (DEG F) : 70.0



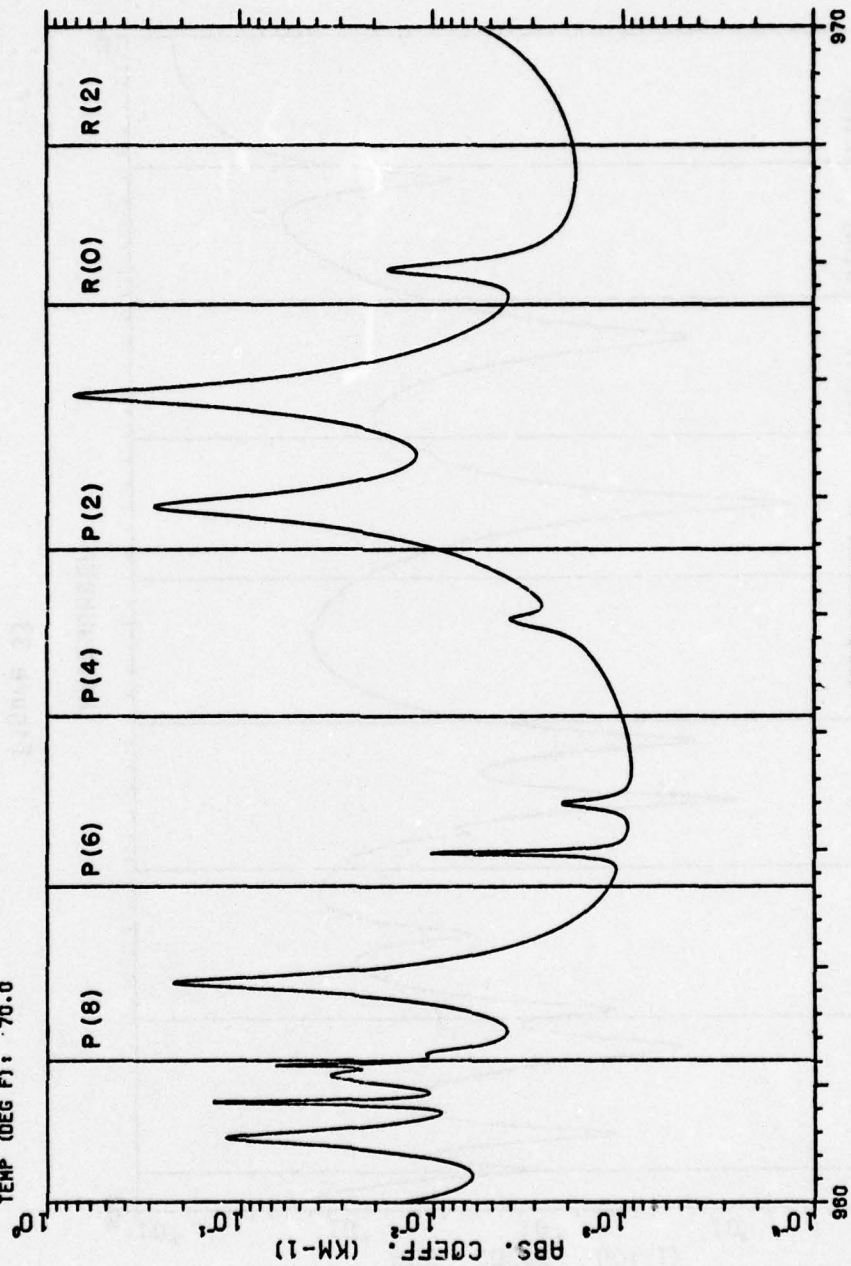
WAVENUMBER

Figure 31

09/02/76
TOTAL PRESSURE (TORR) : 780.0

CARBON-12.OXYGEN-18

ABSORBERS: WATER VAPOR
AMOUNT (TORR) : 15
TEMP (DEG F) : 70.0



WAVENUMBER

Figure 32

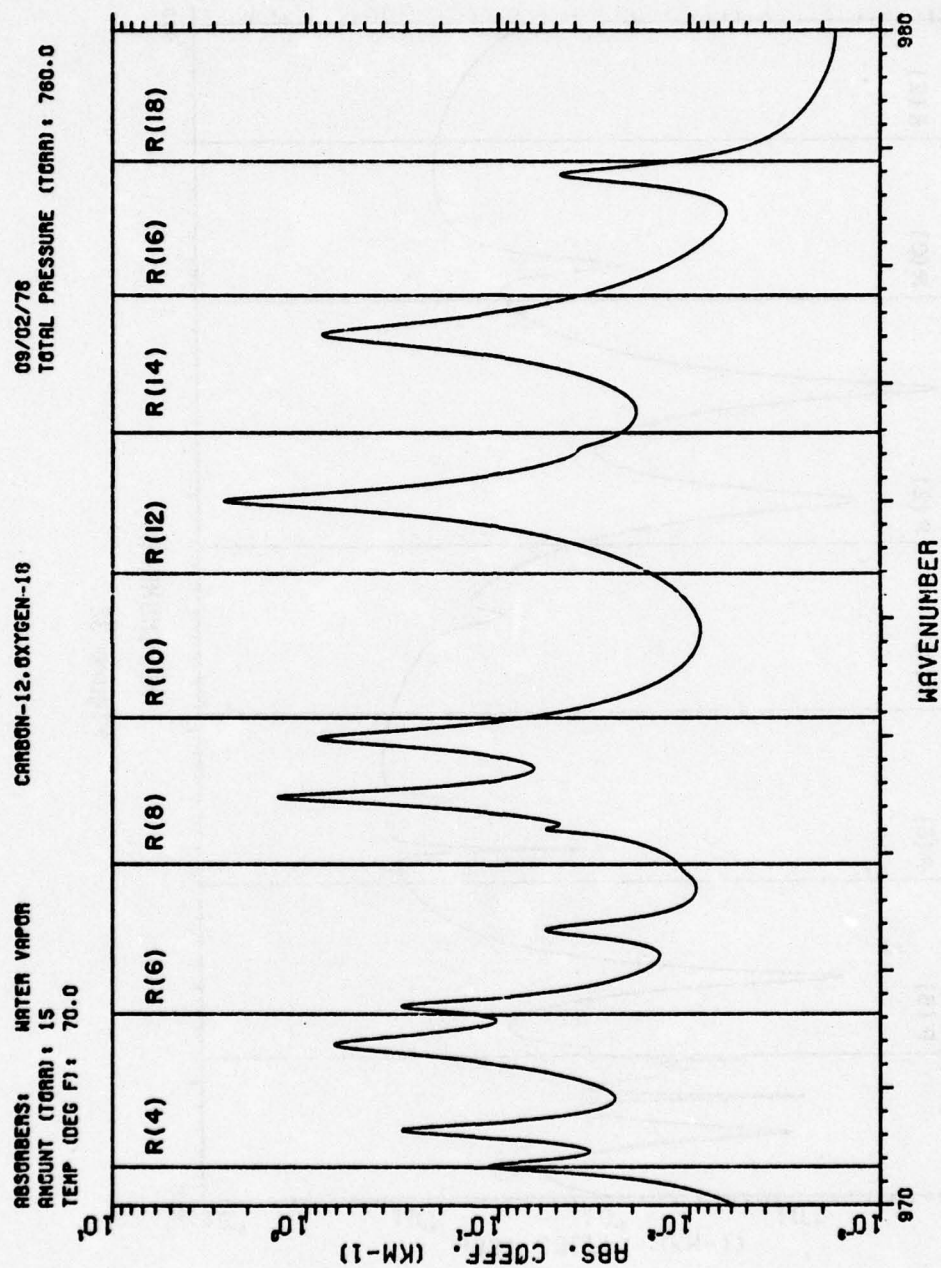


Figure 33

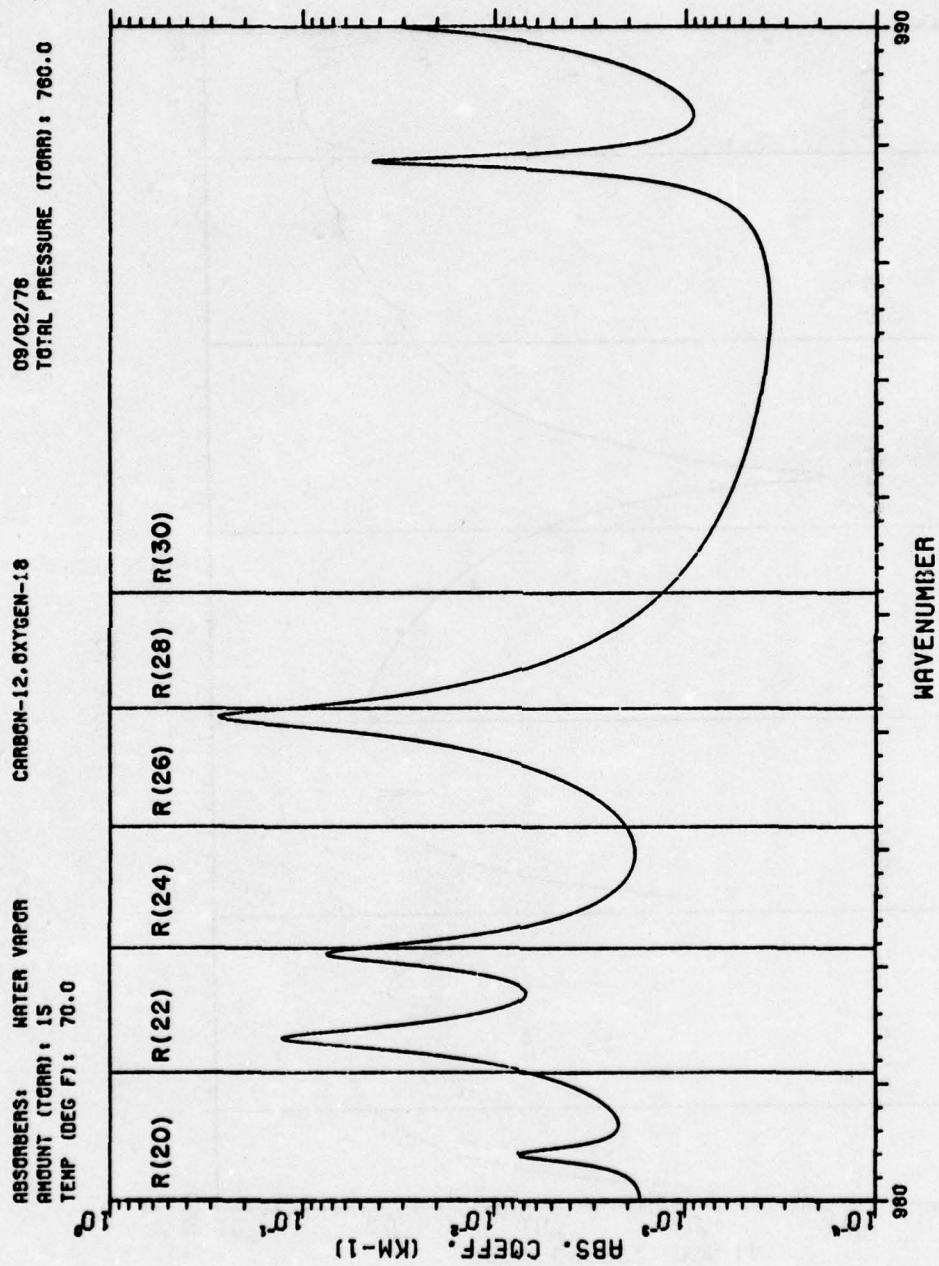


Figure 34

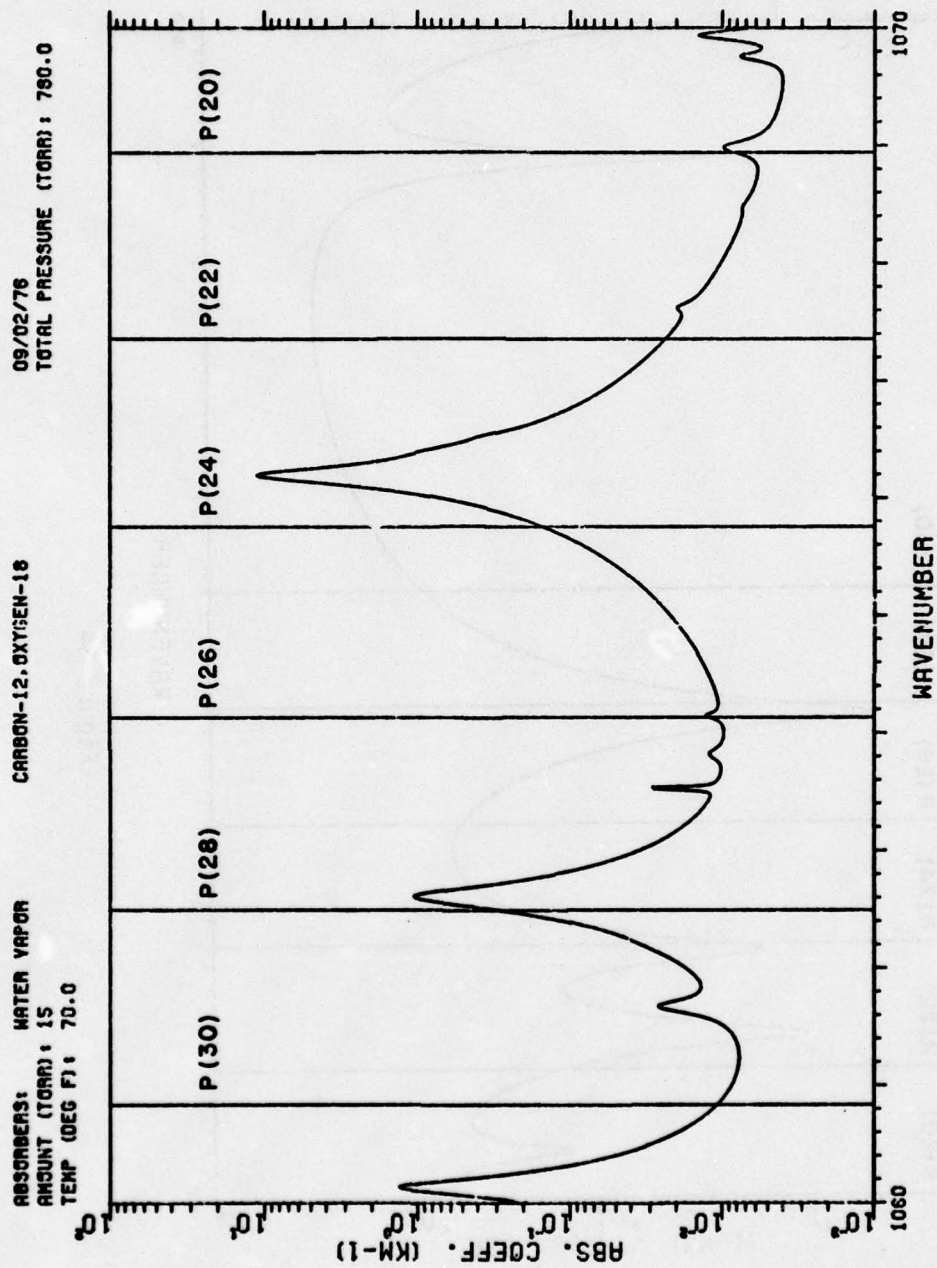


Figure 35

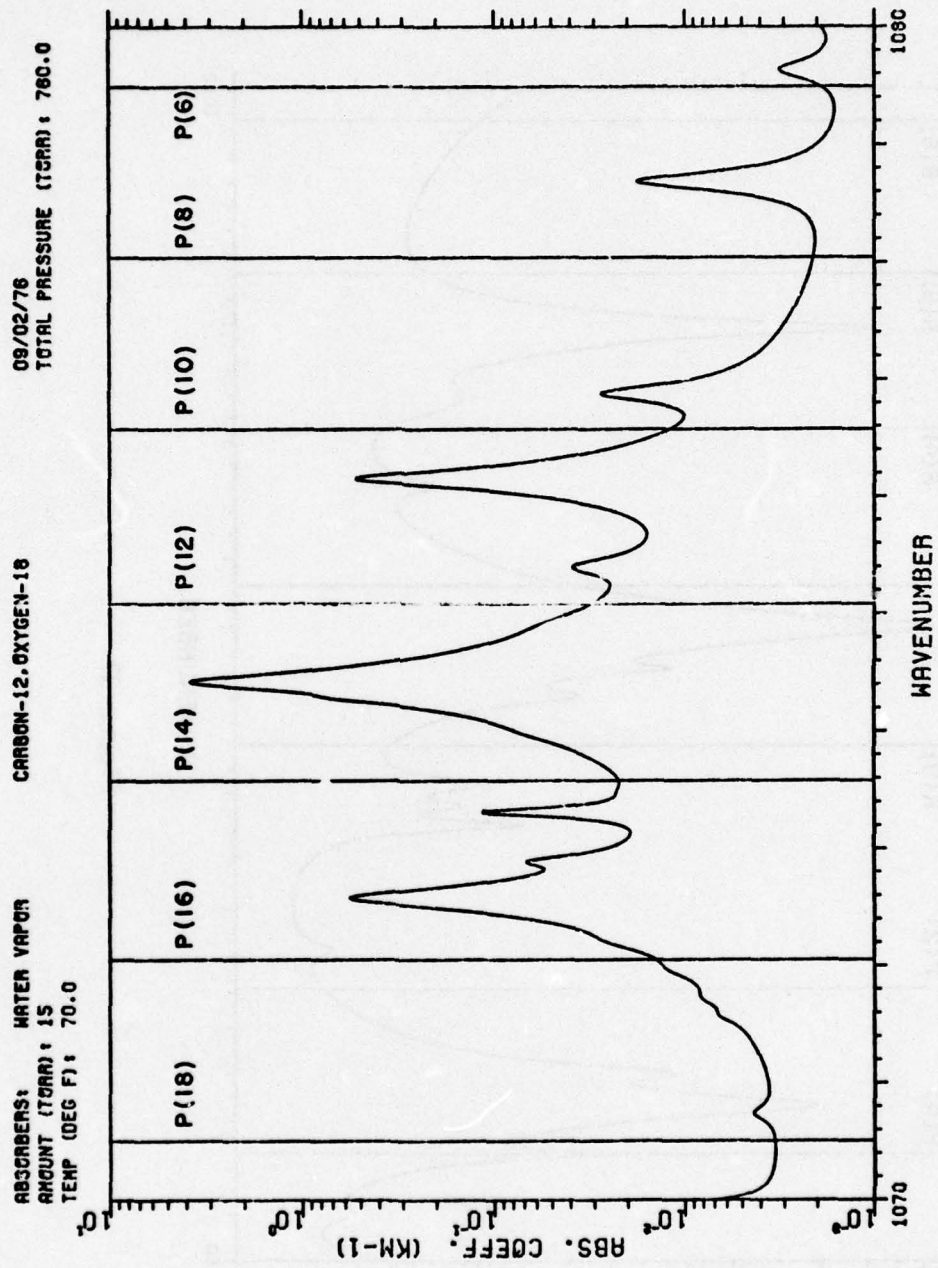


Figure 36

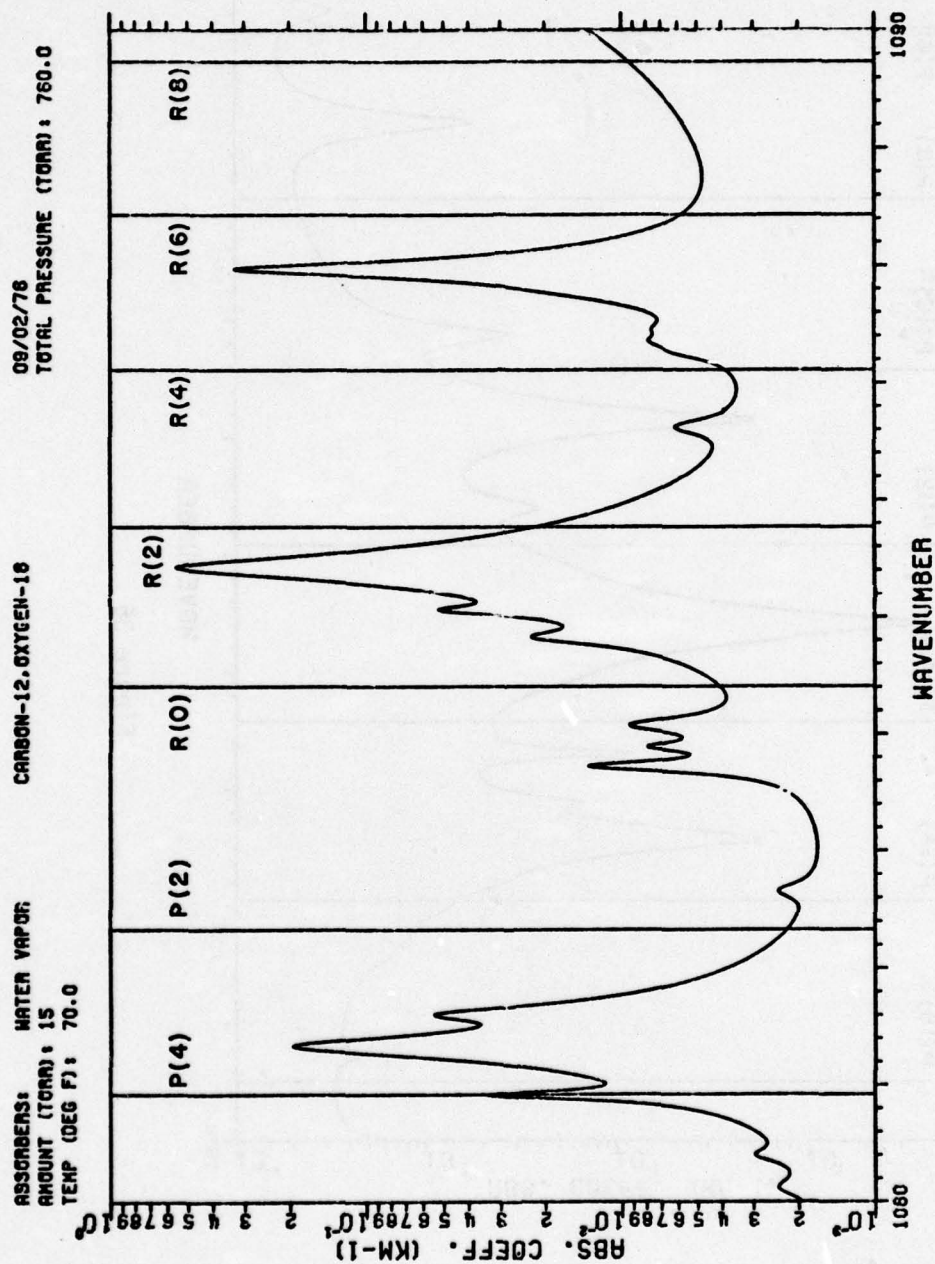
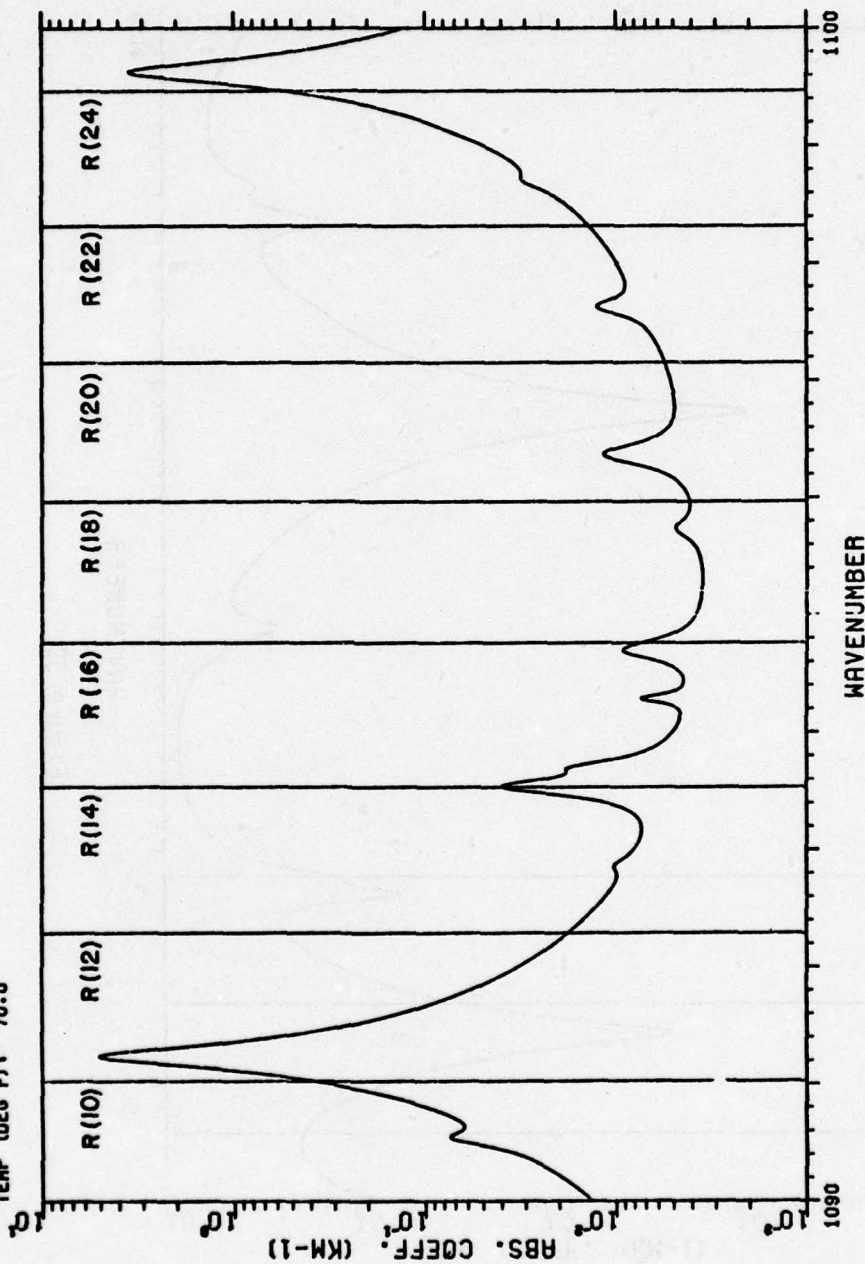


Figure 37

09/02/76
TOTAL PRESSURE (TORR): 760.0

CARBON-12, OXYGEN-18

ABSORBERS: WATER VAPOR
AMOUNT (TORR): 15
TEMP (DEG F): 70.0



WAVENUMBER

Figure 38

09/02/78
TOTAL PRESSURE (TORR): 760.0

CARBON-12.OXYGEN-18

ABSORBERS: WATER VAPOR
AMOUNT (TORR): 15
TEMP (DEG F): 70.0

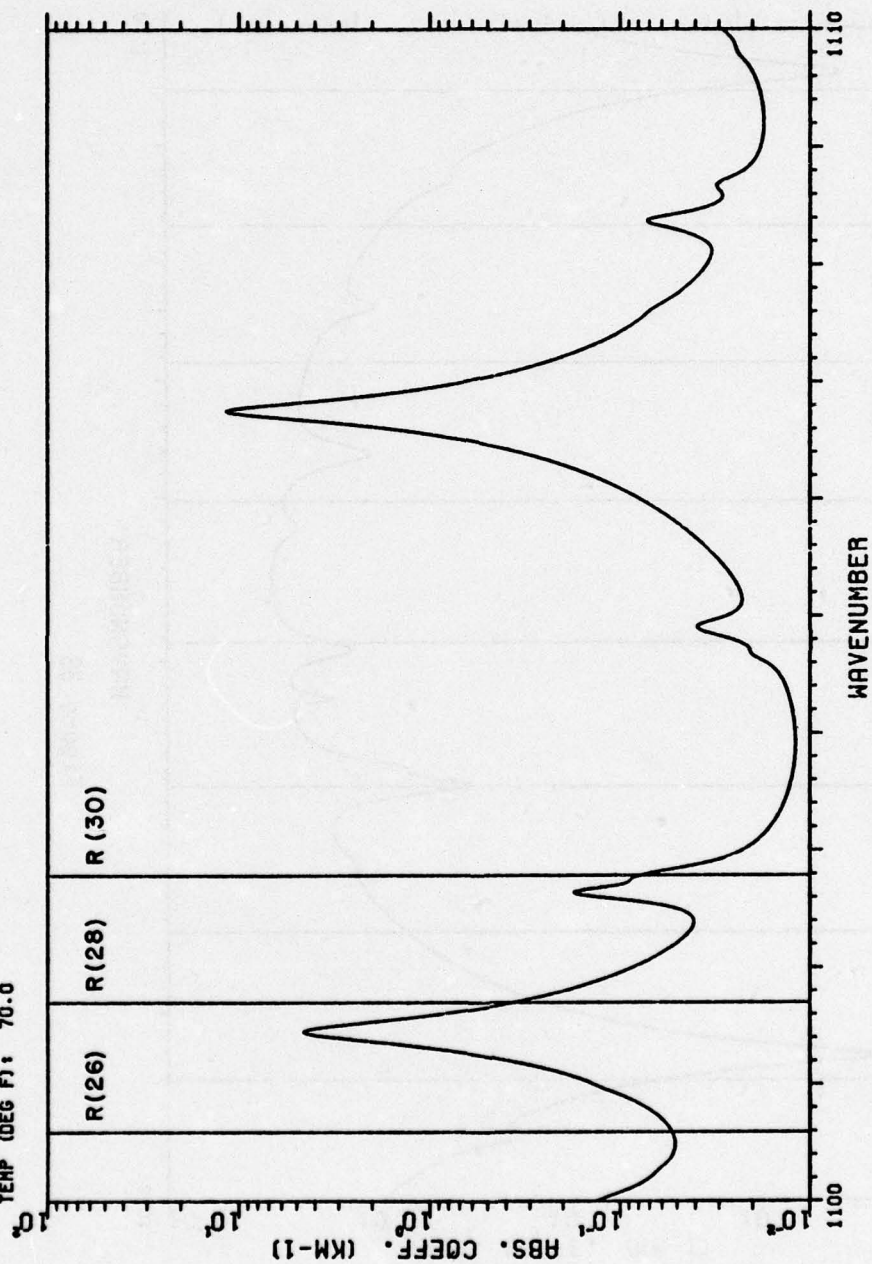


Figure 39

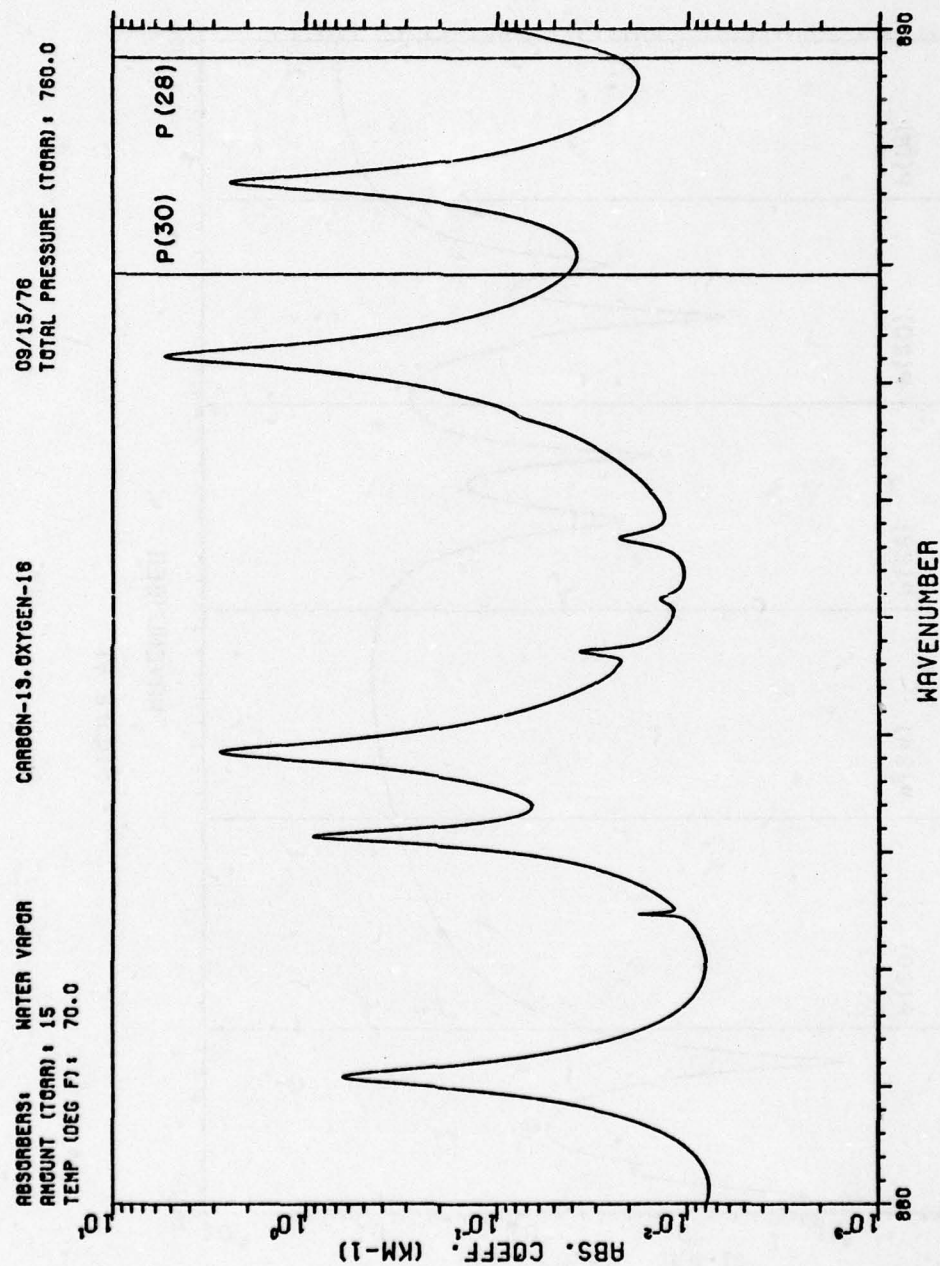


Figure 40

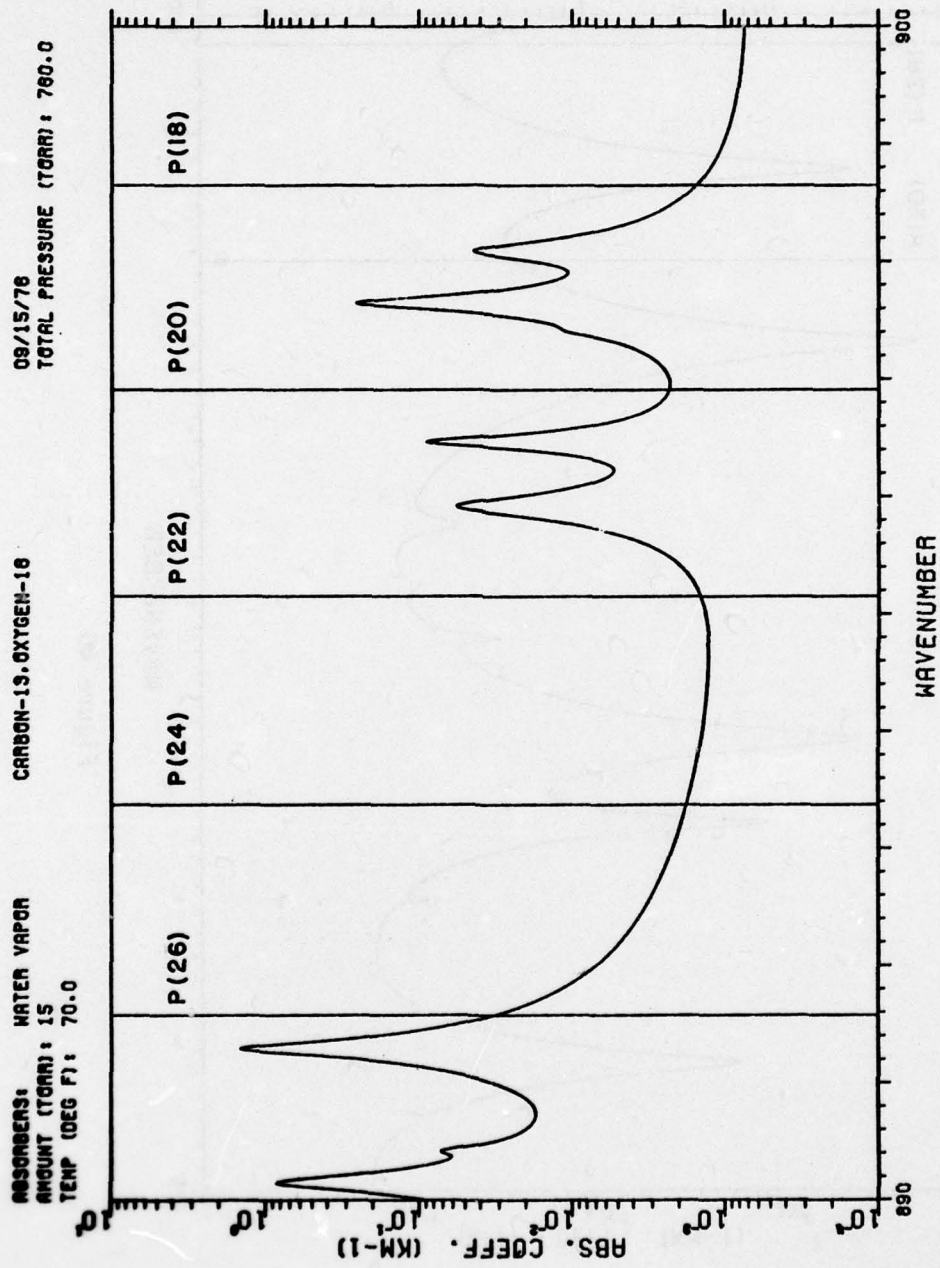
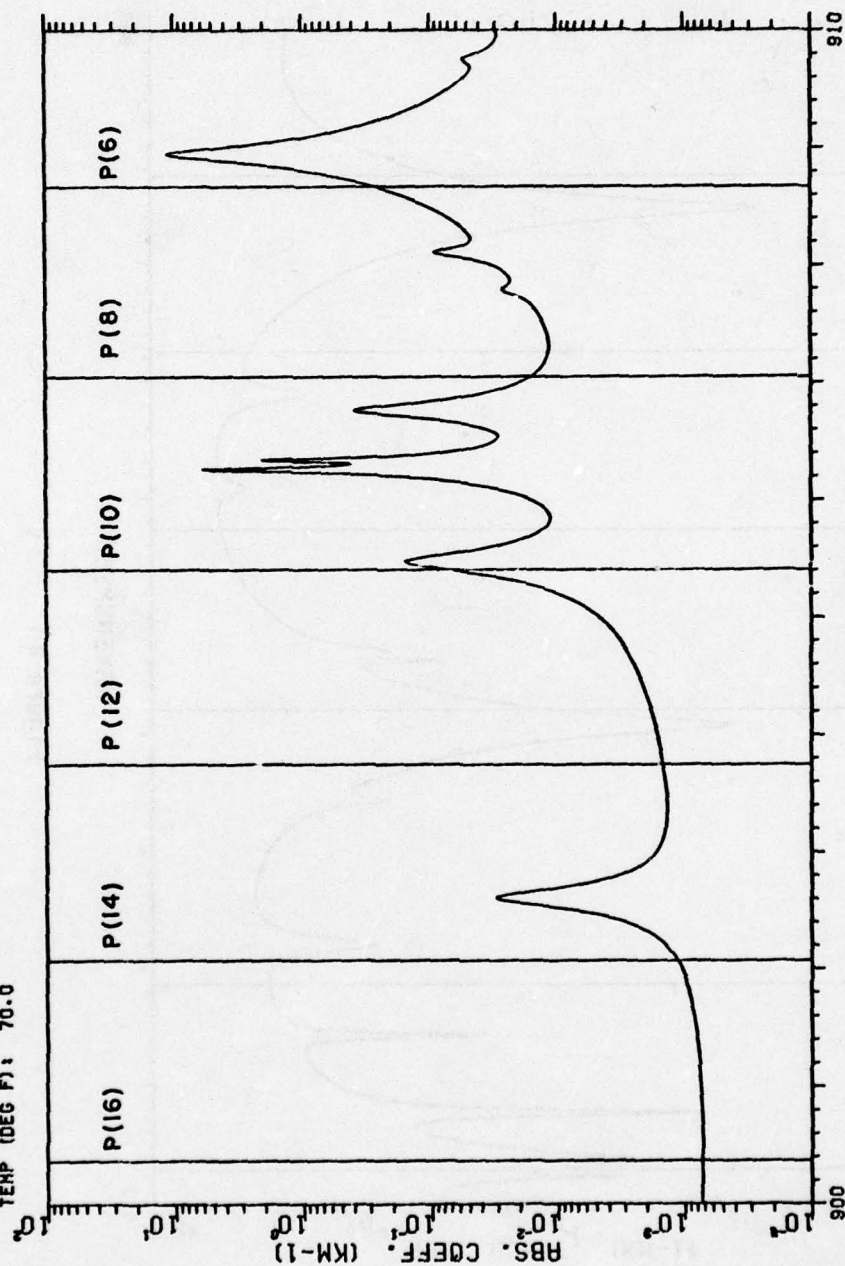


Figure 41

09/15/78
TOTAL PRESSURE (TORR): 760.0

CARBON-13 OXYGEN-18

ABSORBERS: WATER VAPOR
AMOUNT (TORR): 15
TEMP (DEG F): 70.0



WAVENUMBER
Figure 42

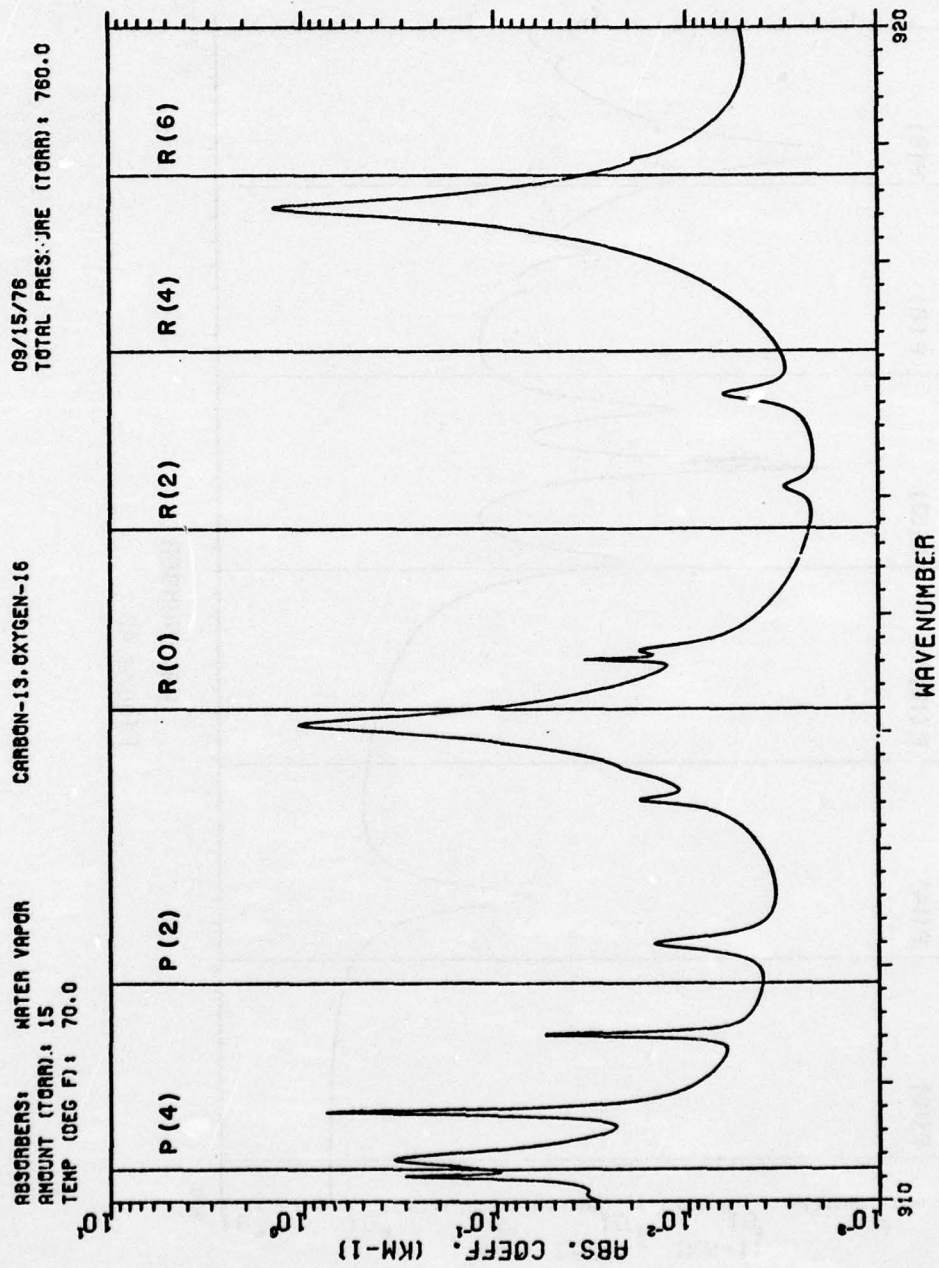


Figure 43

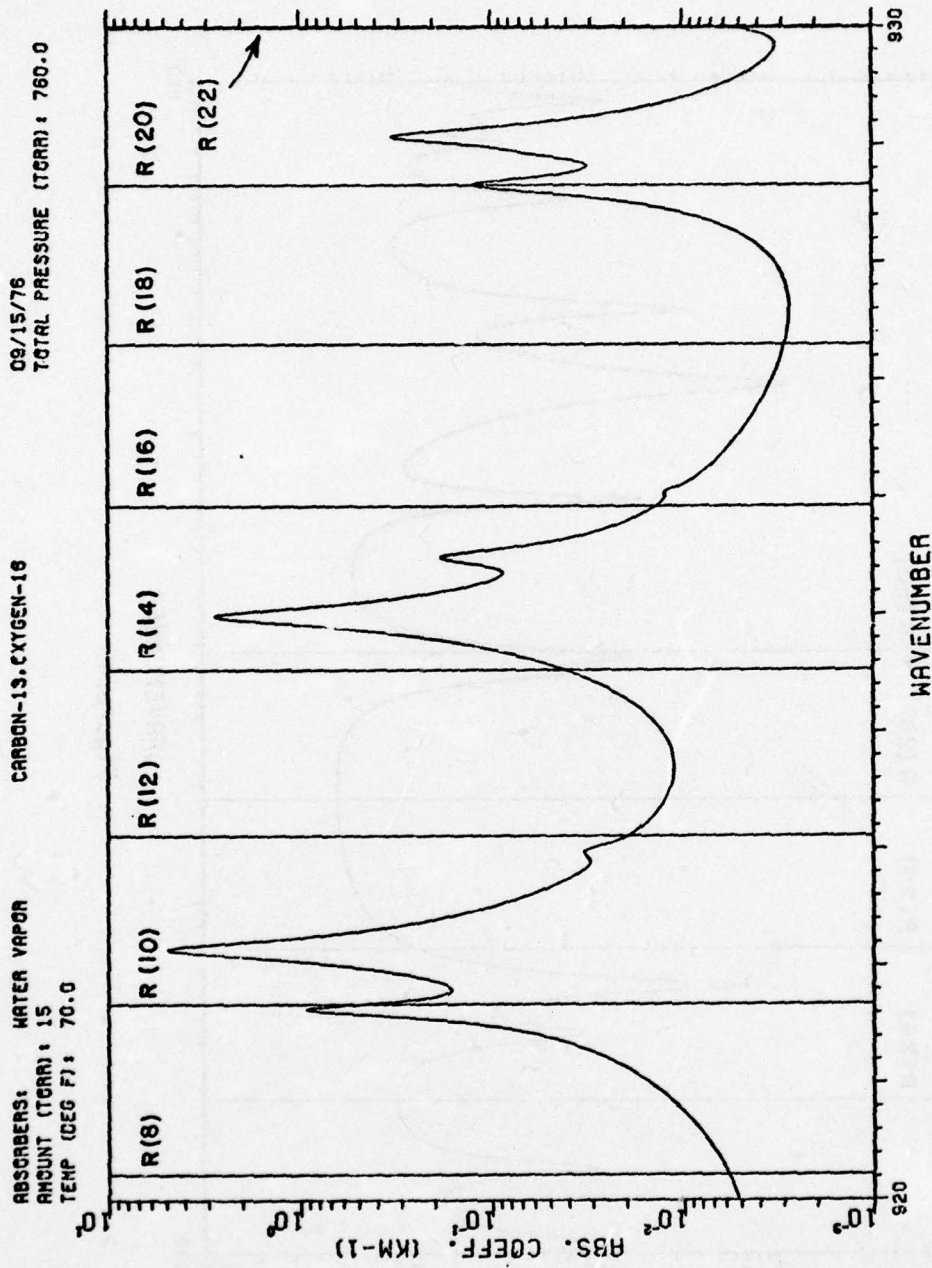
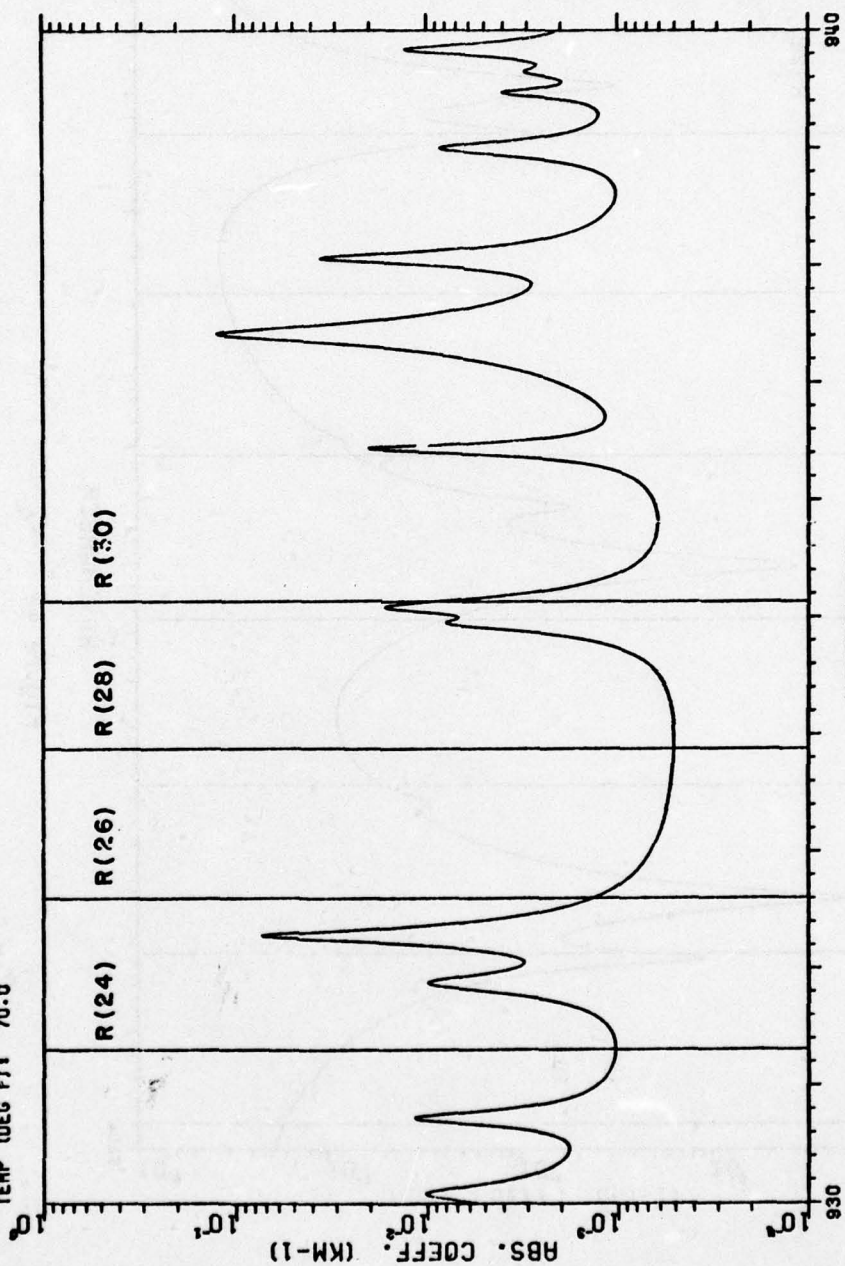


Figure 44

ABSORBERS: WATER VAPOR
 AMOUNT (TORR): 15
 TEMP (DEG F): 70.0
 CARBON-13, OXYGEN-18
 09/15/78
 TOTAL PRE-SURE (TORR): 760.0



WAVENUMBER
 Figure 45

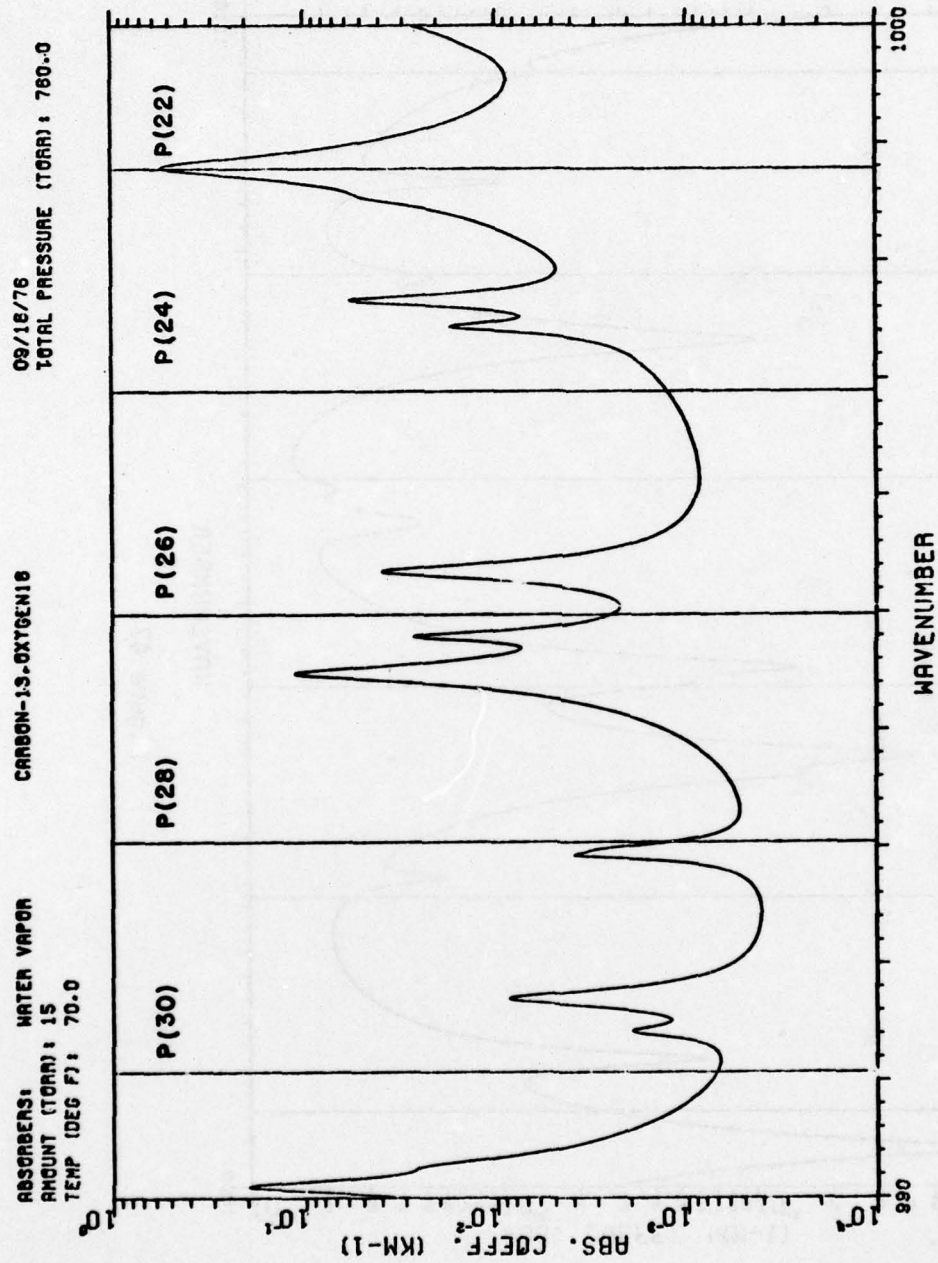


Figure 46

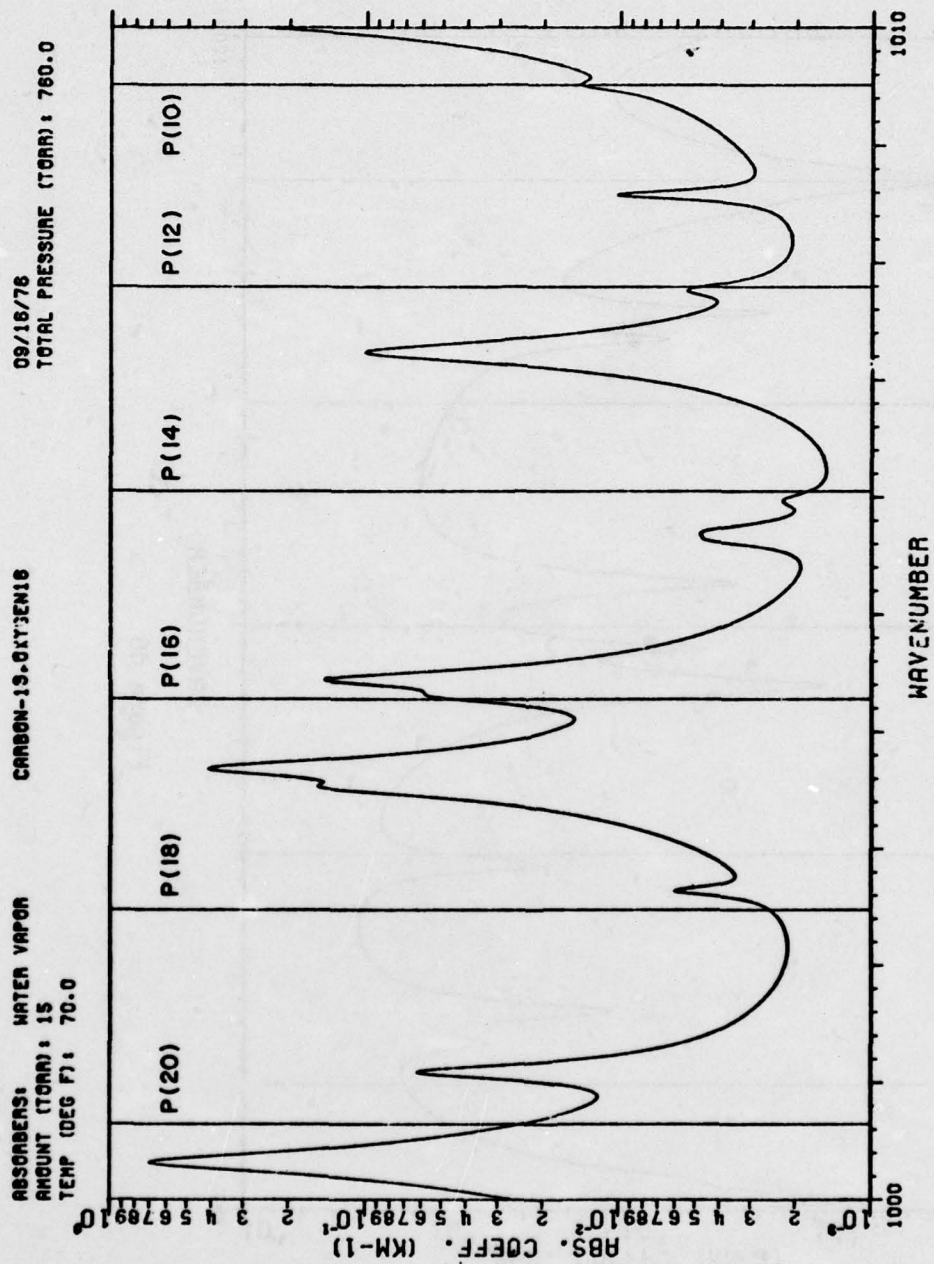


Figure 47

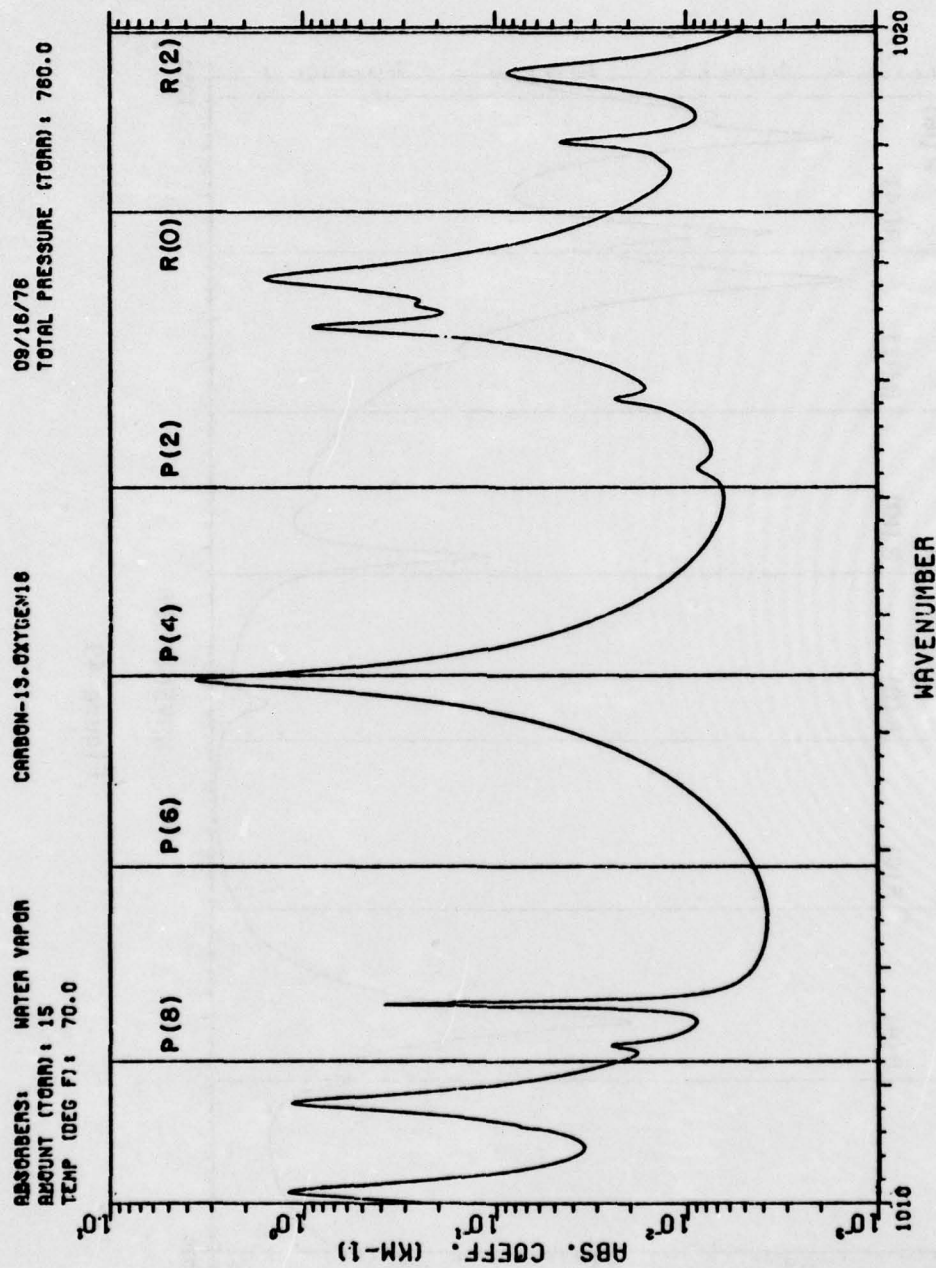


Figure 48

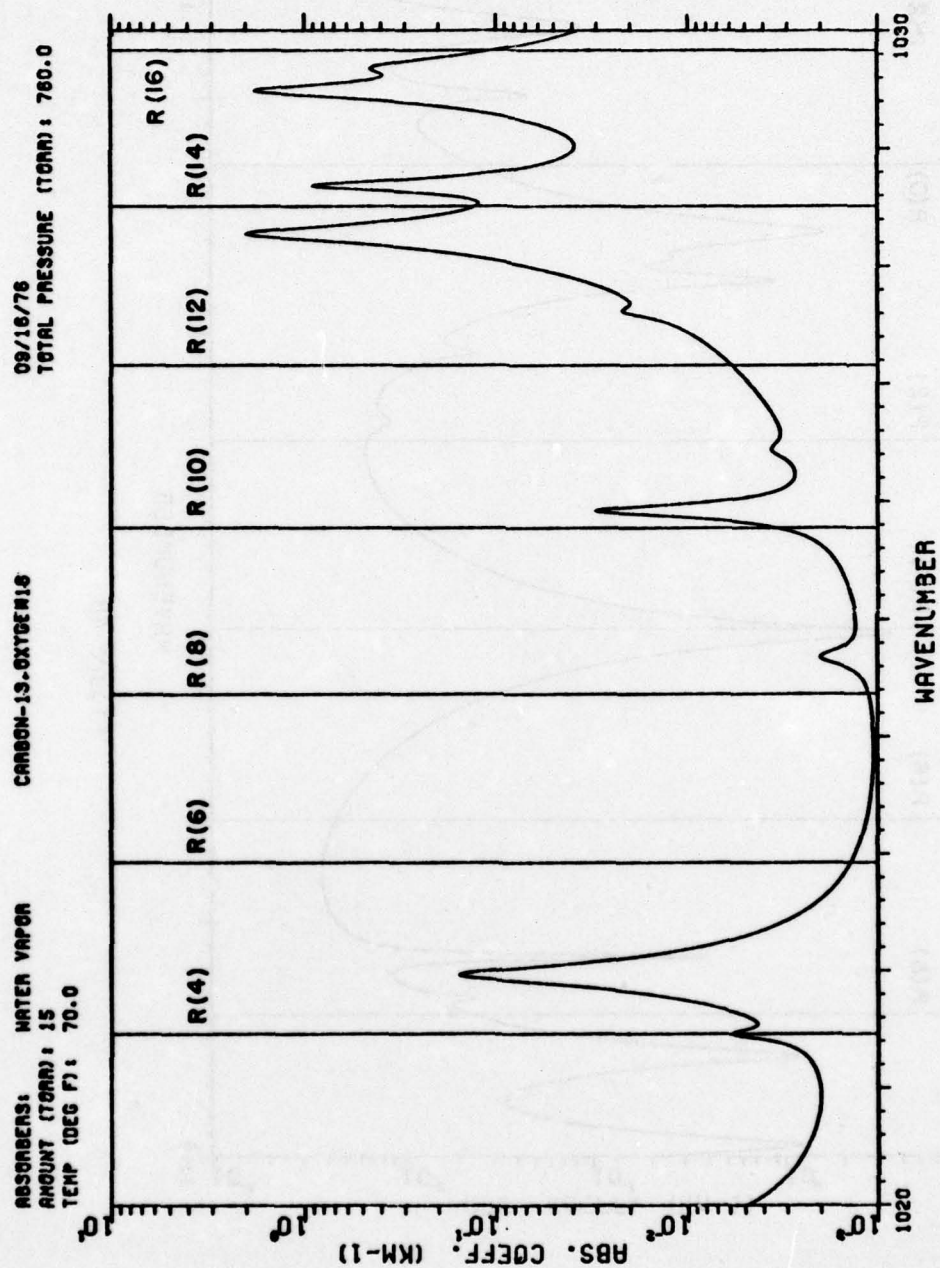


Figure 49

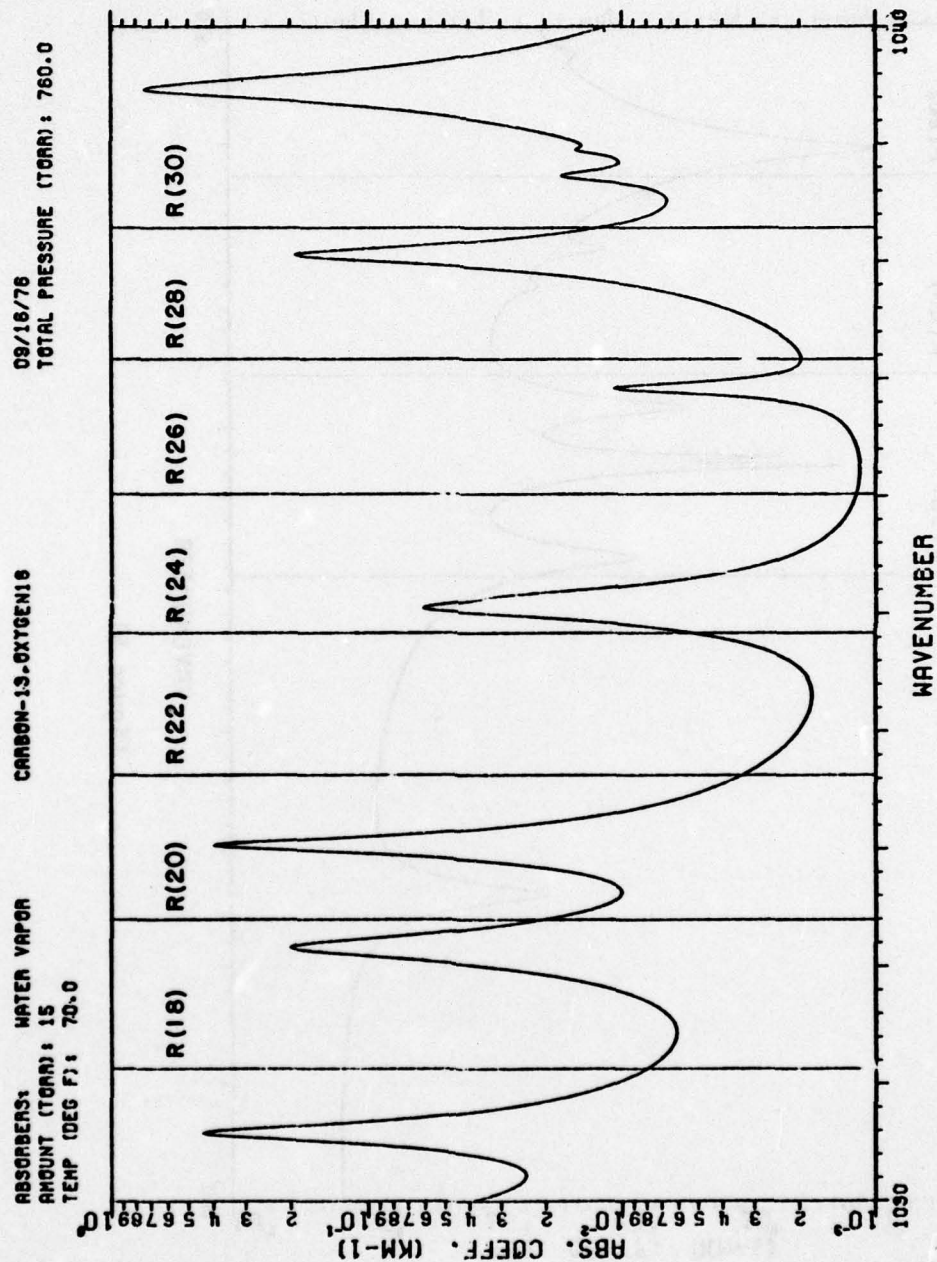


Figure 50

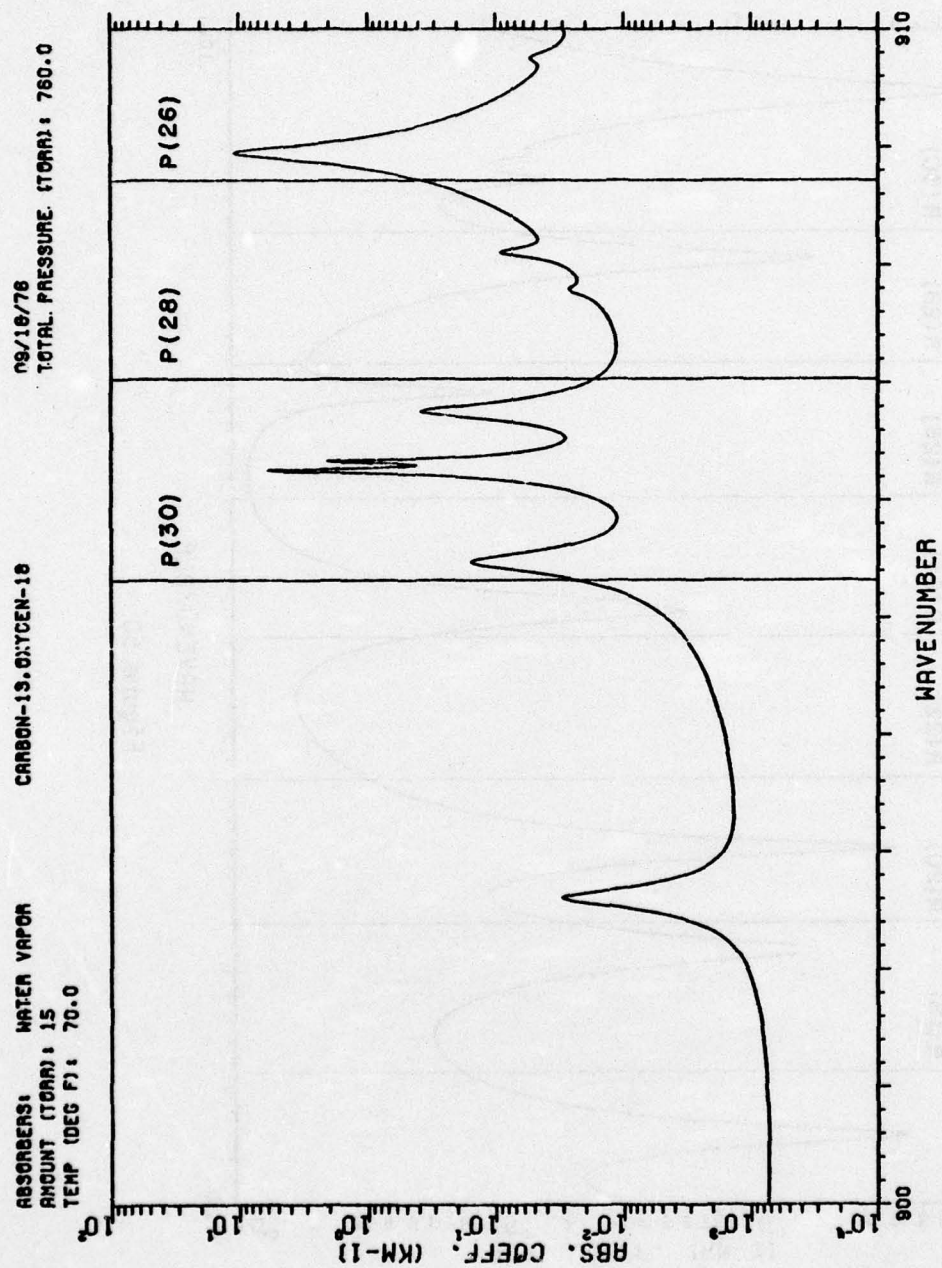


Figure 51

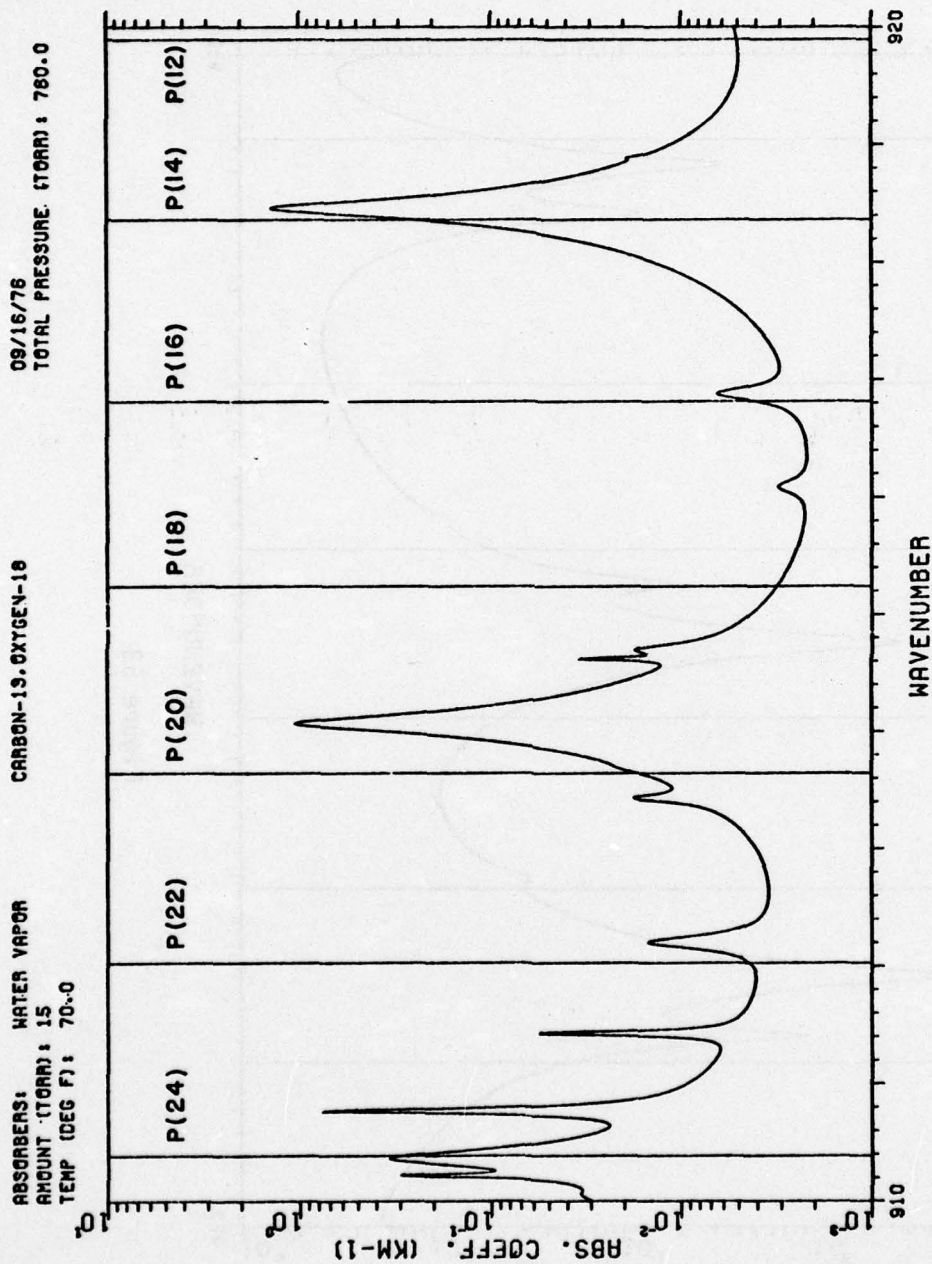


Figure 52

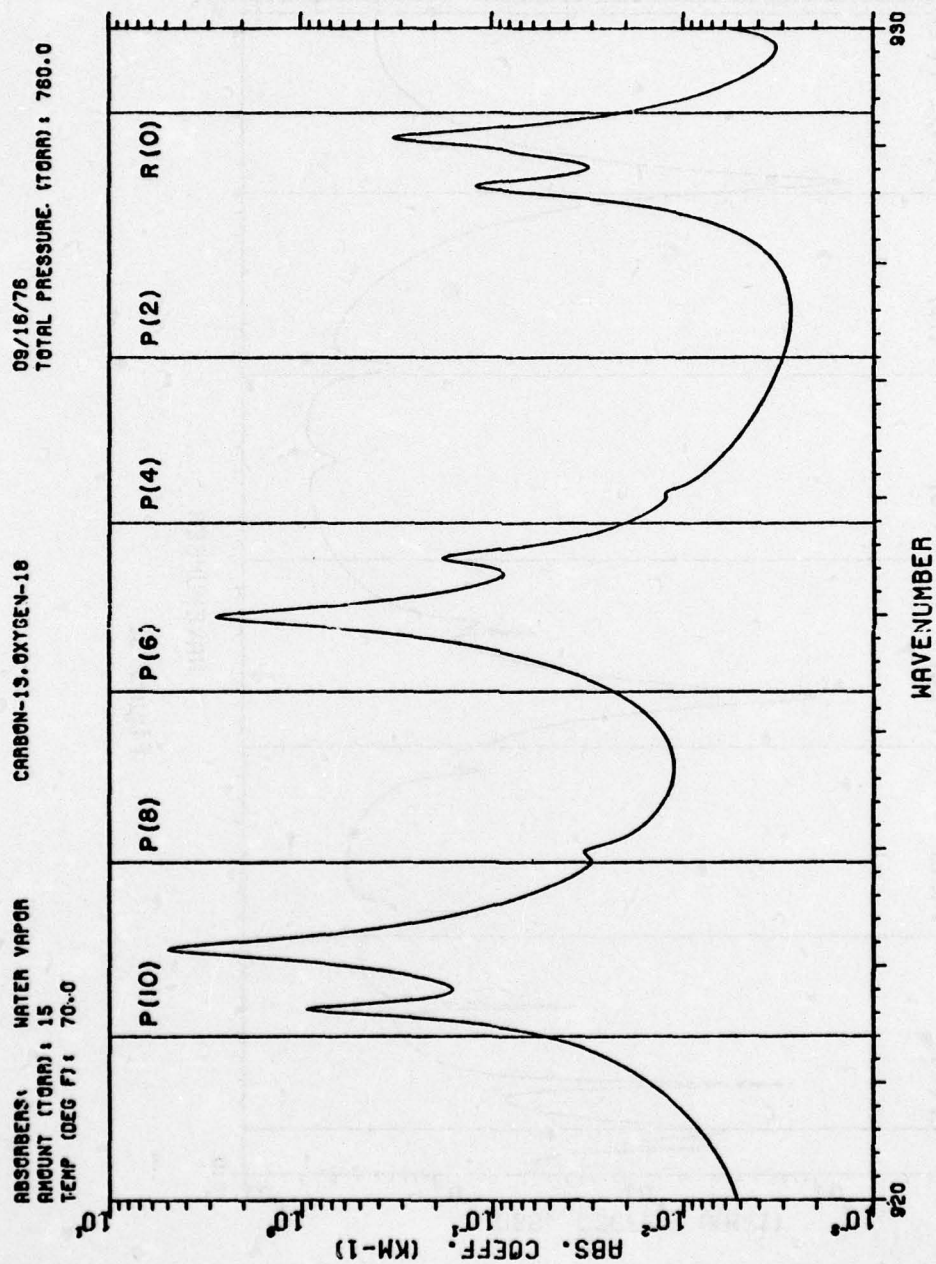
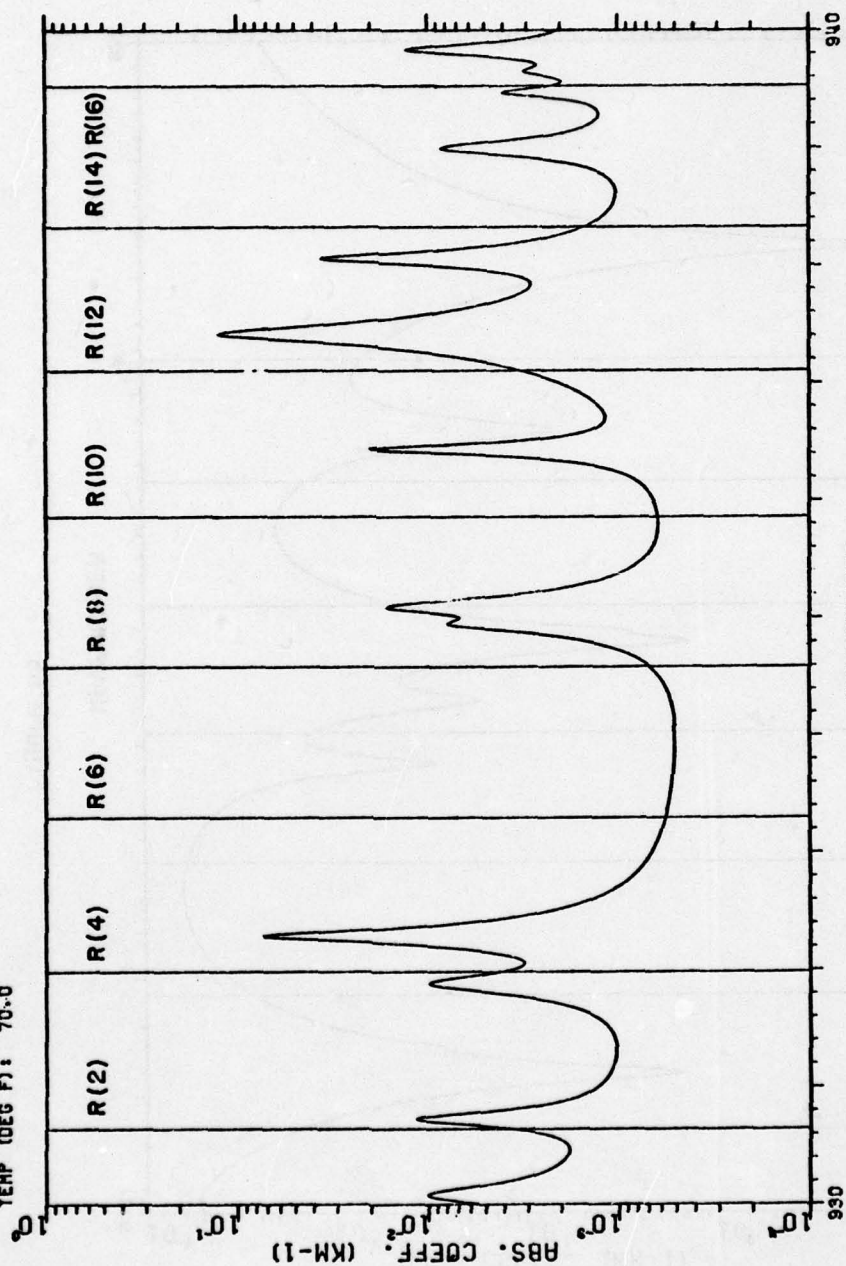


Figure 53

09/16/76
TOTAL PRESSURE (TORR): 760.0

CARBON-13 OXYGEN-18

ABSORBERS: WATER VAPOR
AMOUNT (TORR): 15
TEMP (DEG F): 70.0



WAVENUMBER

Figure 54

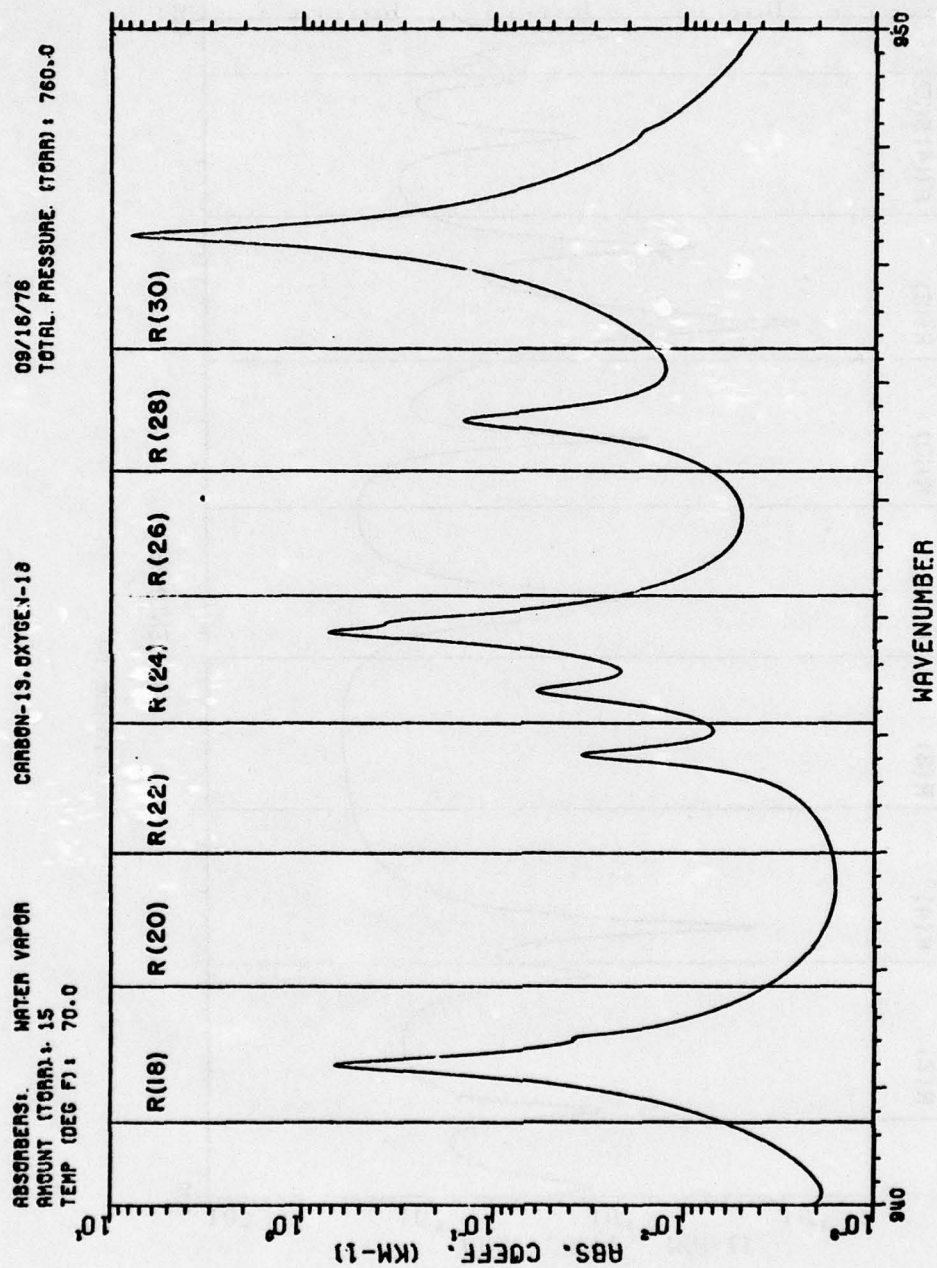


Figure 55

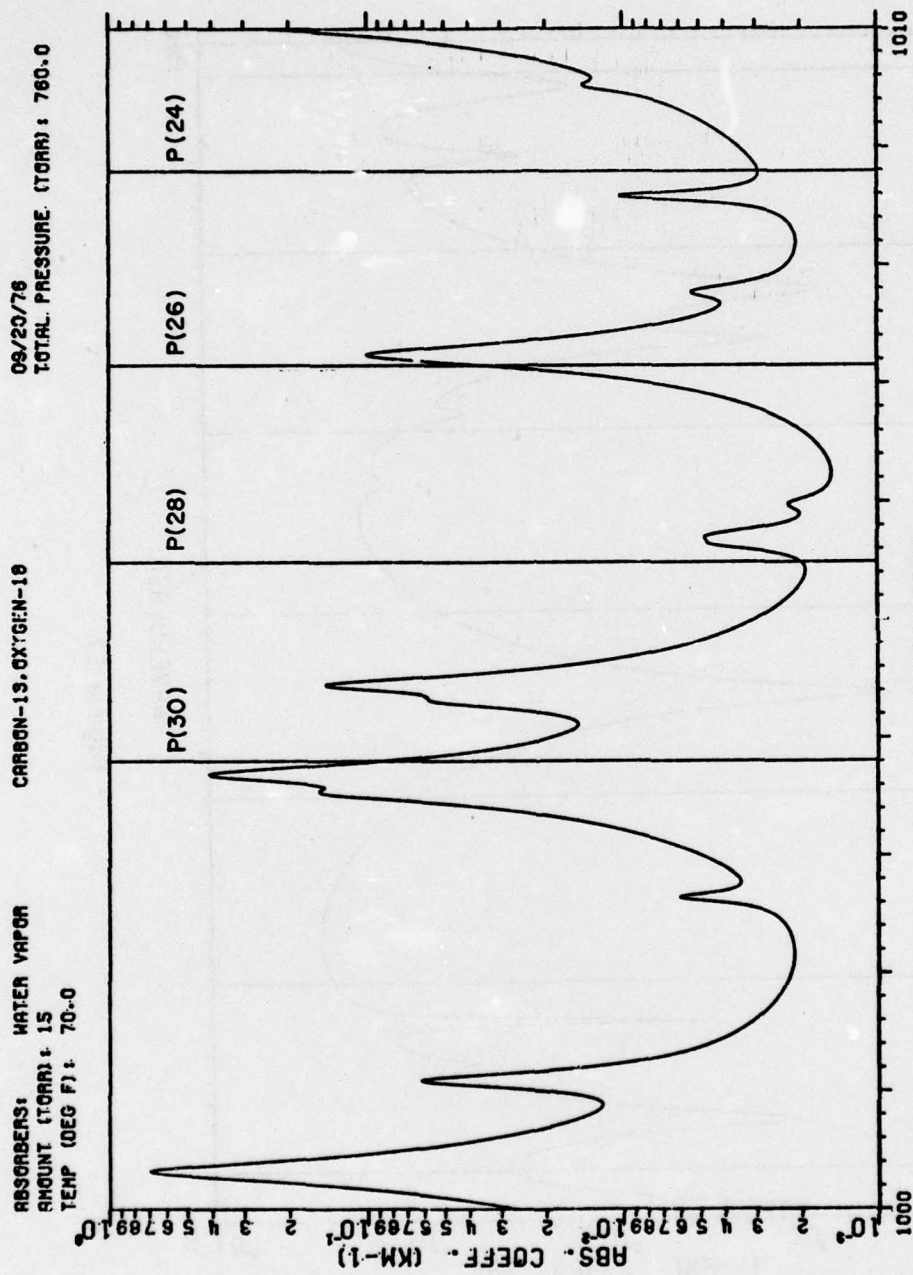


Figure 56

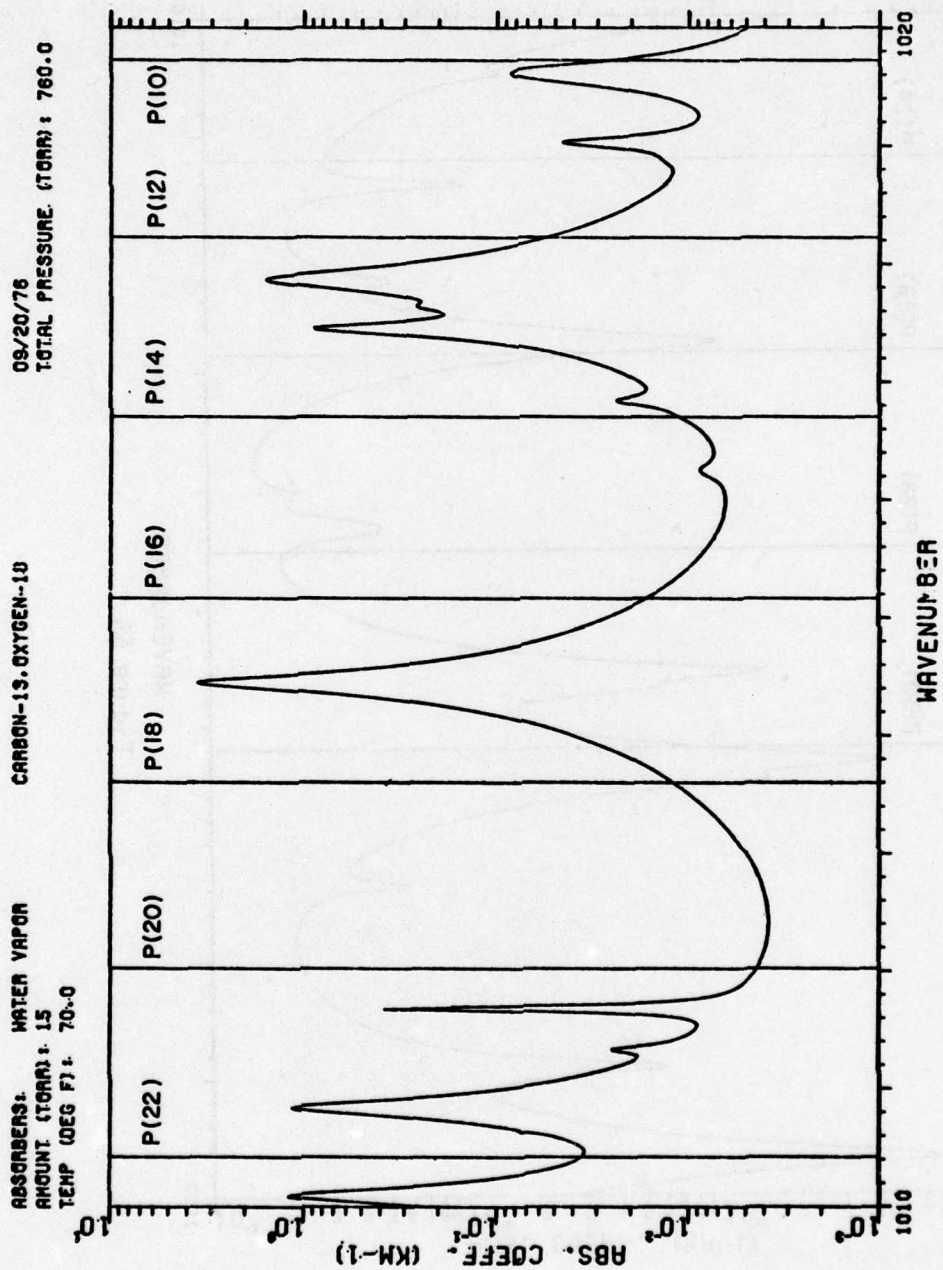


Figure 57

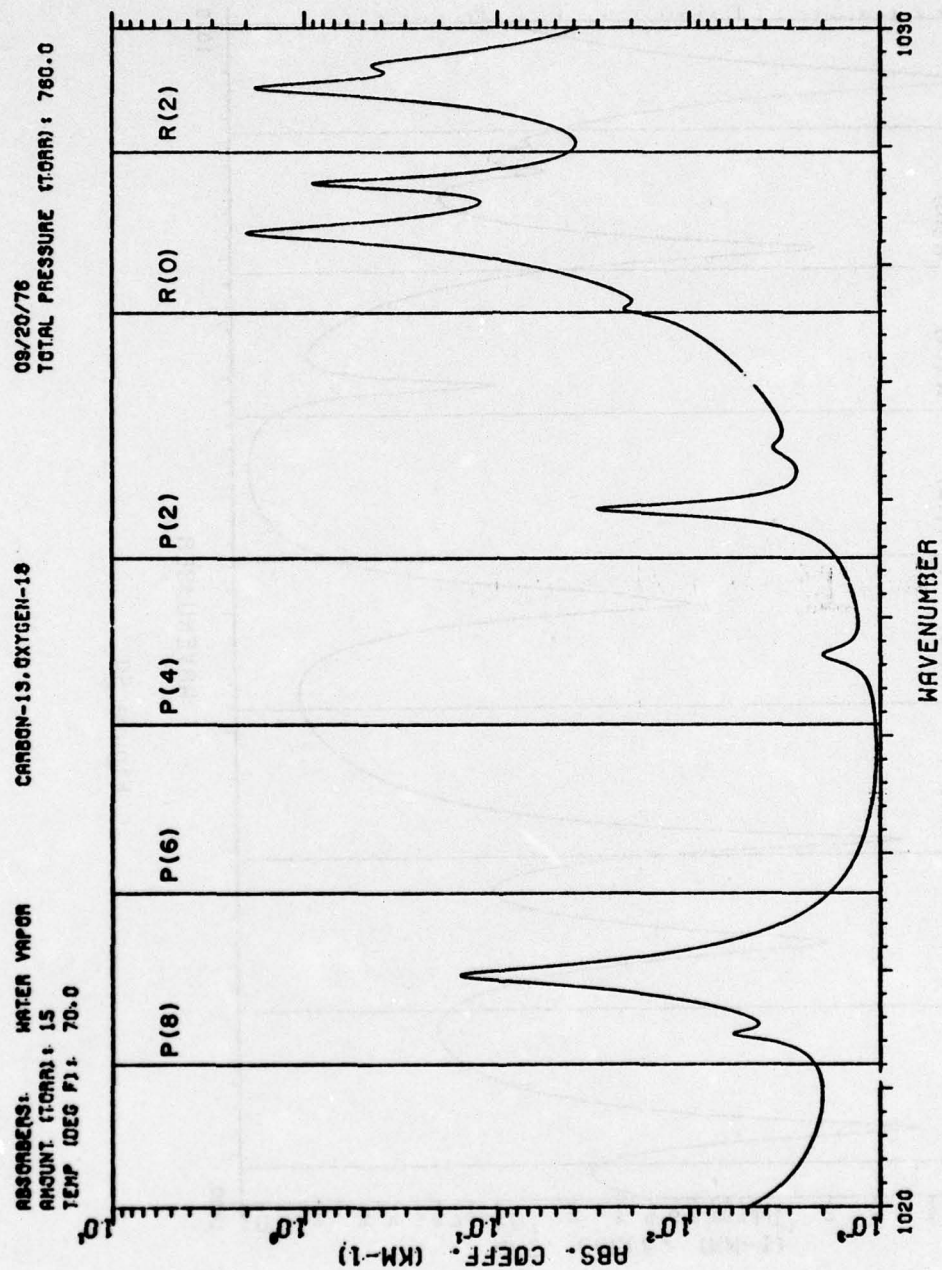


Figure 58

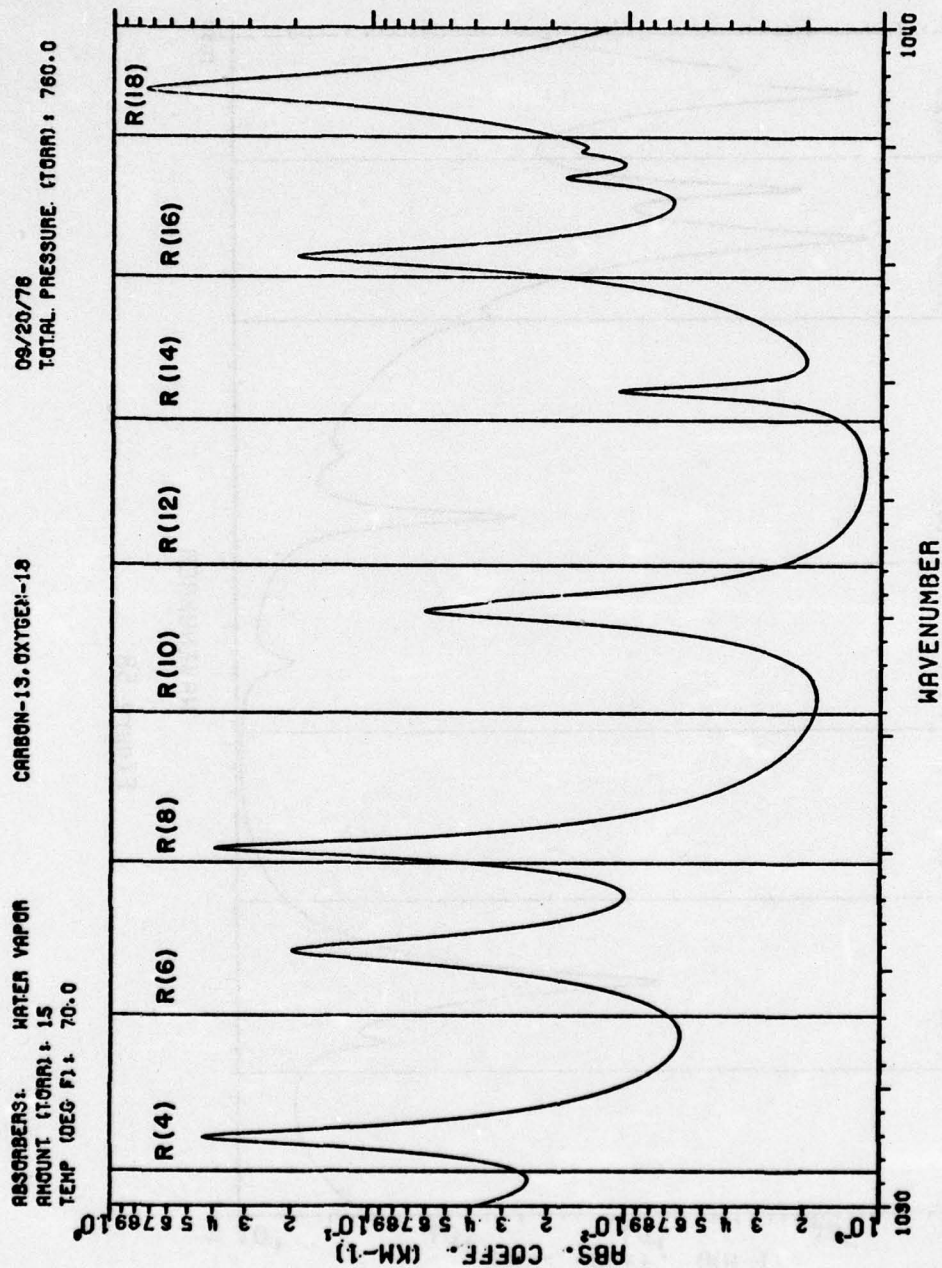


Figure 59

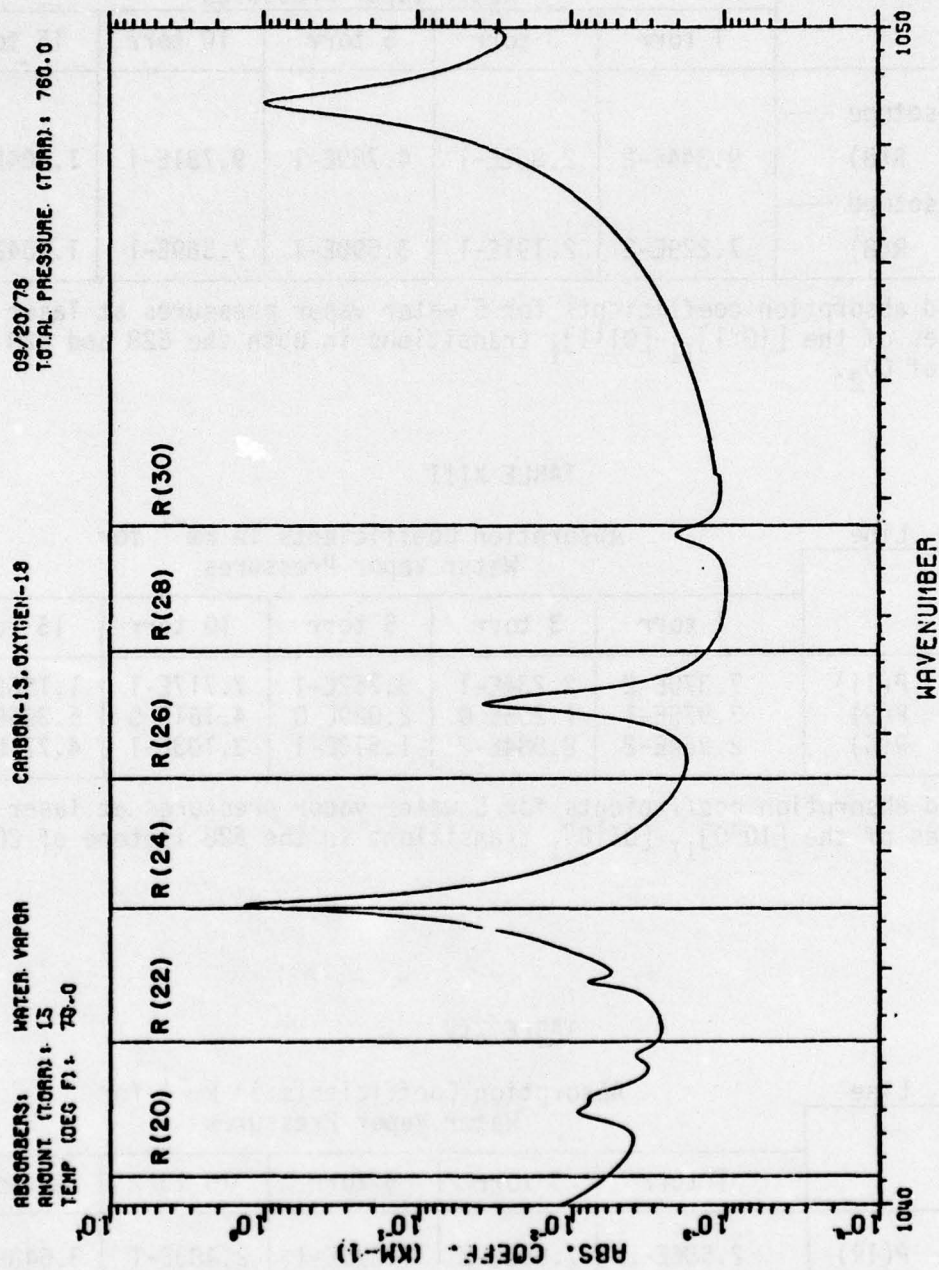


Figure 60

TABLE XII

Frequency Line cm ⁻¹	Absorption Coefficients in km ⁻¹ for Water Vapor Pressures				
	1 torr	3 torr	5 torr	10 torr	15 torr
— 628 isotope —					
595.948 R(8)	9.344E-2	2.832E-1	4.769E-1	9.781E-1	1.504E 0
— 828 isotope —					
572.639 R(8)	7.229E-2	2.191E-1	3.690E-1	7.569E-1	1.164E 0

Calculated absorption coefficients for 5 water vapor pressures at laser frequencies of the $[10^01]_{II}-[01^11]_I$ transitions in both the 628 and 828 isotopes of CO₂.

TABLE XIII

Frequency Line cm ⁻¹	Absorption Coefficients in km ⁻¹ for Water Vapor Pressures				
	1 torr	3 torr	5 torr	10 torr	15 torr
589.275 P(11)	7.370E-2	2.234E-1	3.762E-1	7.717E-1	1.186E 0
590.772 P(9)	3.975E-1	1.205E 0	2.029E 0	4.161E 0	6.396E 0
602.555 R(6)	2.964E-2	8.984E-2	1.513E-1	3.103E-1	4.771E-1

Calculated absorption coefficients for 5 water vapor pressures at laser frequencies of the $[10^00]_{II}-[01^10]_I$ transitions in the 628 isotope of CO₂.

TABLE XIV

Frequency Line cm ⁻¹	Absorption Coefficients in km ⁻¹ for Water Vapor Pressures				
	1 torr	3 torr	5 torr	10 torr	15 torr
2296.739 P(19)	2.586E-2	7.688E-2	1.270E-1	2.483E-1	3.643E-1
2304.147 P(10)	3.293E-3	9.782E-3	1.614E-2	3.152E-2	4.619E-2
2318.034 R(8)	1.030E-4	3.123E-4	5.258E-4	1.078E-3	1.657E-3

Calculated absorption coefficients for 5 water vapor pressures at laser frequencies of the $[10^01]_{II}-[10^00]_{II}$ transitions in the 628 isotope of CO₂.

TABLE XV

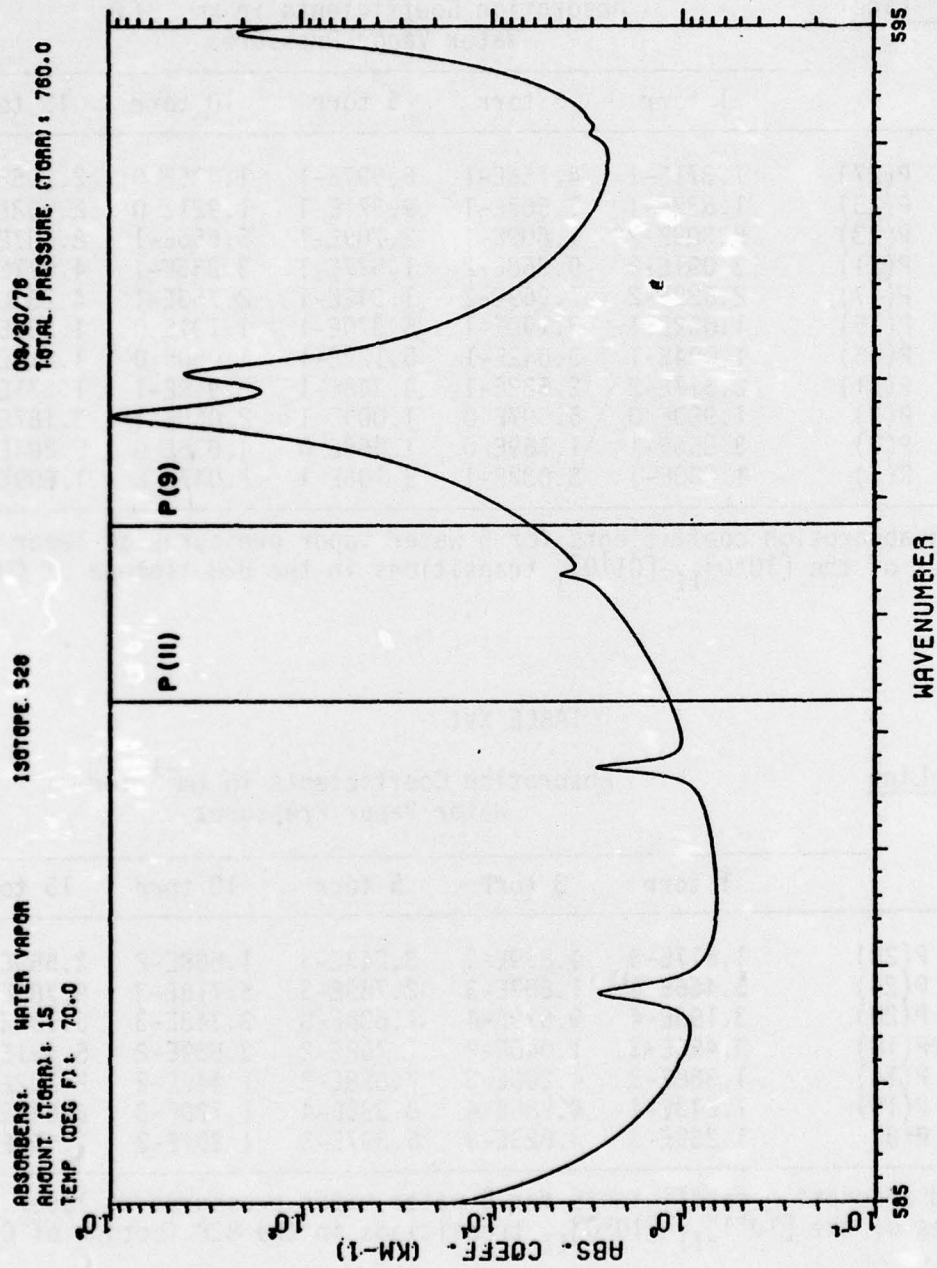
Frequency cm ⁻¹	Line	Absorption Coefficients in km ⁻¹ for Water Vapor Pressures				
		1 torr	3 torr	5 torr	10 torr	15 torr
553.925	P(27)	1.371E-1	4.156E-1	6.997E-1	1.435E 0	2.205E 0
555.247	P(25)	1.837E-1	5.567E-1	9.371E-1	1.921E 0	2.952E 0
556.731	P(23)	5.309E-2	1.609E-1	2.709E-1	5.555E-1	8.537E-1
558.191	P(21)	3.091E-2	9.368E-2	1.577E-1	3.235E-1	4.971E-1
561.136	P(17)	2.629E-2	7.969E-2	1.342E-1	2.753E-1	4.232E-1
562.588	P(15)	1.052E-1	3.190E-1	5.370E-1	1.101E 0	1.692E 0
564.016	P(13)	1.004E-1	3.042E-1	5.122E-1	1.050E 0	1.614E 0
565.483	P(11)	8.517E-2	2.582E-1	4.348E-1	8.918E-1	1.371E 0
566.926	P(9)	1.980E 0	5.997E 0	1.009E 1	2.065E 1	3.167E 1
568.311	P(7)	3.856E-1	1.169E 0	1.968E 0	4.036E 0	6.204E 0
578.704	R(7)	1.000E-1	3.032E-1	5.106E-1	1.047E 0	1.609E 0

Calculated absorption coefficients for 5 water vapor pressures at laser frequencies of the $[10^0 0]_{II} - [01^1 0]_I$ transitions in the 828 isotope of CO₂.

TABLE XVI

Frequency cm ⁻¹	Line	Absorption Coefficients in km ⁻¹ for Water Vapor Pressures				
		1 torr	3 torr	5 torr	10 torr	15 torr
2273.761	P(28)	1.617E-3	4.899E-3	8.243E-3	1.688E-2	2.589E-2
2276.867	P(24)	5.466E-4	1.657E-3	2.789E-3	5.718E-3	8.786E-3
2280.502	P(20)	3.193E-4	9.679E-4	1.630E-3	3.343E-3	5.138E-3
2282.063	P(18)	3.456E-3	1.046E-2	1.758E-2	3.589E-2	5.491E-2
2284.670	P(14)	1.388E-3	4.200E-3	7.058E-3	1.440E-2	2.202E-2
2287.806	P(10)	1.643E-4	4.980E-4	8.385E-4	1.720E-3	2.644E-3
2300.966	R(8)	1.269E-3	3.823E-3	6.397E-3	1.291E-2	1.954E-2

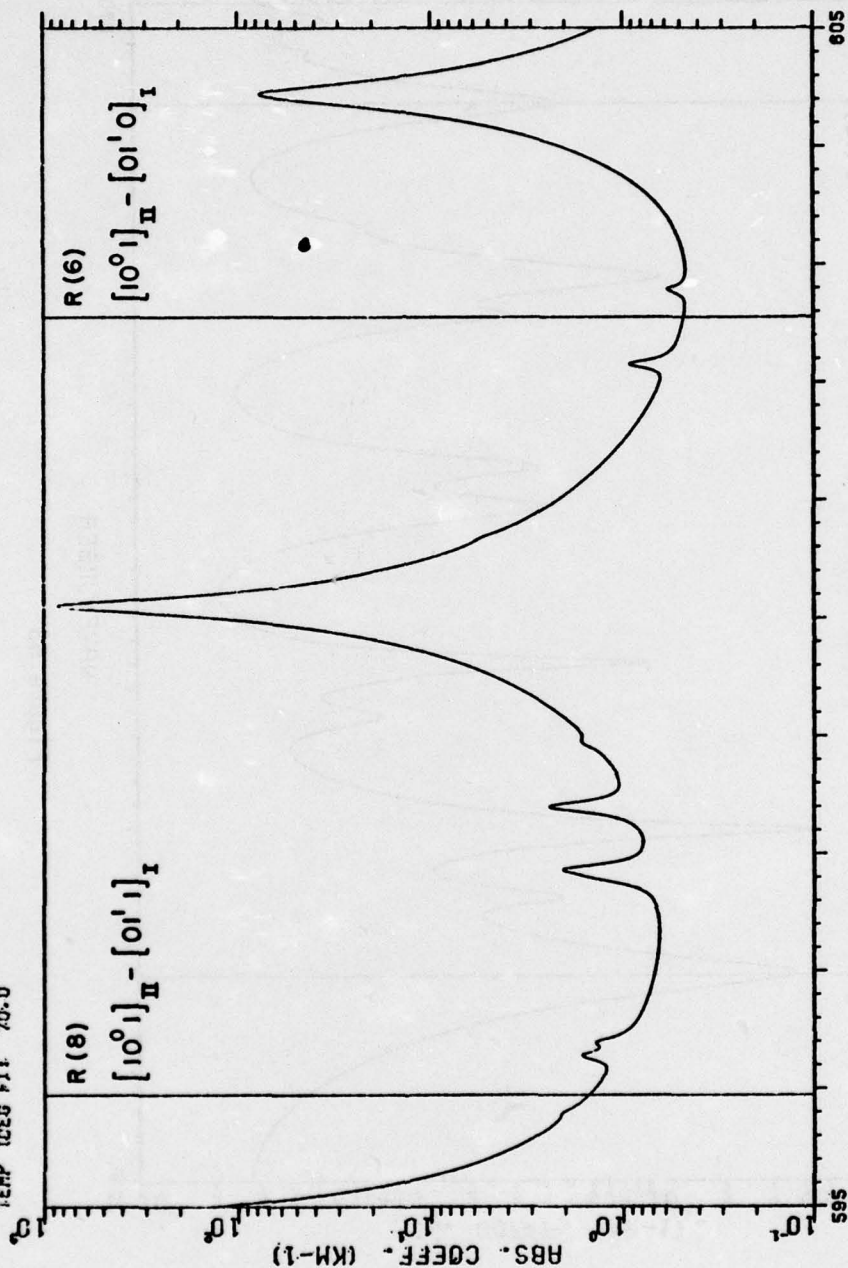
Calculated absorption coefficients for 5 water vapor pressures at laser frequencies of the $[10^0 1]_{II} - [10^0 0]_{II}$ transitions in the 828 isotope of CO₂.



09/20/76
TOTAL PRESSURE (TORR): 760.0

ISOTOPE 620

ABSORBERS: WATER VAPOR
AMOUNT (TORR): 15
TEMP (DEG F): 70.0



WAVENUMBER
Figure 62

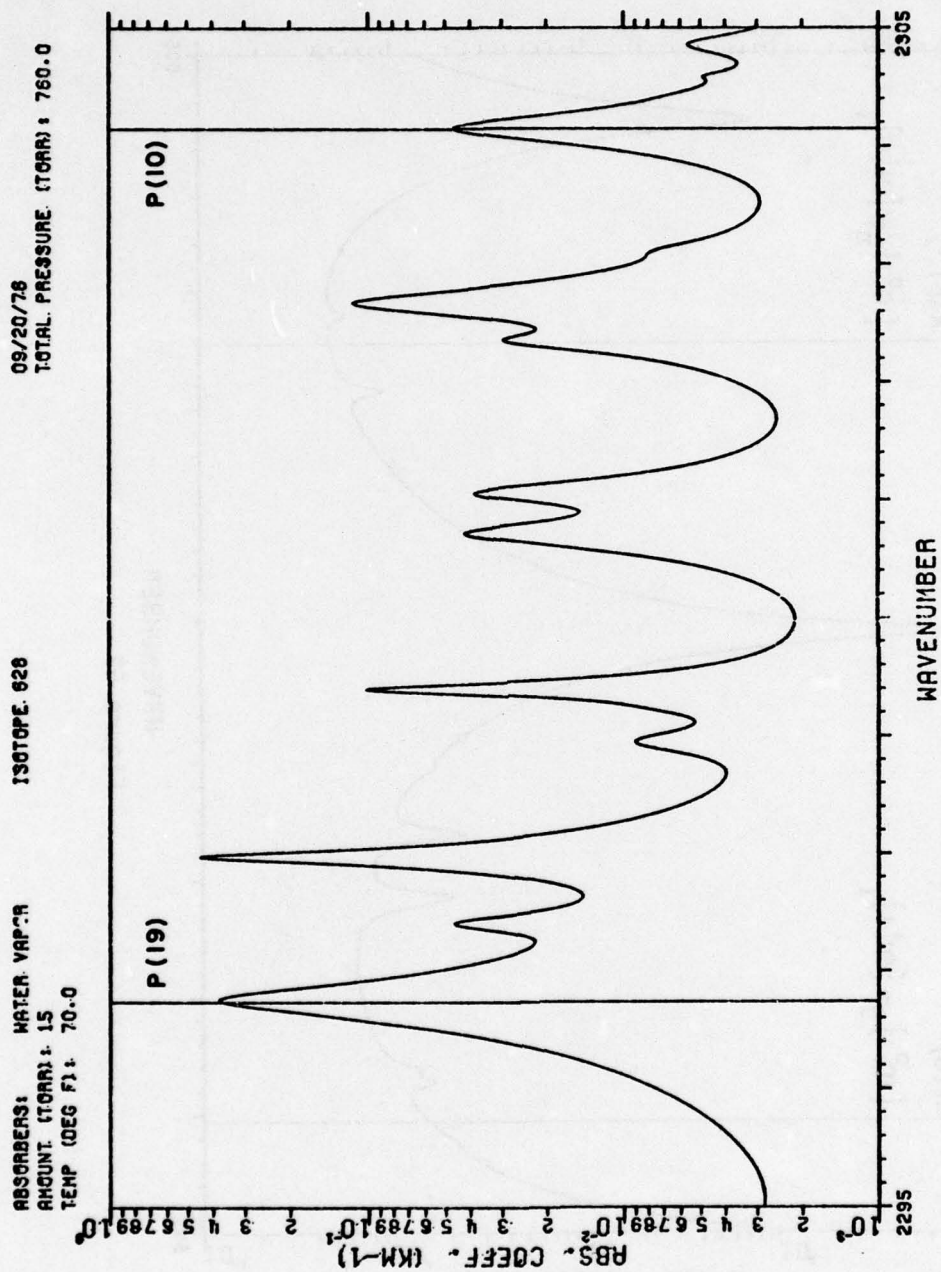


Figure 63

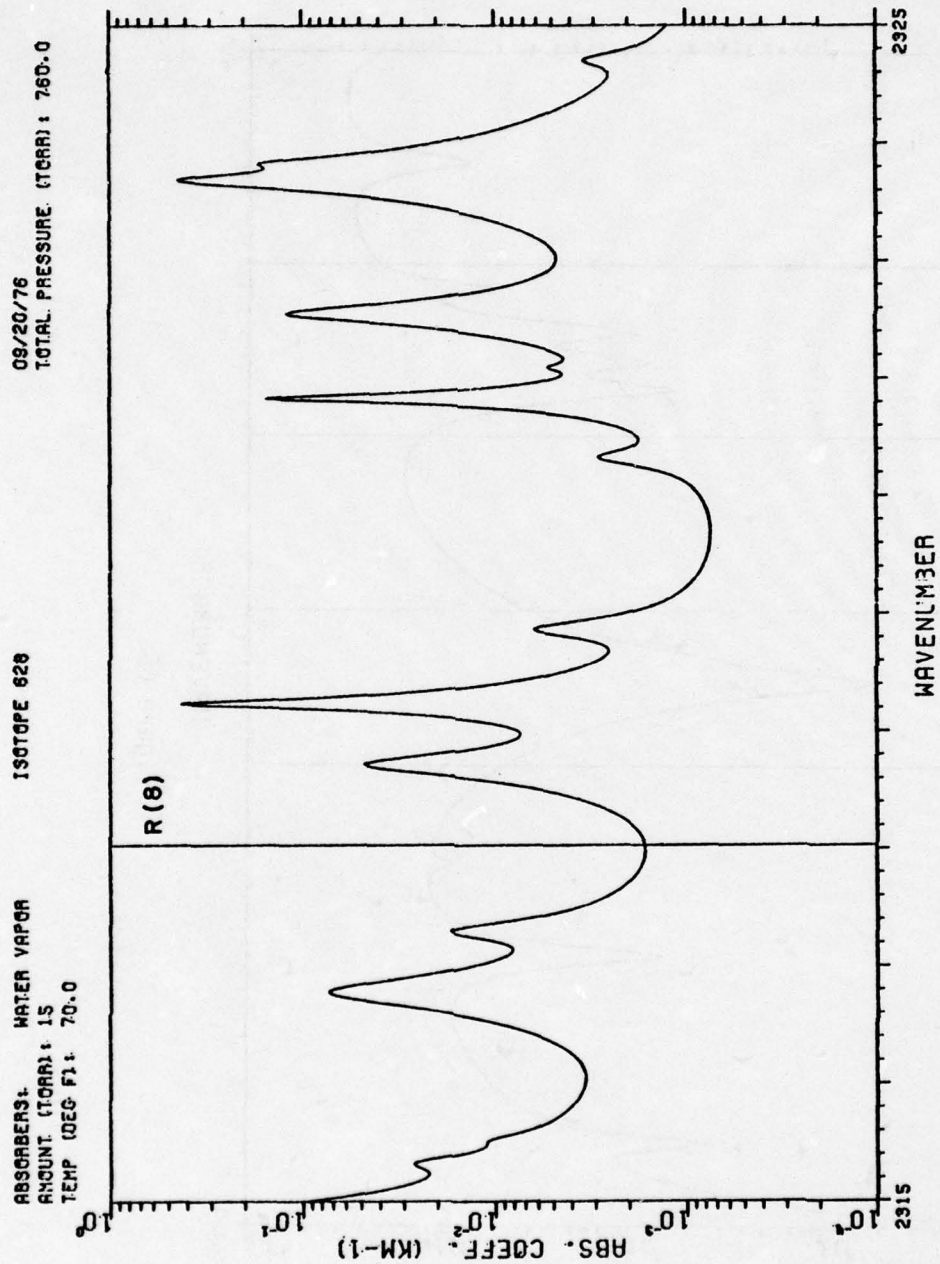


Figure 64

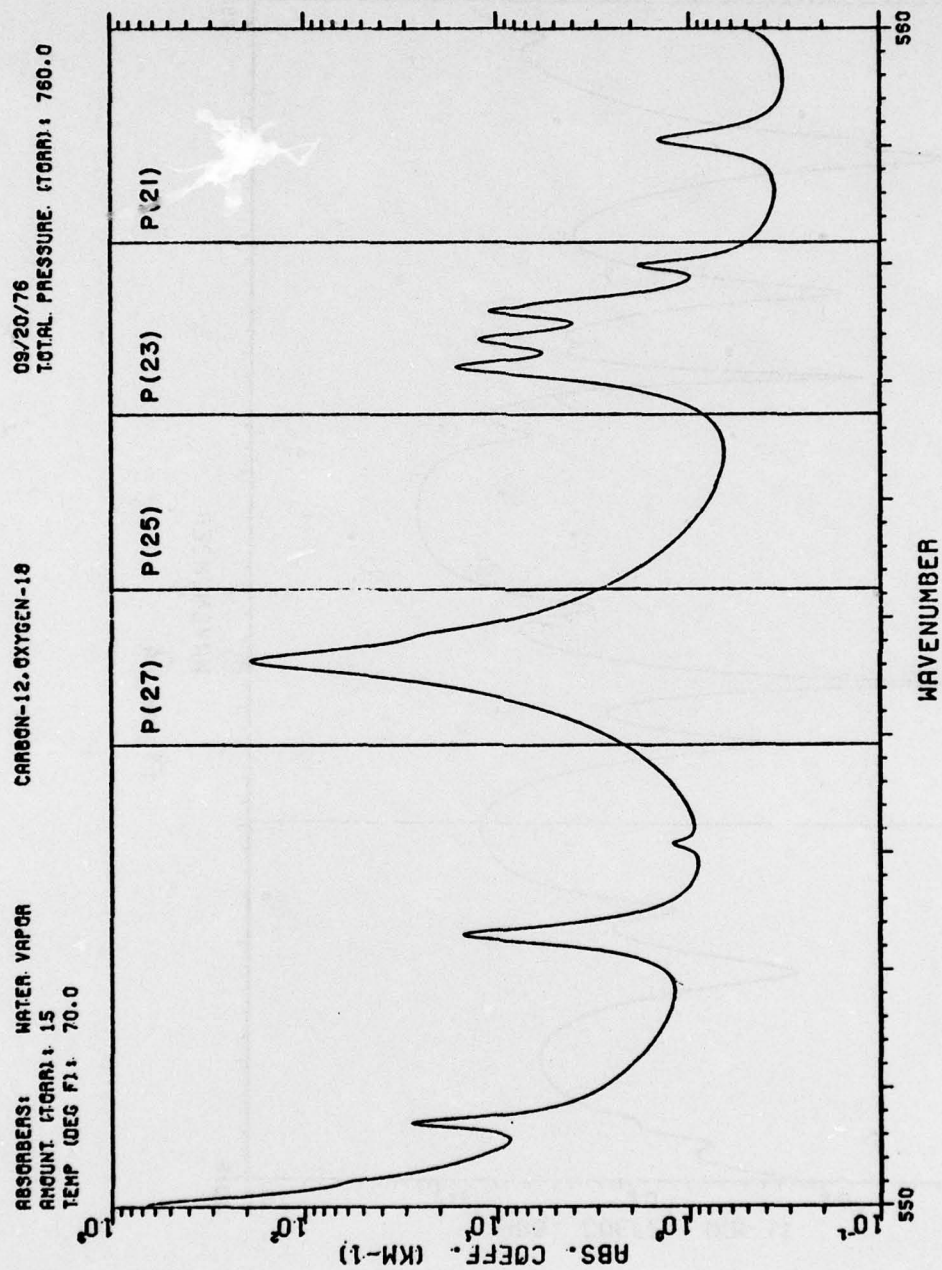
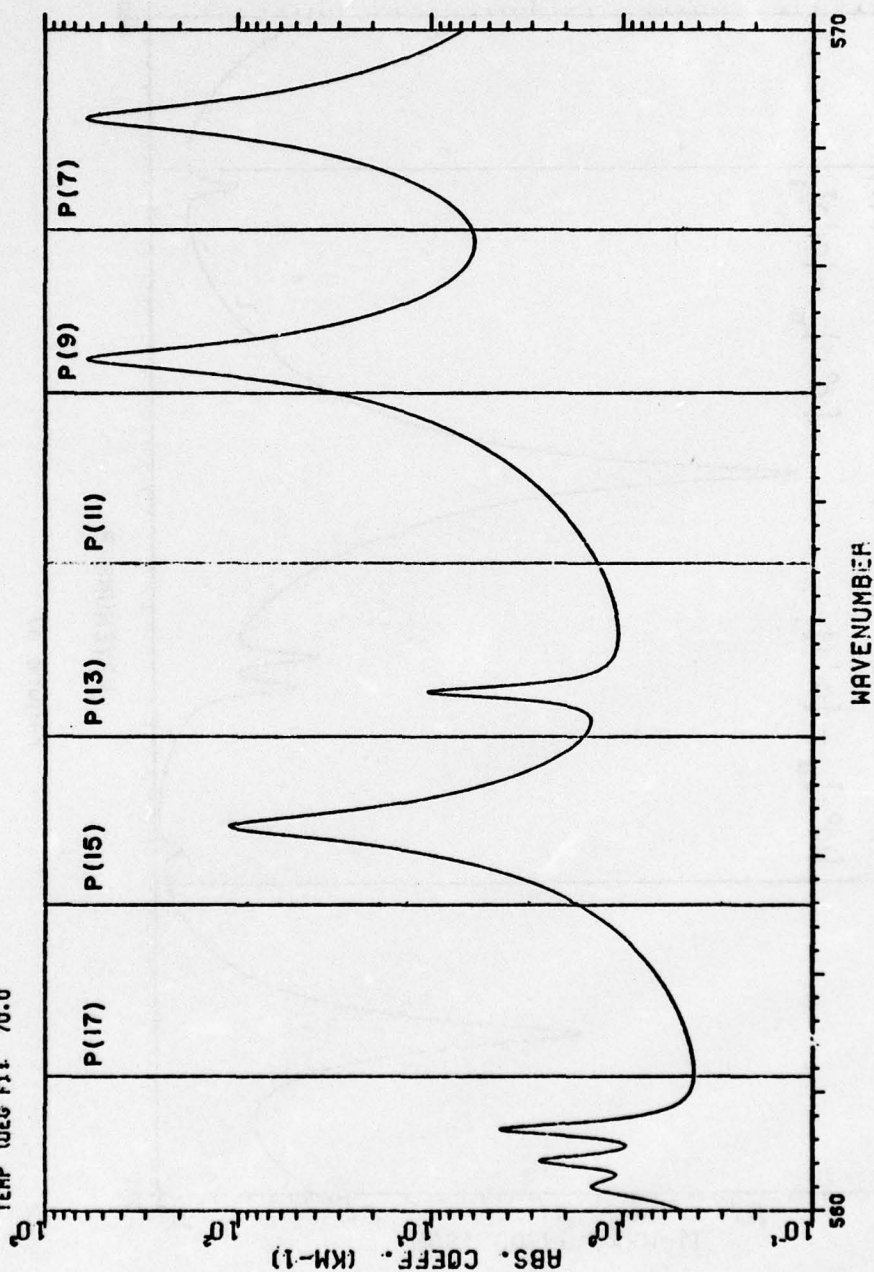


Figure 65

08/20/76
TOTAL PRESSURE (TORR): 780.0

CARBON-12.OXYGEN-18

ABSORBERS: WATER VAPOR.
AMOUNT (TORR): 15
TEMP (DEG F): 70.0



WAVENUMBER

Figure 66

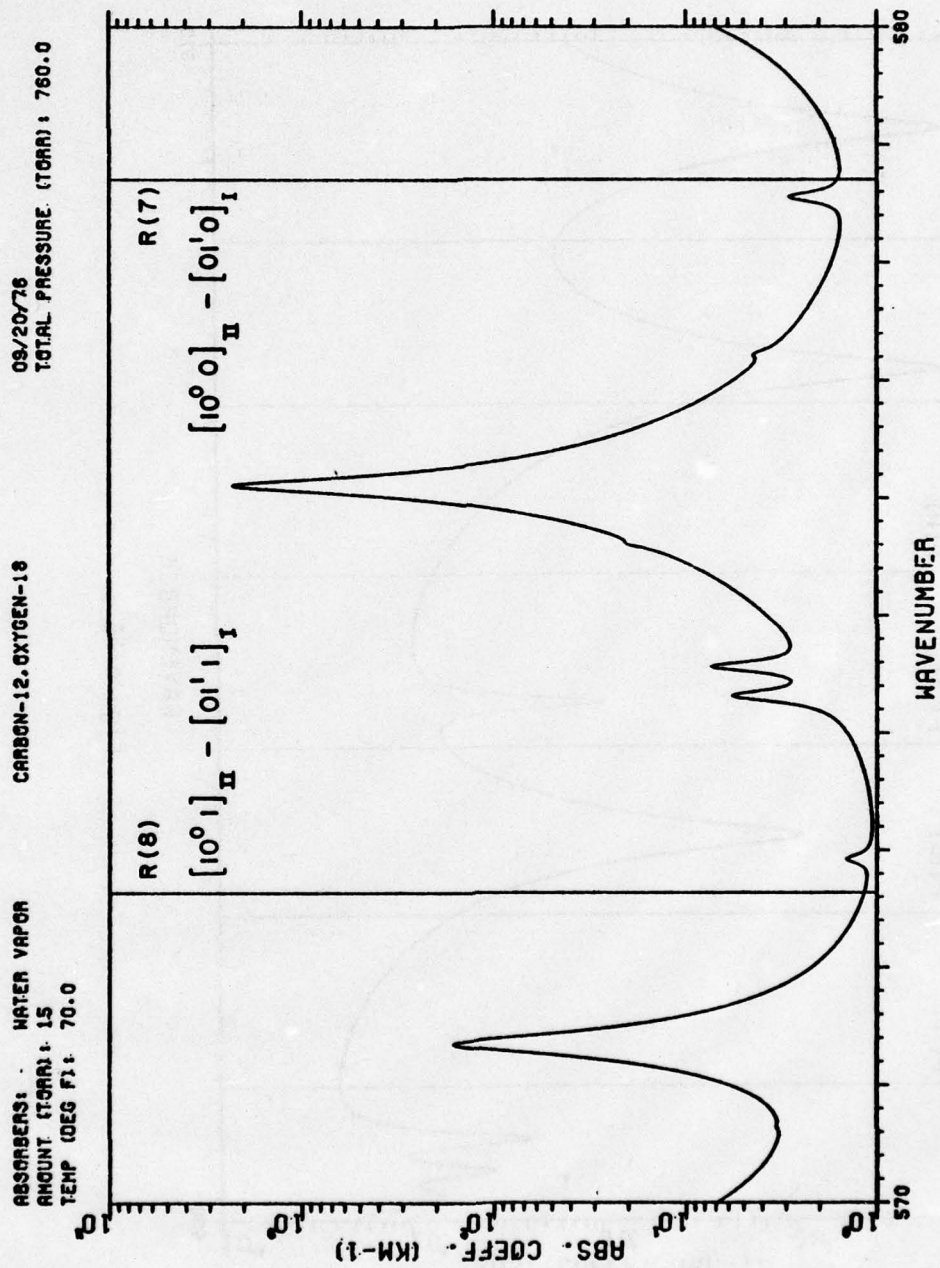


Figure 67

08/20/78
TOTAL PRESSURE (TORR) : 760.0

CARBON-12. OXYGEN-18

ABSORBERS: WATER VAPOR
AMOUNT (TORR) : 15
TEMP (DEG F) : 70.0

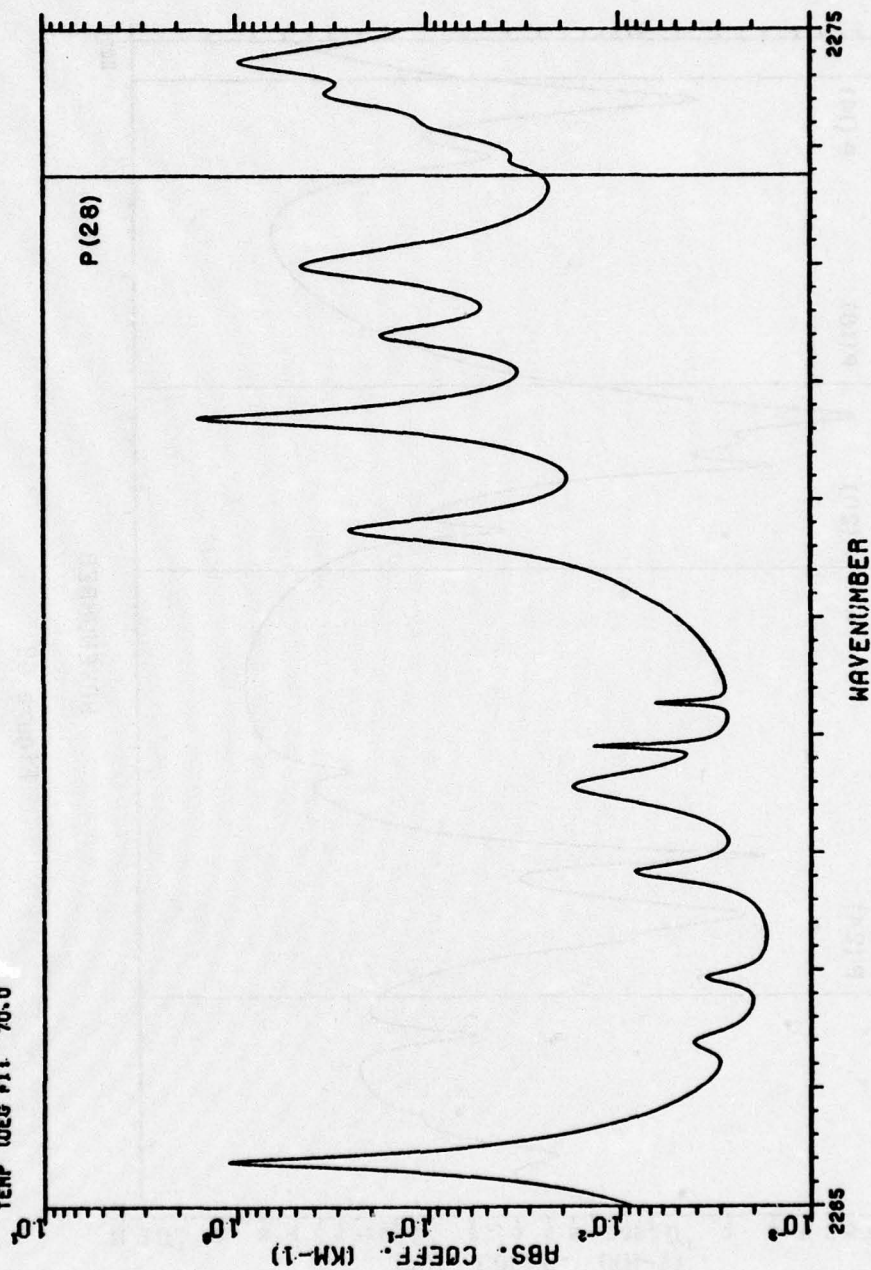


Figure 68

09/20/76
TOTAL PRESSURE (TORR): 760.0

CARBON-12 OXYGEN-18

ABSORBERS: WATER VAPOR
AMOUNT (TORR): 15
TEMP (DEG F): 70.0

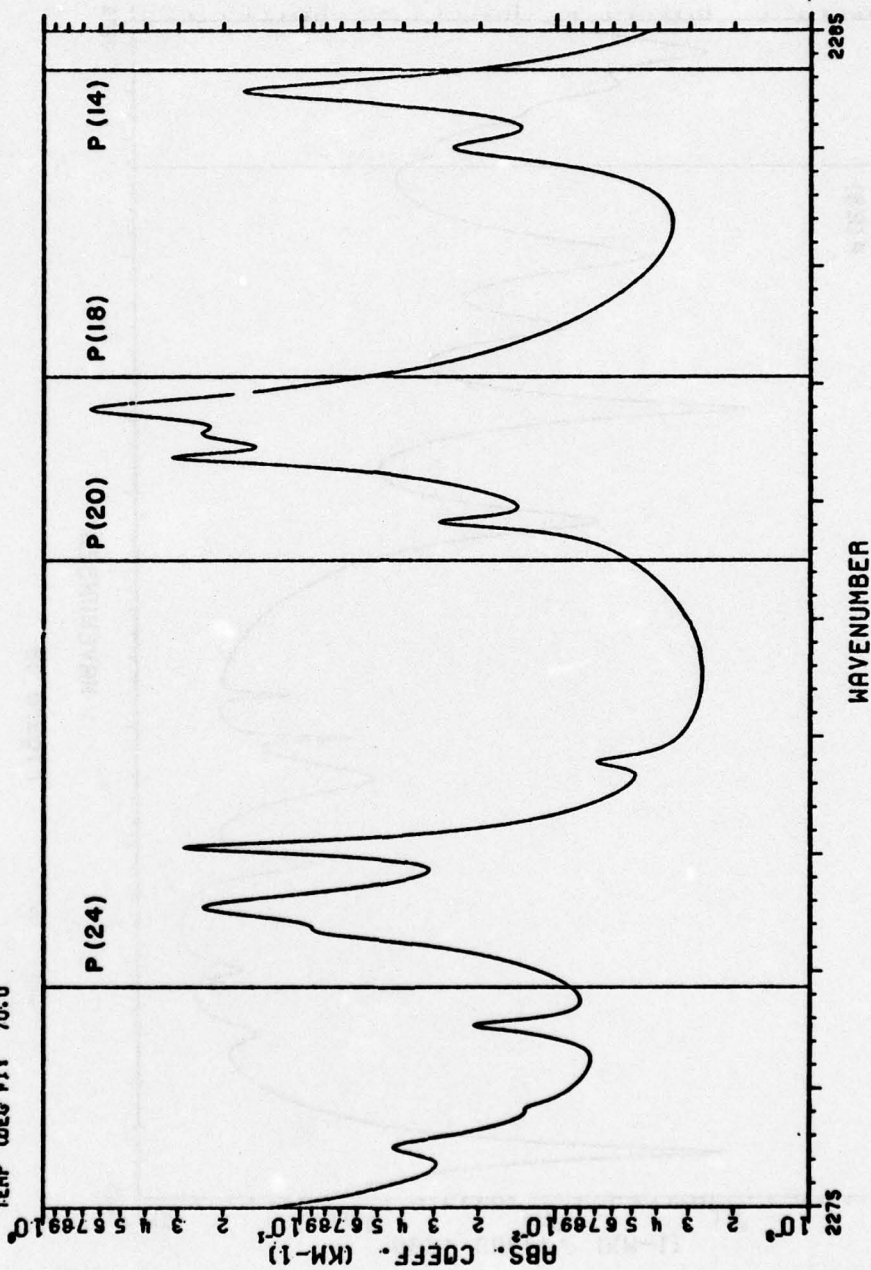


Figure 69

09/20/76
TOTAL PRESSURE (TORR) : 760.0

CARBON-12. OXYGEN-18

ABSORBERS: WATER VAPOR
AMOUNT: (TORR) : 15
TEMP (DEG F) : 70.0

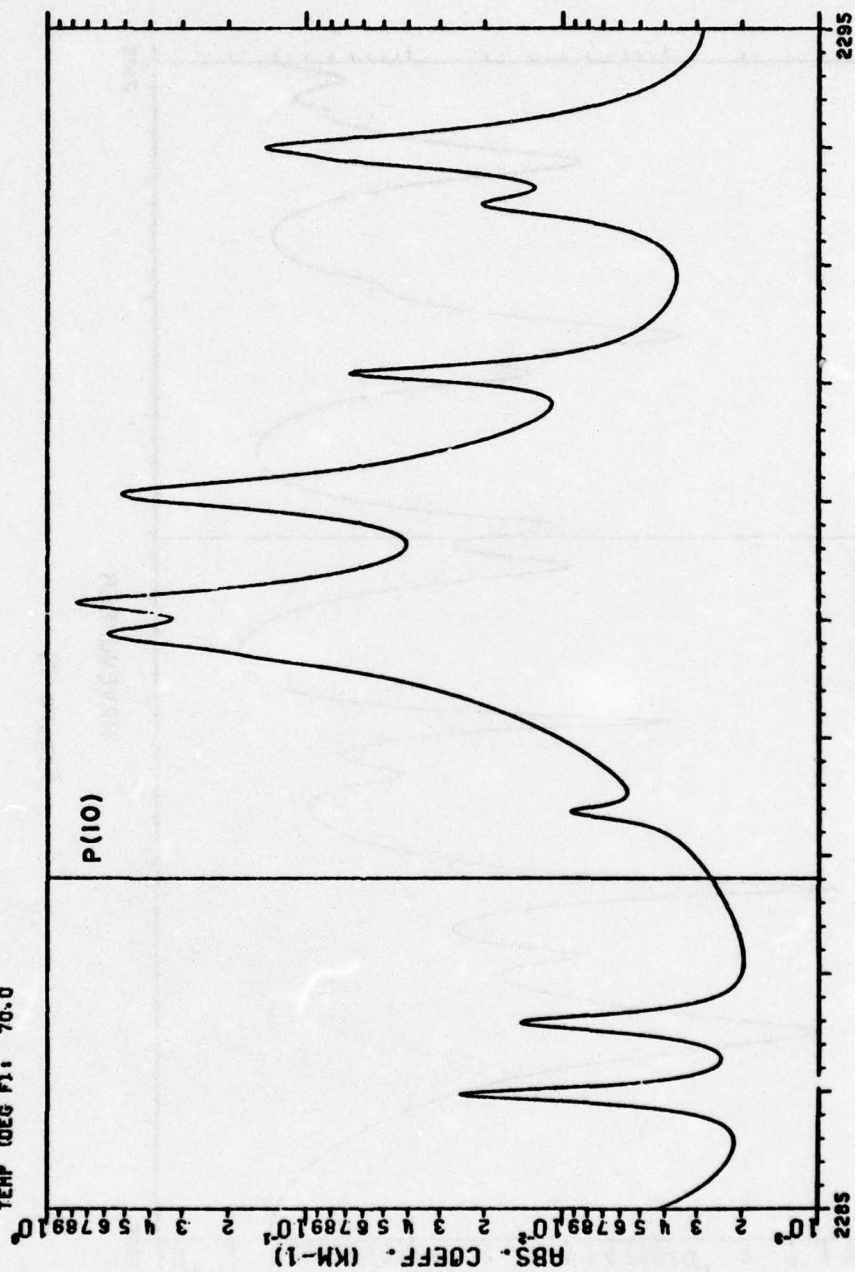


Figure 70

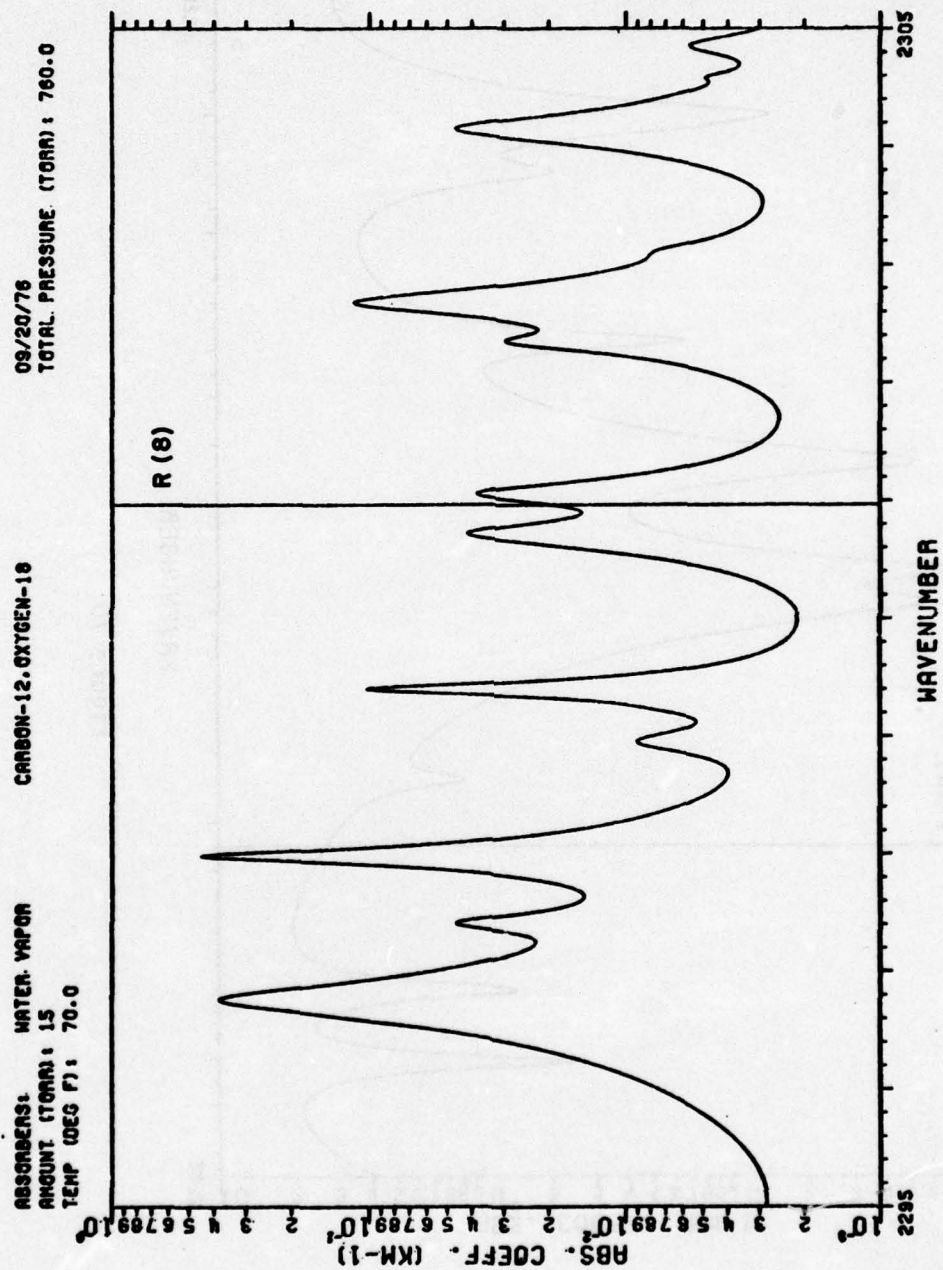


Figure 71

SECTION VIII

CONCLUSION

This report has described the various tasks which comprise the research program of laser atmospheric absorption studies at The Ohio State University. As the work on each of the new stainless steel, temperature controlled absorption cells nears completion, it is anticipated that spectra will be recorded through these cells in the very near future. The temperature controls designed on each absorption cell will offer a greater temperature range than was previously possible.

The new non-resonant, stainless-steel spectrophone is in operation. At the present time, however, there is only a small amount of data which has been collected using this spectrophone. The absorption of CO₂ laser radiation by CO₂ in air has been measured, and these data appear to be correct.

An interesting variation to the familiar White cell and spectrophone studies of the attenuation of CO₂ laser radiation by atmospheric constituents is the use of other isotopic varieties of CO₂ lasers. These lasers would provide new frequencies with which to probe the atmosphere, and could add new data to the magnitude of water vapor continuum absorption. Studies of the attenuation of isotopic CO₂ laser radiation remains a theoretical problem at this laboratory at the present time.

The results of the past year have raised many questions which are both technical and theoretical in scope. During the coming year, these problems will be pursued.

REFERENCES

1. S. P. Langley, Mem. Natl. Acad. Sci. 4, 159 (1888).
2. S. P. Langley, Ann. Ap. Obs., Smithsonian Institution, 1, 1 (1900).
3. A. Adel, Astrophys. J. 87, 198 (1938), 91, 1 (1940), 93, 506 (1941).
4. A. Adel, J. Opt. Soc. America 37 769 (1947).
5. M. V. Migeotte, Phys. Rev. 73, 519 (1948).
6. M. V. Migeotte, Phys. Rev. 75, 1108 (1949).
7. J. H. Shaw, M. L. Oxholm and H. H. Clarssen, Astrophys. J. 116, 554 (1952).
8. W. M. Elsasser, "Heat Transfer by Infrared Radiation in the Atmosphere", Harvard University Press, Cambridge, Mass. (1942).
9. H. W. Yates and J. H. Taylor, "Infrared Transmission of the Atmosphere", NRL Report 5453 (AD 240-88) (1960).
10. A. Adel, Astrophys J. 89, 1 (1939).
11. R. Anthony, Phys. Rev 85, 674 (1952).
12. W. T. Roach and R. W. Goody, Quart. J. Roy. Meterol. Soc. 84, 319 (1958).
13. K. Bignell, F. Saiedy, and P. A. Sheppard, J. Opt. Soc, America 53, 466 (1963).
14. K. J. Bignell, Quart J. Roy. Meterol. Soc. 96, 390 (1970).
15. D. E. Burch, Aeronutronic Publication No. U-4784, "Semi-Annual Technical Report", Air Force Cambridge Research Laboratories, Contract No. F19628-69-C-0263, January, 1970.
16. D. E. Burch, D. A. Gruyvnak, and J. D. Pembroke, Aeronutronic Publication No. U-4897, "Investigation of the Absorption of Infrared Radiation by Atmospheric Gases: Water, Nitrogen, Nitrous Oxide", Air Force Cambridge Research Laboratories, Contract No. F19628-69-C-0263, January, 1971.
17. P. S. Varanasi, S. Chou, and S. S. Penner, J. Quant. Spectrus. Radiat. Transfer 8, 1537 (1968).
18. J. H. McCoy, D. B. Rensch, and R. K. Long, Appl. Opt. 8, 1471 (1969).

19. F. S. Mills, R. K. Long, and E. K. Damon, "Laser Absorption Studies (First Semi-Annual Report)", No. 4054-2, Rome Air Development Center (OCSE), RADC-TR-75-289, November 1975, (A018900).
20. I. I. Ippolitov, Opt. Spektrosc. 27, 246 (1969).
21. V. N. Aref'ev, V. I. Dianov-Klokov, V. N. Radionov, and N. I. Sizov, Opt. Spektrosc, 39, 560 (1975).
22. T. G. Adiks, V. N. Aref'ev, and V. I. Dianov-Klokov, Jor. J. Quant. Electron 5, 481 (1975).
23. R. E. Roberts, L. M. Biberman and J. E. A. Selby, "Infrared Continuum Absorption by Atmospheric Water Vapor in the 8-12 m Window", Institute for Defense Analysis Science and Technology Division, IDA Log No. HQ76-18059, April, 1976.
24. J. E. A. Selby and R. A. McClatchey, "Atmospheric Transmittance From 0.25 to 28.5 μ m: computer Code LOWTRAN 3", AFCRL-TR-75-0255, Air Force Cambridge Research Laboratories Environmental Research Papers, No. 513 (1975).
25. J. E. Lowder, L. A. Kennedy, K. G. P. Sulzmann, and S. S. Penner, J. Quant. Spectrosc. Radiat. Transfer 10, 17 (1969).
26. D. E. Burch, "Radiative Properties of the Atmospheric Windows", presented at the Conference on Atmospheric Radiation sponsored by the American Meteorological Society, Ft. Collins, Colorado, August, 1972.
27. F. S. Mills, "Absorption of Deuterium Fluoride Laser Radiation by the Atmosphere", Report 4054-3, September 1975, The Ohio State University ElectroScience Laboratory, Department of Electrical Engineering; prepared under Contract F30602-75-C-0029 For Rome Air Development Center. (RADC-TR-76-105)(AD/A 025 402)
28. R. E. Meredith, T. W. Tuer, and D. R. Woods, "Investigation of DF Laser Propagation", Research and Development Technical Report, Atmospheric Sciences Laboratory, ECOM-74-4, December 1974.
29. E. K. Damon, J. C. Peterson, F. S. Mills, and R. K. Long, "Spectrophone Measurements of the Water Vapor Continuum at DF Laser Frequencies," Report 4054-1, July 1975, The Ohio State University ElectroScience Laboratory, Department of Electrical Engineering; prepared under Contract F30602-75-C-0029 for the Rome Air Development Center. (RADC-TR-75-203), (A016435).
30. W. H. Thomason and D.C. Elbers, "An Inexpensive Method to Stabilize the Frequency of a CO₂ Laser," 1974, Louisiana State University, Department of Chemistry, private communication.

31. A. D. Wood, M. Camac, and E. T. Gerry, *Applied Optics*, 10, 1971, p. 1877.
32. J. C. Peterson, "A Differential Spectrophone of Unique Design," M.Sc. Thesis, The Ohio State University, 1975.
33. F. S. Mills, private communication, The Ohio State University, ElectroScience Laboratory, Department of Electrical Engineering, Columbus, Ohio.
34. L. Henry, *Commande de Travaux sur Memoire No. 72-147*, Etude de la transmission du rayonnement des lasers a CO₂ dans la région de 10,6 microns, Janvier 1974.
35. T. G. Adiks, V. N. Aref'ev and V. I. Dianov-Klovov, "Influence of Molecular Absorption on Propagation of CO₂ Laser Radiation in Terrestrial Atmosphere (review)," *Sov. J. Quant. Electron.*, Vol. 5, No. 5.
36. M. Schumate et al., to be published in *Applied Optics*.
37. N. Deju, *Appl. Phys. Lett.* 23, 309 (1973).
38. P. Brachignac, J. P. Martin, and G. Taieb, *J. Quant. Electron.*, IEEE 10, 797 (1974).
39. P. Brechignac and J. P. Martin, *J. Quant. Electron*, IEEE 2, 80 (1976).
40. J. U. White, *J. Opt. Soc. Amer.* 32, 285 (1942).
41. D. J. McCaa and J. H. Shaw, *J. Mol. Spectrosc.* 25, 374 (1968).
42. A. G. Maki, *J. Mol. Spectrosc.* 57, 416 (1975).
43. E. C. Y. Inn and Y. Tanaka, "Ozone Chemistry and Technology", *Advances in Chemistry*, No. 21, American Chemical Society, Applied Publication, 265 (1959).
44. R. Blickensderfer, G. Ewing, and R. Leonard, *Appl. Opt.* 7, 2114 (1968).
45. G. L. Trusty, "Absorption Measurements of the 10.4 m Region Using a CO₂ Laser and a Spectrophone," Report 2819-4, January 1973, The Ohio State University ElectroScience Laboratory, Department of Electrical Engineering; prepared under Contract F33615-69-C-1807 for Air Force Avionics Laboratory. (AFAL-TR-72-413) (AD 907549)
46. E. L. Kerr and J. G. Atwood, *Appl. Opt.* 7, 915 (1968).
47. C. F. Dewey, Jr., R. D. Kamm, and C. F. Hackett, *Appl. Phys. Lett.* 23, 633 (1973).

48. P. D. Goldman and K. Goto, J. Appl. Phys. 45, 4350 (1974).
49. L. G. Rosengren, Appl. Optics 14, 1960 (1975).
50. J. C. Peterson, "A Differential Spectrophone of Unique Design," M.S. Thesis, The Ohio State University, 1976.
51. R. R. LaPelle, Practical Vacuum Systems, McGraw-Hill, New York, 1972.
52. D. F. Shriver, The Manipulation of Air Sensitive Compounds, McGraw-Hill, New York, 1969.
53. R. G. Pike and D. Hubbard, J. Res. Nat. Bur. Stand. 59, 127 (1957).
54. W. J. Witteman, IEEE J. Quant. Electron. 2, 377 (1966).
55. F. S. Mills, "Absorption of Deuterium Fluoride Laser Radiation by the Atmosphere," Report 4054-3, September 1975, The Ohio State University ElectroScience Laboratory, Department of Electrical Engineering; prepared under Contract F30602-75-C-0029 for Rome Air Development Center. (RADC-TR-76-105) (AD/A 025402)
56. I. Wieder and G. B. McCurdy, Phys. Rev. Lett. 16, 1966, p. 565.
57. G. B. Jacobs and H. C. Bowers, J. Appl. Phys. 38, 1967, p. 2629.
58. C. Freed, A. H. M. Ross, and R. G. O'Donnell, J. Molec. Spectrosc. 49, 1974, p. 439.
59. M. I. Buchwald, C. R. Jones, H. R. Fetterman, H. R. Schlossberg, Appl. Phys. Lett. 29, 1976, p. 300.
60. R. A. McClatchey, R. W. Fenn, J. E. A. Selby, F. E. Voltz, and J. S. Garing, "Optical Properties of the Atmosphere (Third Edition)," AFCRL-70-0527, 1970.
61. R. A. McClatchey, W. S. Benedict, S. A. Clough, D. E. Burch, R. F. Calfee, K. Fox, L. S. Rothman, and J. S. Garing, "AFCRL Atmospheric Absorption Line Parameters Compilation," AFCRL-TR-73-0096, 1973.
62. W. R. Skinner and R. J. Nordstrom, to be published in Applied Optics, November 1976.
63. F. S. Mills, "Absorption of Deuterium Fluoride Laser Radiation by the Atmosphere," Report 4054-3, The Ohio State University ElectroScience Laboratory, Department of Electrical Engineering; prepared under Contract F30602-75-C-0029 for Rome Air Development Center. (RADC-TR-76-105) (AD/A 025 402).

APPENDIX A

This appendix is a paper which has been accepted for publication to Applied Optics. The results discussed here come from a great deal of work on the elimination of contaminants from spectrophones.

A SUBTLE SOURCE OF CONTAMINATION IN SPECTROPHONES*

by

J.C. Peterson, R.J. Nordstrom, and R.K. Long

The Ohio State University ElectroScience Laboratory
Department of Electrical Engineering
Columbus, Ohio 43212

August 1976

*The work reported in this paper was supported in part by Contract F30602-76-C-0058 between Rome Air Development Center and The Ohio State University Research Foundation.

The laser illuminated spectrophone has proved itself to be a very sensitive instrument for measuring absorption of electromagnetic radiation by gases. Kerr and Atwood [1] were the first to use laser sources in conjunction with the spectrophone device. Absorptivities as low as 10^{-6} cm^{-1} to 10^{-7} cm^{-1} were measured using pulsed ruby and continuous CO_2 lasers.

The original concept of the spectrophone was developed by A. G. Bell [2,3]. Rather than measuring a ratio of output power to input power through an absorber as conventional transmittance studies do, the spectrophone measures absorptivity directly by monitoring a pressure change caused by absorption of the radiation within the confined gas. Sensitivities achieved by Kerr and Atwood in their original experiments were limited by a false pressure signal which was proportional to laser power and associated with absorption of the radiation by the end windows. These erroneous signals can be considerably reduced by employing a differential spectrophone design [4,5].

The relatively small volume of the spectrophone and its very high sensitivity make this apparatus particularly vulnerable to erroneous measurements caused by small amounts of an absorbing contaminant. Therefore, every effort must be taken to keep the spectrophone system as clean as possible. Present sensitivities of 10^{-8} cm^{-1} are not uncommon in a properly cleaned system.

Spectrophones can be divided into two general categories: the resonant and the nonresonant types. We have used nonresonant spectrophones in this laboratory for several years to measure the attenuation of laser radiation by various atmospheric gases [6,7]. A CO_2 laser has been

used to study water vapor absorption in the $10\mu\text{m}$ spectral region, and a deuterium fluoride (DF) laser has been used to study the absorption of several gases including water vapor, nitrous oxide, and methane in the $3.8\mu\text{m}$ spectral region. Results of spectrophone measurements of the absorption of P(20) CO_2 laser radiation at $10.59\mu\text{m}$ by nitrogen broadened water vapor samples are in good agreement with the earlier long-path absorption cell measurements of McCoy et al [8].

However, on occasion, an apparent contaminant in the water vapor samples has interfered with the measurements of water vapor absorption. At first, a foreign substance dissolved in the water was suspected. It was thought that this contaminant might be ammonia since ammonia has been reported to be a problem in water samples [9]. Another potential source of contamination was plastic from the walls of the containers in which the distilled water was stored.

These possibilities were pursued by recording infrared spectra of large amounts of water vapor in an absorption cell with a total path of 170m. These spectra were recorded with a Fourier transform instrument. No bands of ammonia were observed in the $10\mu\text{m}$ region or elsewhere in the spectra. There are very strong absorption bands of ammonia at $10.5\mu\text{m}$ and $6.2\mu\text{m}$ along with a weaker band at $3.0\mu\text{m}$. None of these features was observed.

Every precaution to eliminate plastic as a contaminant was taken. All water samples used are now doubly-distilled in Pyrex and bottled in glass vessels.

The source of our contamination was finally traced to a fluid used to clean the mirror in the EG and G model 992 dew-point hygrometer which

was used to monitor the amount of water vapor in the spectrophone. This fluid, provided by the manufacturer, has a very strong infrared absorption in the $10\mu\text{m}$ spectral region as can be seen in Figure 1. The manufacturer's nomenclature for this fluid is CSO Type "A" Solvent. This cleaner is primarily methanol (CH_3OH). Several spectra of methanol are included in Figure 1. These spectra show that the methanol is responsible for the strong absorption in Type "A" Solvent near 1025 cm^{-1} . It is this absorption band which causes the interference with the CO_2 laser measurements.

The methanol spectra were recorded by injecting a certain amount of methanol into a multiple-transversal absorption cell and filling the cell to 700 torr with high-purity nitrogen. Total path length in the absorption cell was 255m. A spectrum was then recorded at a resolution of 1.0 cm^{-1} with a Fourier transform instrument. The spectrum of Type "A" Solvent was recorded by evaporating a few drops of the liquid into a 40 cm long single pass absorption cell and bringing the total pressure within the cell to 1.0 atm with nitrogen. The same Fourier transform instrument was used to record the spectrum of the solvent.

In order to verify that this compound was causing the false absorption in the spectrophone experiments, an important check was made. The experimental apparatus used for this test of the influence of Type "A" Solvent is shown in Figure 2. The spectrophone was irradiated by the P(20) CO_2 laser line at $10.59\mu\text{m}$. A nitrogen sample was introduced into the system and circulated through the spectrophone, first with only valve 1 open and next with valve 1 closed and valves 2 and 3 open. The measured background absorptivity in the system was the same for both circulation paths.

The 2.5 inch stainless steel tubing was then removed from the system and cleaned with the Type "A" Solvent. A cotton swab was used to rub the solvent onto the inner wall of the tubing. The tubing was then blown dry with helium gas, and filled with nitrogen. The tubing was then replaced onto the spectrophone system.

Then, 10 torr water vapor in nitrogen (total pressure was 760 torr) was injected into the spectrophone and was circulated with valve 1 open. The measured absorption coefficient was 0.13 km^{-1} . This value is slightly higher than other measurements made in a cleansed system, and indicates that the spectrophone probably contained contamination from previous experiments.

Next, valve 1 was closed and valves 2 and 3 were opened. The sample of water vapor in nitrogen was circulated for 60 seconds through the 2.5 inch stainless steel tubing which had been cleaned with the solvent. The absorption coefficient was measured to be 0.216 km^{-1} . This value is 1.7 times as great as the original measurement and clearly demonstrates that contamination of the water sample by even minute amounts of solvent can be serious.

The spectrophone was then evacuated and flushed with nitrogen. The experiment was repeated with a 5 torr water vapor sample in nitrogen. The results of this series of tests are shown in Figure 3.

It is our experience that once this solvent has contaminated a spectrophone system it is very difficult to purify the system once again. Repeated flushing with large amounts of water seems to work best since the solvent appears to be soluble in water.

A very subtle feature of this contaminant is the fact that it seems to lie dormant on the mirror surface when absorption by gases other than water vapor are studied. However, as soon as water vapor is injected into the system, the contaminant is picked up and causes interference with the measurements. For this reason, a great deal of time was spent in studying the water vapor itself for contamination.

A clean mirror is important in the reflection-type dew-point hygrometers. However extreme caution must be taken when selecting a cleaning fluid to be sure that the cleaner does not interfere with the experiment. For studies of the absorption of CO_2 laser radiation by water vapor, it would appear that spectroscopic grade carbon tetrachloride is a suitable cleaner, provided that it is used in small amounts. The infrared spectrum of carbon tetrachloride shows absorption at 790 cm^{-1} . The CO_2 laser region is free from strongly absorbing features.

The authors wish to thank J. H. Shaw for providing the Fourier transform instrument and we greatly appreciate the assistance of W. H. Chan and W. M. Uselman in collecting the methanol spectra.

REFERENCES

1. E.L. Kerr and J.G. Atwood, Appl. Opt 7, 915 (1968).
2. A.G. Bell, Proc. Am. Assoc. Advance Sci. 29, 115 (1880).
3. A.G. Bell, Phil. Mag. 11, 510 (1881).
4. T.F. Deaton, D.A. Depatie, and T.W. Walker, Appl. Phys. Lett. 26, 300 (1975).
5. J.C. Peterson, "A Differential Spectrophone of Unique Design," Thesis, The Ohio State University, (1976).
6. E.K. Damon, F.S. Mills, J.C. Peterson, and R.K. Long, "Spectrophone Measurement of the Water Vapor Continuum at DF Laser Frequencies," Interim Technical Report RADC-TR-75-203, August 1975, (A016435).
7. G.L. Trusty, "Absorption Measurements of the 10.4 Micron Region Using a CO₂ Laser and a Spectrophone," Report 2819-4, Air Force Avionics Laboratory, AFAL-TR-72-413, January 1973.
8. J.H. McCoy, D.B. Rensch, and R.K. Long, Appl. Opt. 8, 1471 (1969).
9. D.E. Burch, Aeronutronic Publication No. U-4784, "Semi-Annual Technical Report," Air Force Cambridge Research Laboratories, Contract No. F 19628-69-C-0263, January 1970.

CAPTIONS FOR FIGURES

Figure 1

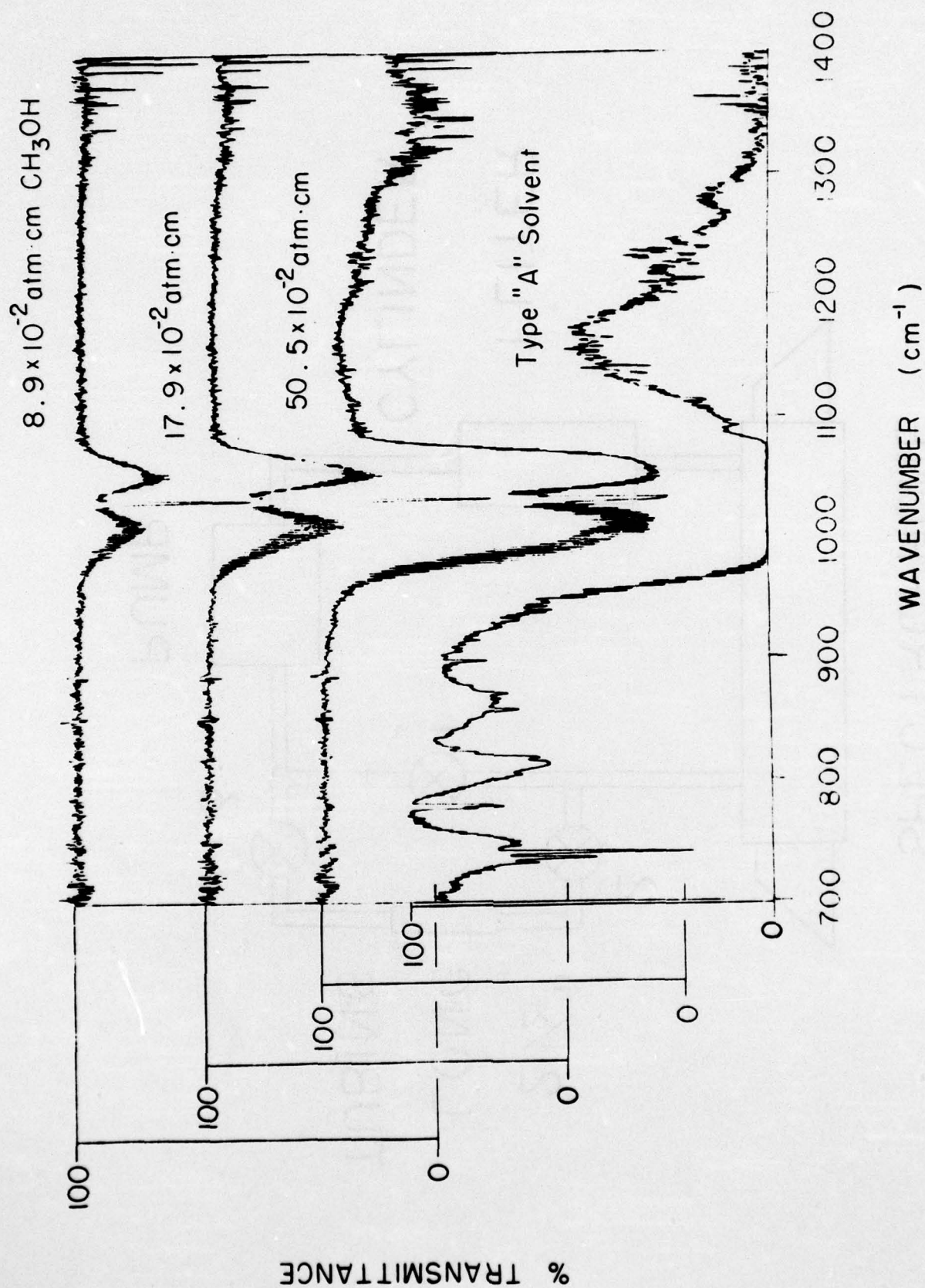
Spectrum of CSO Type "A" Solvent along with spectra of methanol (CH_3OH). All spectra are 1.0 cm^{-1} resolution.

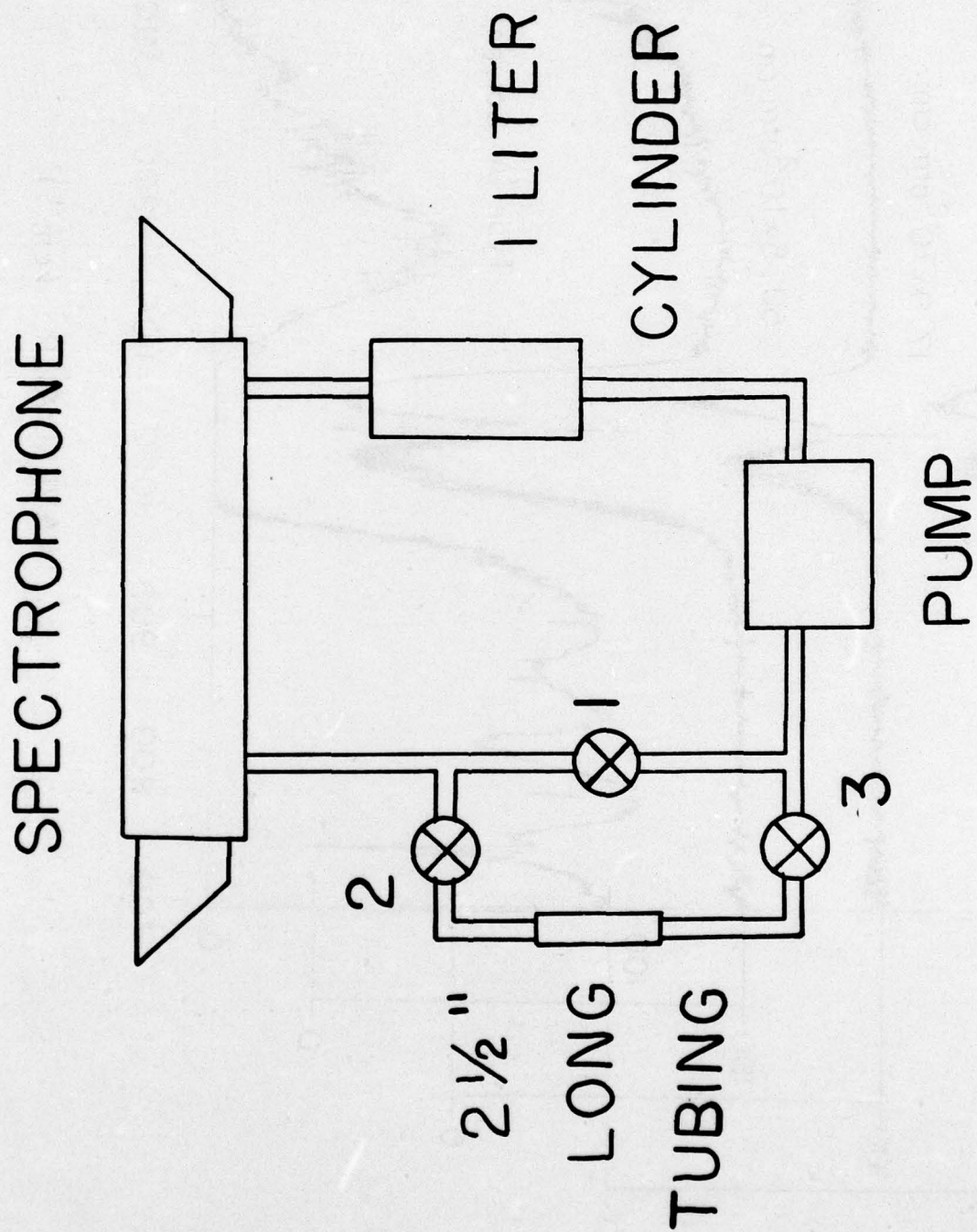
Figure 2

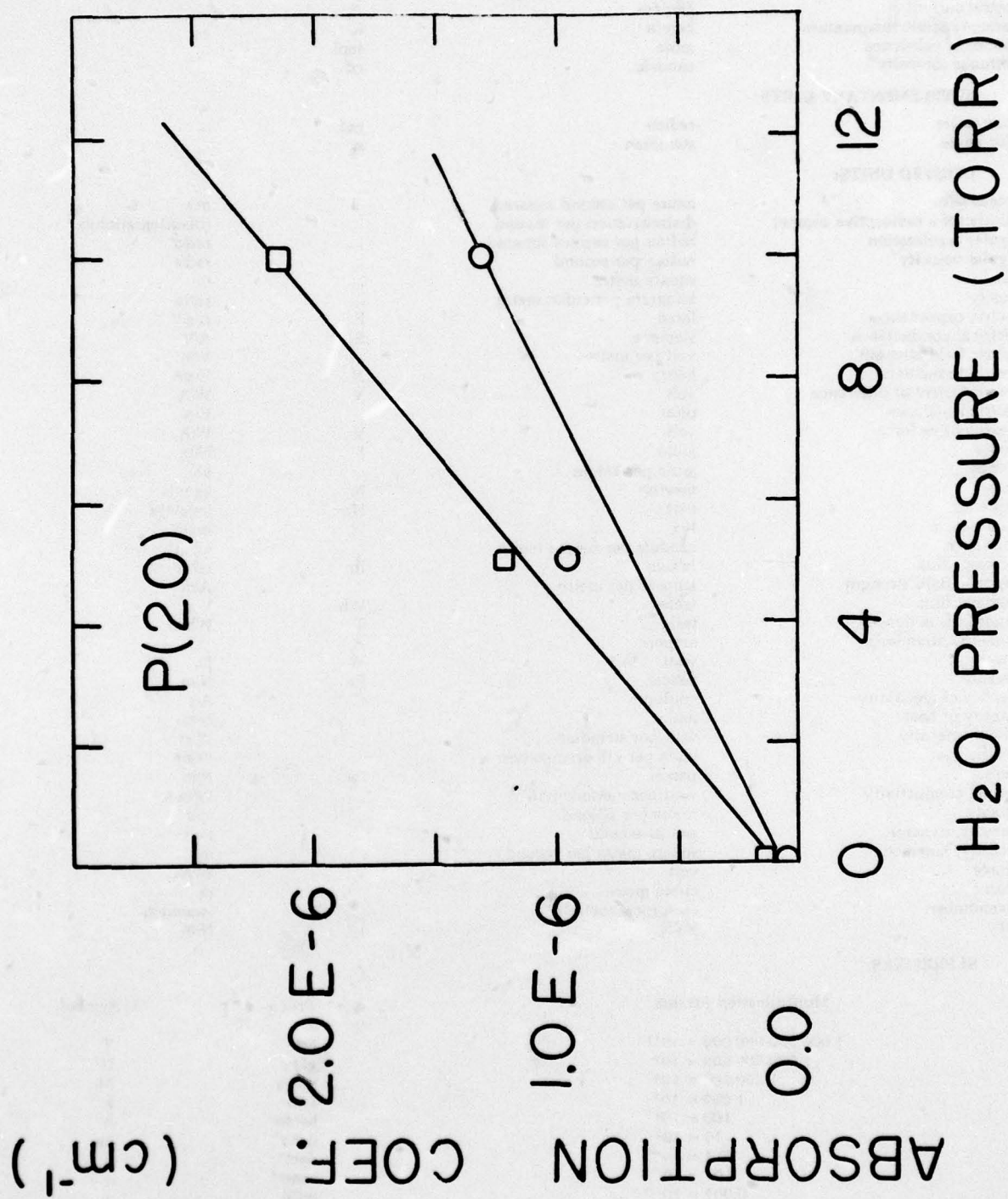
Experimental apparatus used to test the influence of Type "A" Solvent on spectrophone measurements of the absorptivity of water vapor. All parts are stainless steel except the spectrophone.

Figure 3

Plots of absorption coefficient vs the pressure of water vapor in the spectrophone system. All measurements made with a total pressure of 760 torr with N_2 . The circles are uncontaminated measurements and squares show the results of contamination caused by Type "A" Solvent. The circle near 5 torr shows residual contamination from previous experiment.







METRIC SYSTEM

BASE UNITS:

Quantity	Unit	SI Symbol	Formula
length	metre	m	...
mass	kilogram	kg	...
time	second	s	...
electric current	ampere	A	...
thermodynamic temperature	kelvin	K	...
amount of substance	mole	mol	...
luminous intensity	candela	cd	...

SUPPLEMENTARY UNITS:

plane angle	radian	rad	...
solid angle	steradian	sr	...

DERIVED UNITS:

Acceleration	metre per second squared	...	m/s
activity (of a radioactive source)	disintegration per second	...	(disintegration)/s
angular acceleration	radian per second squared	...	rad/s
angular velocity	radian per second	...	rad/s
area	square metre	...	m
density	kilogram per cubic metre	...	kg/m
electric capacitance	farad	F	A·s/V
electrical conductance	siemens	S	A/V
electric field strength	volt per metre	...	V/m
electric inductance	henry	H	V·s/A
electric potential difference	volt	V	W/A
electric resistance	ohm	...	V/A
electromotive force	volt	V	W/A
energy	joule	J	N·m
entropy	joule per kelvin	...	J/K
force	newton	N	kg·m/s
frequency	hertz	Hz	(cycle)/s
illuminance	lux	lx	lm/m
luminance	candela per square metre	...	cd/m
luminous flux	lumen	lm	cd·sr
magnetic field strength	ampere per metre	...	A/m
magnetic flux	weber	Wb	V·s
magnetic flux density	tesla	T	Wb/m
magnetomotive force	ampere	A	...
power	watt	W	J/s
pressure	pascal	Pa	N/m
quantity of electricity	coulomb	C	A·s
quantity of heat	joule	J	N·m
radiant intensity	watt per steradian	...	W/sr
specific heat	joule per kilogram-kelvin	...	J/kg·K
stress	pascal	Pa	N/m
thermal conductivity	watt per metre-kelvin	...	W/m·K
velocity	metre per second	...	m/s
viscosity, dynamic	pascal-second	...	Pa·s
viscosity, kinematic	square metre per second	...	m/s
voltage	volt	V	W/A
volume	cubic metre	...	m
wavenumber	reciprocal metre	...	(wave)/m
work	joule	J	N·m

SI PREFIXES:

Multiplication Factors	Prefix	SI Symbol
1 000 000 000 000 = 10 ¹²	tera	T
1 000 000 000 = 10 ⁹	giga	G
1 000 000 = 10 ⁶	mega	M
1 000 = 10 ³	kilo	k
100 = 10 ²	hecto*	h
10 = 10 ¹	deka*	da
0.1 = 10 ⁻¹	deci*	d
0.01 = 10 ⁻²	centi*	c
0.001 = 10 ⁻³	milli	m
0.000 001 = 10 ⁻⁶	micro	μ
0.000 000 001 = 10 ⁻⁹	nano	n
0.000 000 000 001 = 10 ⁻¹²	pico	p
0.000 000 000 000 001 = 10 ⁻¹⁵	femto	f
0.000 000 000 000 000 001 = 10 ⁻¹⁸	atto	a

* To be avoided where possible.